Second Harmonic Based Method to Detect Geomagnetically Induced Currents in Power Transformers

by

Eric Walter Zundel

Bachelor of Science in Engineering, UNB, 2022

A Thesis Submitted in Partial Fulfillment of
the Requirements for the Degree of

Masters of Science in Engineering

in the Graduate Academic Unit of Electrical and Computer Engineering

Supervisor:	Saleh A. Saleh, PhD, Electrical and Computer Engineering
Examining Board:	Brent Petersen, PhD, Electrical and Computer Engineering, Chair
	Julian Meng, PhD, Electrical and Computer Engineering
	Othman Nasir, PhD, Civil Engineering

This thesis is accepted by the
Dean of Graduate Studies

THE UNIVERSITY OF NEW BRUNSWICK

April, 2024

© Eric Walter Zundel, 2024

Abstract

Geomagnetically Induced Currents (GICs) are quasi-dc currents triggered by interactions between the Earth's magnetic field and charged particles released by the sun during coronal mass ejections. These currents flow through grounding circuits (such as grounded power transformers) into power systems, and can damage power system components. A power transformer with a GIC flow experiences half-cycle saturation, causing harmonic distortion and increased reactive power demands. As a result, power transformers can suffer damage, mal-operation of protective devices, tripping of compensation devices, and degraded power quality.

Various methods have been developed to respond to GIC flows, the majority of which identify the need for blocking of GIC flows. To block GIC flows, a method to accurately detect GIC is required. This thesis focuses on the development of an effective measure to detect the GIC flow. The desired detection measure is based on the second harmonic component extracted from power transformer differential currents.

Acknowledgements

I would like to thank my supervisor, Dr. Saleh, for his guidance throughout my masters and thesis. Dr. Saleh brought me onto the project that would eventually inspire this research and learning, and supported me through the complexities of this degree.

I am grateful to my family and friends for their support throughout my learning journey, and especially my partner Jordyn for her unwavering dedication and inspiration.

Lastly, I would like to thank the Atlantic Digital Grid project group and the MITACS Program for the scholarship and funding that they have provided.

Table of Contents

Abstract ii

Acknowledgments iii

Table of Contents iv

List of Tables vii

List of Figures viii

1 Introduction 1

1.1 General 1

1.2 Motivation 2

1.3 Literature review 2

1.3.1 Effects of GIC 3

1.3.2 Management of GIC 5

1.3.3 Other Sources of Harmonics 5

1.3.4 Detection of GIC 6

1.3.5 Transformer Protection 7

1.3.5.1 Processing Unbalanced Signals 9

1.4 Second Harmonic Based Method to Detect GIC Flows 9

1.5 Thesis Objective 11

1.6 Thesis Outline 12

2 Transformer and GIC Saturation Modelling 13

2.1 General . . . 13

2.2 Modelling Transformer Saturation . . . 14

2.2.1 Standard Transformer Wiring . . . 15

2.2.1.1 Harmonics . . . 17

2.2.2 Autotransformer Wiring . . . 19

2.2.2.1 Harmonics . . . 22

2.2.3 Effect of the Loading Level . . . 23

2.2.3.1 Harmonics . . . 25

2.2.4 Effect of Grounding System . . . 27

2.3 Summary . . . 28

3 Analysis of Harmonic Distortion Due to GIC in Power Transformers 29

3.1 General . . . 29

3.2 Test Power Transformers . . . 30

3.3 Test Results . . . 31

3.4 Harmonics Due to a GIC Flow . . . 32

3.4.1 5 kVA Transformer . . . 32

3.5 Effect of the Loading Level . . . 34

3.5.1 5 kVA Transformer . . . 36

3.6 Effect of the Grounding Impedance . . . 37

3.6.1 5 kVA Transformer . . . 39

3.7 Non-GIC Events . . . 42

3.7.1 5 kVA Transformer . . . 43

3.8 Summary . . . 45

4 Analysis of Harmonic Distortion Due to GIC in Autotransformers 46

4.1 General . . . 46

4.2 Test Autotransformers 47
4.3 Harmonics due to a GIC Flow in Autotransformers 48
4.3.1 5 kVA Autotransformer 48
4.3.2 35 kVA Autotransformer 50
4.4 Effect of the Loading Level 54
4.4.1 5 kVA Autotransformer 54
4.4.2 35 kVA Autotransformer 57
4.5 Non-GIC Events 58
4.5.1 5 kVA Autotransformer 58
4.5.2 35 kVA Autotransformer 61
4.6 Summary 63

5 Conclusion **64**
5.1 Summary 64
5.2 Conclusions 65
5.3 Contributions 66
5.4 Future Works 67

References **68**

A 35 kVA Power Transformer Results **75**
A.1 Harmonics Due to a GIC Flow 75
A.2 Effect of the Loading Level 78
A.3 Effect of the Grounding Impedance 81
A.4 Non-GIC Events 84

Vita

List of Tables

3.1 Specifications of the Laboratory Power Transformers 30

4.1 Specifications of the Laboratory Autotransformers 47

List of Figures

1.1 Effect of dc flux, resulting in half-cycle saturation, compared to normal operation. 3

1.2 A typical differential protection scheme. 8

2.1 A linearized approximation of a transformer saturation curve experiencing a dc flux [3], [47]. 15

2.2 A per-phase equivalent circuit of a 3ϕ power transformer 15

2.3 Effect of GIC level on harmonics in power transformers. 19

2.4 A per-phase equivalent circuit of a 3ϕ Y-connected autotransformer. . 19

2.5 A per-phase equivalent circuit of a 3ϕ, Y-connected autotransformer with electrical coupling components [48]. 20

2.6 A simplified per-phase equivalent circuit of a 3ϕ, Y-connected autotransformer with GIC. 21

2.7 Effect of GIC level on harmonics in autotransformers. 23

2.8 Effect of loading level on harmonics due to GIC flows in power transformers [42]. 27

3.1 A schematic of the test system used for the GIC tests with the power transformers. 31

3.2 Primary side current waveforms showing the distortion caused by GIC in the 5 kVA power transformer. 33

3.3 Secondary-side voltage waveforms showing the distortion caused by GIC in the 5 kVA power transformer. 33

3.4 Calculated harmonics for the voltages and currents caused by GIC in the 5 kVA power transformer as: a) DC Component; b) Fundamental Component; c) 2^{nd} Harmonic Component; d) 3^{rd} Harmonic Component; e) 4^{th} Harmonic Component; f) 5^{th} Harmonic Component; g) 6^{th} Harmonic Component; and h) 7^{th} Harmonic Component. 35

3.5 Calculated THD for the current and voltage and power/reactive power for the 5 kVA power transformer: a) THD for the current and voltage, and b) Calculated power and reactive power. 36

3.6 Primary side current waveforms showing the distortion caused by I_{GIC} = 12 A in the 5 kVA power transformer for each load level. 36

3.7 Calculated harmonics for the currents caused by GIC in the 5 kVA power transformer for each load level as: a) DC Component; b) Fundamental Component; c) 2^{nd} Harmonic Component; d) 3^{rd} Harmonic Component; e) 4^{th} Harmonic Component; f) 5^{th} Harmonic Component; g) 6^{th} Harmonic Component; and h) 7^{th} Harmonic Component. 38

3.8 Calculated THD for the current and reactive power for the 5 kVA power transformer at each loading level: a) THD for the current, and b) Calculated reactive power. 39

3.9 Primary side current waveforms showing the distortion caused by I_{GIC} = 12 A in the 5 kVA power transformer for each grounding system tested. 40

3.10 Calculated harmonics for the currents caused by GIC in the 5 kVA power transformer for each grounding type used as: a) DC Component; b) Fundamental Component; c) 2nd Harmonic Component; d) 3rd Harmonic Component; e) 4th Harmonic Component; f) 5th Harmonic Component; g) 6th Harmonic Component; and h) 7th Harmonic Component. 41
3.11 Calculated THD for the current and reactive power for the 5 kVA power transformer for each grounding type: a) THD for the current, and b) Calculated reactive power. 42
3.12 Primary side current waveforms showing the distortion caused for each test case for a 5 kVA power transformer at a load level of 100%. . . . 44
3.13 A comparison of the 2nd harmonic ratio for each event for the 5 kVA power transformer. 45

4.1 A schematic of the test diagram used for the GIC tests with the Y-Y autotransformers [43]. 48
4.2 Primary side current waveforms showing the distortion caused by GIC in the 5 kVA autotransformer. 49
4.3 Secondary-side voltage waveforms showing the distortion caused by GIC in the 5 kVA autotransformer. 49
4.4 Calculated harmonics for the voltages and currents caused by GIC in the 5 kVA autotransformer as: a) DC Component; b) Fundamental Component; c) 2nd Harmonic Component; d) 3rd Harmonic Component; e) 4th Harmonic Component; f) 5th Harmonic Component; g) 6th Harmonic Component; and h) 7th Harmonic Component. 51
4.5 Calculated THD for the current and voltage and power/reactive power for the 5 kVA autotransformer: a) THD for the current and voltage, and b) Calculated power and reactive power. 52

4.6 Primary side current waveforms showing the distortion caused by GIC in the 35 kVA autotransformer. 52
4.7 Secondary-side voltage waveforms showing the distortion caused by GIC in the 35 kVA autotransformer. 52
4.8 Calculated harmonics for the voltages and currents caused by GIC in the 35 kVA autotransformer as: a) DC Component; b) Fundamental Component; c) 2^{nd} Harmonic Component; d) 3^{rd} Harmonic Component; e) 4^{th} Harmonic Component; f) 5^{th} Harmonic Component; g) 6^{th} Harmonic Component; and h) 7^{th} Harmonic Component. 53
4.9 Calculated THD for the current and voltage and power/reactive power for the 35 kVA autotransformer: a) THD for the current and voltage, and b) Calculated power and reactive power. 54
4.10 Primary side current waveforms showing the distortion caused by I_{GIC} = 16 A in the 5 kVA autotransformer for each load level. 55
4.11 Calculated harmonics for the currents caused by GIC in the 5 kVA autotransformer for each load level as: a) DC Component; b) Fundamental Component; c) 2^{nd} Harmonic Component; d) 3^{rd} Harmonic Component; e) 4^{th} Harmonic Component; f) 5^{th} Harmonic Component; g) 6^{th} Harmonic Component; and h) 7^{th} Harmonic Component 56
4.12 Calculated THD for the current and reactive power for the 5 kVA autotransformer at each loading level: a) THD for the current, and b) Calculated reactive power. 57
4.13 Primary side current waveforms showing the distortion for $I_{GIC} = 30$ A in the 35 kVA autotransformer for each load level. 57

4.14 Calculated harmonics for the currents caused by GIC in the 35 kVA autotransformer for each load level as: a) DC Component; b) Fundamental Component; c) 2nd Harmonic Component; d) 3rd Harmonic Component; e) 4th Harmonic Component; f) 5th Harmonic Component; g) 6th Harmonic Component; and h) 7th Harmonic Component. 59

4.15 Calculated THD for the current and reactive power for the 35 kVA autotransformer at each loading level: a) THD for the current, and b) Calculated reactive power. 60

4.16 Primary side current waveforms showing the distortion caused by each test case for a 5 kVA autotransformer at a load level of 100%. 60

4.17 A comparison of the 2nd harmonic ratio for each event for a 5 kVA autotransformer. 61

4.18 Primary side current waveforms showing the distortion caused by each test case for a 35 kVA autotransformer at a load level of 12%. 62

4.19 A comparison of the 2nd harmonic ratio for each event for a 35 kVA 3-limb autotransformer. 63

A.1 Primary side current waveforms showing the distortion caused by GIC in the 35 kVA power transformer. 76

A.2 Secondary-side voltage waveforms showing the distortion caused by GIC in the 35 kVA power transformer. 76

A.3 Calculated harmonics for the voltages and currents caused by GIC in the 35 kVA power transformer as: a) DC Component; b) Fundamental Component; c) 2nd Harmonic Component; d) 3rd Harmonic Component; e) 4th Harmonic Component; f) 5th Harmonic Component; g) 6th Harmonic Component; and h) 7th Harmonic Component. 77

A.4 Calculated THD for the current and voltage and power/reactive power for the 35 kVA power transformer: a) THD for the current and voltage, and b) Calculated power and reactive power. 78

A.5 Primary side current waveforms showing the distortion for $I_{GIC} = 30$ A in the 35 kVA power transformer for each load level. 79

A.6 Calculated harmonics for the currents caused by GIC in the 35 kVA power transformer for each load level as: a) DC Component; b) Fundamental Component; c) 2^{nd} Harmonic Component; d) 3^{rd} Harmonic Component; e) 4^{th} Harmonic Component; f) 5^{th} Harmonic Component; g) 6^{th} Harmonic Component; and h) 7^{th} Harmonic Component. 80

A.7 Calculated THD for the current and reactive power for the 35 kVA power transformer at each loading level: a) THD for the current, and b) Calculated reactive power. 81

A.8 Primary side current waveforms showing the distortion caused by I_{GIC} = 12 A in the 35 kVA power transformer for each grounding system tested. 82

A.9 Calculated harmonics for the currents caused by GIC in the 35 kVA power transformer for each grounding type used as: a) DC Component; b) Fundamental Component; c) 2^{nd} Harmonic Component; d) 3^{rd} Harmonic Component; e) 4^{th} Harmonic Component; f) 5^{th} Harmonic Component; g) 6^{th} Harmonic Component; and h) 7^{th} Harmonic Component. 83

A.10 Calculated THD for the curren and reactive power for the 35 kVA power transformer for each grounding type: a) THD for the current, and b) Calculated reactive power. 84

A.11 Primary side current waveforms showing the distortion caused by each test case for a 35 kVA power transformer at a load level of 12%. . . . 85
A.12 A comparison of the 2nd harmonic ratio for each event for the 35 kVA power transformer. 85

Chapter 1

Introduction

1.1 General

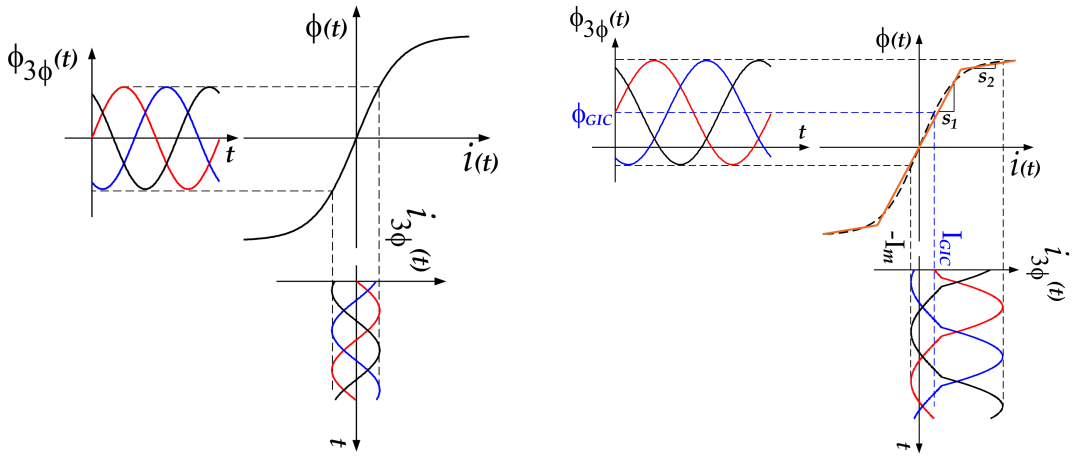
One of the fundamental objectives of any power system is to ensure safe, reliable, and cost-efficient delivery of electric power to its loads. Such a fundamental objective is achieved both through design (of power system components) and operation procedures (control, protection, etc.). Among many design practices in power systems are the grounding systems, where the neutral point of Y-connected power transformers and generators are connected to the system grounding through a grounding impedance. This grounding design allows for a safe path for currents during fault events. The selection of a grounding impedance is typically dependent on power system ratings (power and voltage), ground capacity, protection system, etc. The ground connection, however, leaves a power transformer vulnerable to quasi-dc currents triggered by geomagnetic disturbances (GMDs). Geomagnetically induced currents (GICs) can cause severe operational disruptions, damage to power system components, and have an adverse impact on its stability.

1.2 Motivation

The presence of GIC in power transformers can result in harmonic distortion, increased reactive power consumption, and overheating of the transformer. The harmonic distortion can result in the tripping off of transmission lines and power system components, while the reactive power consumption can impact power system stability and reliability. A GIC flow can be blocked by using a series capacitor in the grounding circuit. However, practices for grounding system design may then not be met. In addition, the accurate and fast detection of a GIC allows for an effective response that can prevent the adverse impact of GIC flows on power systems. The simple and non-intrusive detection and identification of a GIC flow can be achieved by introducing a signature, which can be extracted from differential 3ϕ currents. The development, implementation, and verification of such a signature is the main motivation of this research work.

1.3 Literature review

In general, GMDs are caused by the interaction between solar weather and earth's magnetic field. Solar flares and coronal mass ejections can eject charged particles. When these charged particles interact with the earth's magnetic field, they can cause an increase in the strength of high-altitude electrojets. These electrojets interact with the earth's surface, generating potential differences across different areas. When transformers with grounded neutral points are connected across these potential differences, the grounding connections provide a path for GIC flows into the power system [1], [2].



(a) Normal Operation

(b) Operation under dc bias

Figure 1.1: Effect of dc flux, resulting in half-cycle saturation, compared to normal operation.

1.3.1 Effects of GIC

The GIC, a quasi-dc current, can have significant effects on transmission systems, power transformers, shunt devices, generating units, loads, and protective devices. When a GIC flows through a transformer grounding circuit, the magnetic flux in the transformer core will have a large dc component. This dc flux component causes a half-cycle saturation of the magnetic core, as illustrated in Figure 1.1 [3]. During the normal operation, a transformer core stays within the linear region of its B-H curve. In the presence of GIC (and its associated dc flux), the dc flux pushes the transformer core past the knee point of its B-H curve (only during the positive half-cycle of the magnetizing current). As a result, significant distortion takes place in the magnetizing currents, as well as the 3ϕ currents flowing in the grounded windings of the affected transformer [1], [3].

The resulting harmonics can damage or disrupt the power system. Known effects include [1], [3]–[7]:

- Tripping of static var compensators and capacitor banks;
- Tripping of power electronic converters, such as high voltage direct current

(HVDC) links, battery storage devices, and renewable intermittent sources;

- Tripping of protection devices, both correctly and erroneously;
- Tripping of transmission lines; and
- Overheating of transformers.

The increase in reactive power consumption can result in voltage drops if there are inadequate reactive power reserves [1]. The combination of a dc current flow and current harmonics can result in overheating of the transformer, which can cause damage, as was the case during the 1989 geomagnetic storm that resulted in the failure of the Quebec power system. During that event, several transformers suffered damage to their windings [8]. Further research indicates that overheating may only be a problem for older transformers and may not be significant for most transformers due to the short duration of peak GIC flow [8], [9]. This indicates that the main threat of GICs is the resulting harmonics and the instability it can cause on the power system.

Research has shown certain core topologies to be more vulnerable to GICs than others. 3ϕ multi-core transformers, with three separate single-phase cores, and five-limb 3ϕ cores have low reluctance paths for dc flux, making them more susceptible to saturation [1], [10], [11]. 3ϕ three-limb cores present a high reluctance path for dc flow, reducing the effects of GIC flows but presenting an increased risk of overheating [1], [3]. Additionally, core topology has an effect on the harmonics generated from GICs. In 3ϕ bank transformers, the harmonics tend to be the same in each phase while in 3ϕ three- and five-limb transformers, differences exist between phase B and the other phases due to the magnetic coupling that exists between the different phases [1], [10], [12], [13].

1.3.2 Management of GIC

There exist a variety of methods to block or manage the flow of GICs into the transformer neutral, including both passive and active protection devices. Passive devices include a neutral point capacitor with a form of overvoltage protection [14], [15], neutral point reactors [16], and neutral point reactors with series capacitors [17]. Active protection devices are often capacitive blocking devices with unique detection and switching methods such as fuzzy logic controllers [18], [19], but can include switching devices that intermittently block the GIC flow [20]. Any neutral-based method will require widespread application to be effective on the power system due to the presence of autotransformers. Autotransformers, lacking electrical isolation, can allow GIC to flow through part of their windings regardless of the presence of neutral-blocking devices if there is an alternate path through the neutrals of other transformers in the system [21].

Other methods exist to manage GIC flow, including the use of a current source on transformer auxiliary windings to counter the half-cycle saturation [22], adjusting the configuration of the transmission system to reduce the overall amount of GIC [23], and the use of dc diverting transformers on overhead lines [24].

1.3.3 Other Sources of Harmonics

In addition to GIC, current harmonics are caused by a variety of sources. Faults, overexcitation, and transformer energization can generate harmonics due to transformer saturation [25]. Overexcitation, where the voltage is increased above the nominal voltage of the transformer, can result in saturation that generates exclusively odd harmonics, such as the third and fifth harmonic. This is due to the saturation occurring in both parts of the cycle, rather than the half-cycle saturation that is common for GIC events [25], [26]. Inrush currents, caused by transformer energization, can be very large, but are comprised largely of even harmonics [25],

[27]. However, the exact values of the inrush currents are difficult to predict due to their dependence on remnant flux and location that they occur in the voltage cycle [27].

Harmonics can also be generated externally, due to non-linear loads and HVDC systems. The harmonics generated by HVDC systems depend on their design and topology. However, the 11^{th} and 13^{th} harmonics are often generated by HVDC systems, in addition to high order harmonics [28]. These often have dedicated filters to minimize their effects on the rest of the system, reducing their effect on detecting GIC.

1.3.4 Detection of GIC

There exist a number of methods to detect GIC in the power system. The most basic method is simply to monitor the grounding point of transformers for a dc current. A more advanced version of this involves monitoring for the dc current flow on the 3ϕ system itself [29], or monitoring for a dc voltage drop across a portion of the line [30].

Taking advantage of the effects that GIC has on the system, symptoms based monitoring methods are possible. As previously discussed, GIC will cause an increased demand for reactive power. This reactive power demand has been used a method of detecting and quantifying GIC in transformers [31], [32]. Additionally, the harmonic signature of GIC can be used. The presence of 2^{nd} harmonic distortion has been shown to be an effective indicator of the presence of GIC, with a sustained 2^{nd} harmonic differentiating it from other power system events [33]–[35]. An alternative method of detection based on the 2^{nd} harmonic involves differentiating it by examining the sequence of the 2^{nd} harmonic components of each phase, with a GIC event having negative sequence components [36]. Examining the shape of the 3ϕ currents can also indicate the presence of GIC, with the waveforms having asym-

metric distortion [37]. The previous two detection method can also be combined for increased accuracy [38].

Machine learning has also been incorporated into GIC detection, being used alongside wavelet transformations to detect the presence of GIC [39]. It has also been used to detect GIC using both the reactive power and presence of even harmonics as indicators [40].

1.3.5 Transformer Protection

There exist many tools to detect faults and issues with transformers and engage protection methods. While there are tools that detect faults through mechanical methods (pressure relays, gas accumulation/detection, temperature rise detection, etc.), electrical detection methods allow for more precise operation of protection, including restraint conditions to prevent erroneous tripping [25]. Electrical fault detection uses current transformers (CTs) to monitor the currents of the transformer, and can include overcurrent and differential protection. Overcurrent protection, particularly instantaneous overcurrent protection, offers fast response to serious faults. Differential protection offers more adjustable protection in the form of percentage differential protection. A typical differential protection scheme can be seen in Figure 1.2. CTs on each phase measure the phase currents. The CTs all share the same rating, with the microprocessor-based controller accounting for any differences in current due to phase shift or transformer ratio. The differential current for each phase n, I_{Opn}, is determined by the difference between the primary and secondary current, as:

$$I_{Opn} = I_{norm1n} - I_{norm2n} \tag{1.1}$$

where I_{norm1n} and I_{norm2n} are the primary and secondary currents for each phase n, normalized to account for the transformer ratio and phase shift [25].

This form of protection activates when the differential current exceeds a cer-

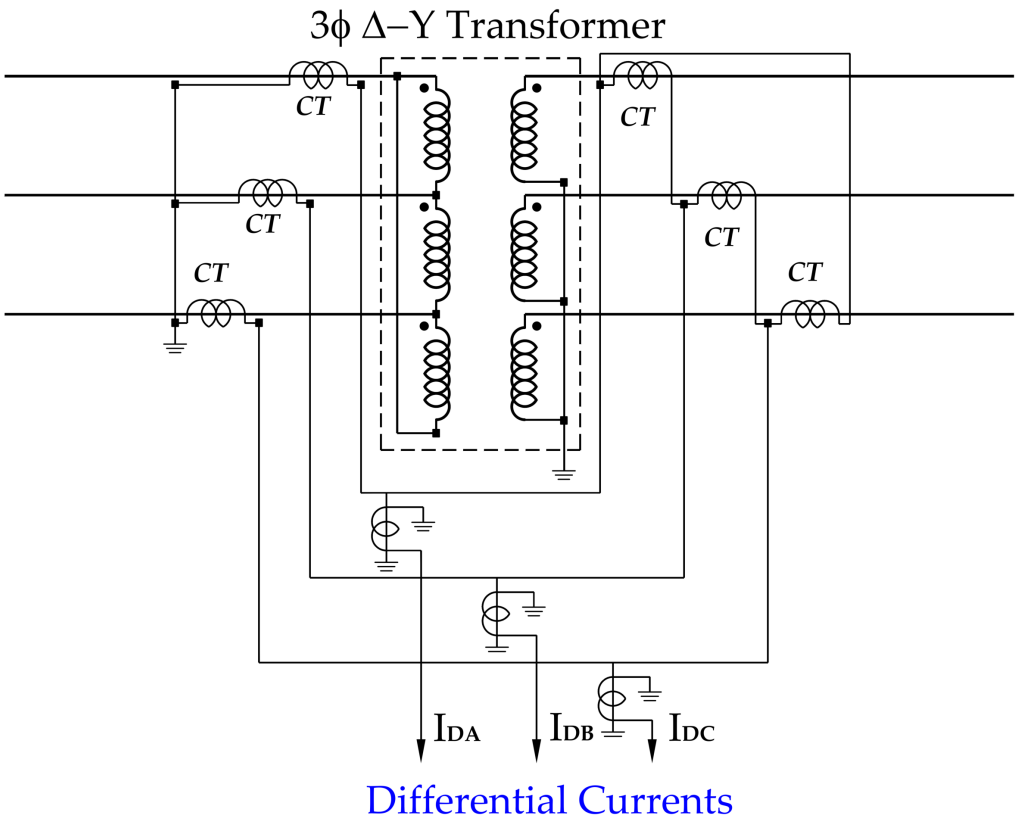


Figure 1.2: A typical differential protection scheme.

tain percentage of a restraining current. This restraining current can be calculated as:

$$I_{res} = k(|I_{w1}| + |I_{w2}|) \tag{1.2}$$

where I_{w1} is the primary winding current, I_{w2} is the secondary winding current, I_{Res} is the restraining current, and k is a constant of proportionality (usually 0.5 or 1) [25].

To prevent tripping, a number of restraining schemes can be used. Even-harmonic restraint and 2^{nd}-harmonic restraint are used to prevent tripping during transformer inrush by preventing the operation of protection relays if the percentage of certain harmonics is too high. This can be calculated as:

$$I_{Op} > s_{res}|I_{res}| + k_{harm}|I_{harm}| + ... \tag{1.3}$$

where I_{Op} is the fundamental of the differential current, s_{res} is the slope of the restraining curve, I_{res} is the restraining current, k_{harm} is a weighting factor for each harmonic, and I_{harm} is the harmonic component of the differential current being examined for the restraint [25]. Even-harmonic restraint can be more reliable, in the case of a low 2^{nd}-order harmonic.

To prevent tripping in the case of an overvoltage, the fifth harmonic is used as signature. As the third harmonic can be reduced due to the presence of a delta winding, overvoltage restraint is based on the fifth harmonic. This is often combined with 2^{nd} harmonic restraint to prevent tripping due to both inrush conditions and overvoltage [25].

1.3.5.1 Processing Unbalanced Signals

Inrush events produce different levels of harmonics depending on where in the voltage cycle the inrush occurs. Additionally, depending on core topology, the harmonics caused by GIC in each phase will be different [10], [13]. To account for this difference, the three phases can be processed in a variety of ways. These include engaging protection if any of the phases exceed the restraining current, if all the phases exceed the restraining current, if two or more phases exceed the restraining current, or if the average of the phases exceeds the restraining current. This last method provides a robust approach that is more reliable than other methods of restraint [27].

1.4 Second Harmonic Based Method to Detect GIC Flows

The previous review has identified several methods to detect a GIC flow in a power transformer. The majority of existing methods are based on a direct measurement of the ground current to detect the presence of a GIC. Despite their simplicity, these

methods require the use of a dc current measurement that can be expensive and may create complications for power system grounding design. Other methods require the measurement of reactive power flow through a power transformer. These methods can suffer inaccuracy due to the dependence on the reactive power demand on the secondary side of a power transformer. Pattern recognition, data-driven models, and magnetic circuit models have been proposed to detect and identify a GIC flow in power transformers. These methods require significant data for training, have to be developed for each transformer (can not be generalized), and may depend on approximated models.

The analysis of impacts created by a GIC flow (presented in Chapter 3 and Chapter 4) shows that harmonic components are triggered by a GIC flow in a power transformer [3], [35], [41]–[44]. Such harmonic components are created in the 3ϕ currents of the grounded windings in a power transformer, thus their strong presence in the transformer differential currents. The harmonic analysis of the 3ϕ differential currents in a power transformer, during a GIC flow, shows that the second harmonic dominates all induced harmonic components by a GIC flow. This thesis proposes the use of the second harmonic component extracted from the 3ϕ differential currents as a signature of a GIC flow in a power transformer. The proposed approached can be quantified as a ratio of the second harmonic to the fundamental component as:

$$R2 = \frac{I_{D2}}{I_{D1}} = \frac{(I_{D2})_A + (I_{D2})_B + (I_{D2})_C}{(I_{D1})_A + (I_{D1})_B + (I_{D1})_C} \tag{1.4}$$

If the ratio is above a predetermined value, GIC may be present. The specific magnitude of the ratio depends on the transmission system design and voltage level. Additional consideration should be given to designating a level that limits operation to dangerous levels of GIC, minimizing needless operation. The magnitude of the 2^{nd} harmonic should not exceed 1.5% for an extended period of time on systems above 169 kV [45]. The test results of several GIC flows in power transformers

under different loading conditions and grounding impedance values indicated that the ratio $R2$ remains above 45% for the tested transformers. Examples of $R2$ for non-GIC events on the same transformers are:

- Normal load changes: $R2 \leq 10\%$;
- Line-to-ground fault: $R2 \leq 10\%$;
- Line-to-fault fault: $R2 \leq 5\%$;
- Transformer energization: $R2 \leq 37\%$;

To distinguish a GIC event from transformer energization, which may have a similar high 2^{nd} harmonic component, the protection should not operate until a certain amount of time has passed. The time must exceed the expected decay time of inrush events, which can depend heavily on the transformer design. At a minimum, this time restraint should last several cycles, but should not exceed three seconds [45].

1.5 Thesis Objective

The literature review has identified the half-cycle magnetic saturation as one of the direct effects of a GIC flow in a power transformer. This type of magnetic saturation induces even harmonic components in the transformer magnetizing currents, which affects the harmonic contents of the 3ϕ differential currents of a power transformer. The use of 2^{nd} harmonic components extracted from the 3ϕ differential currents as a signature for a GIC flow is the main focus of thesis. The objectives of this thesis can be summarized as:

- to perform harmonic analysis of differential currents under different levels of GIC flows;

- to assess possible impacts of the core type and transformer configuration on the harmonic components triggered by a GIC flow;
- to examine possible impacts of the transformer loading levels on the harmonic components triggered by a GIC flow; and
- to investigate possible impacts of the transformer grounding design on the harmonic components triggered by a GIC flow.

1.6 Thesis Outline

This thesis is composed of the following chapters:

- Chapter 2 reviews models for the magnetic core of a power transformer, especially during a GIC flow. This chapter also discusses the effects of the loading level and grounding impedance on the magnetic core models.
- Chapter 3 presents experimental test results obtained from laboratory power transformers during different levels of GIC flows, grounding impedances, and loading levels. Moreover, Chapter 3 provides a comparison between the harmonic distortion due to GIC flows and the harmonic distortions created by other non-GIC events.
- Chapter 4 expands on the work of Chapter 3, and presents experimental test results obtained from several laboratory power autotransformers during different levels of GIC flows and loading levels. It also provides a comparison between the harmonic distortion due to GIC flows and the harmonic distortions created by other non-GIC events in autotransformers.
- Chapter 5 summarizes the work done, provides conclusions, and lists the contributions made by this thesis. In addition, Chapter 5 suggests avenues for future works.

Chapter 2

Transformer and GIC Saturation Modelling

2.1 General

Power transformers are key components in any power system, where they provide connections between voltages zones, electrical isolation between certain power system parts, points-for-ground connections, etc. Due to physical limitations of the transformer magnetic core, high levels of excitation can initiate a magnetic saturation of the core triggering non-linearities in the magnetizing currents. The modeling of such cases require connecting the electrical excitation and the magnetic flux generated. The fundamental relationship between the induced voltage and magnetic flux (induced by magnetizing currents) can be stated using Faraday's law as [46]:

$$v(t) = -N\frac{d\phi}{dt} \tag{2.1}$$

where $v(t)$ is the induced voltage, N is the number of turns linked by the flux ϕ, and $\Delta\Phi/\Delta t$ is the time-varying magnetic field.

In the case of a GIC flow, the magnetic flux in a power transformer core has

a dc component induced by the quasi-dc GIC. This chapter discusses the modeling of a power transformer core during normal and GIC flow conditions. The presented models focus on the distortion created in the magnetizing currents due to a GIC flow.

2.2 Modelling Transformer Saturation

In general, any magnetic material (including the core of any power transformer) is characterized by its $B-H$ hysteresis curve. Such a curve is meant to identify levels of magnetic flux handled by a magnetic material without saturation. Figure 2.1 provides an example for a magnetic core in a 3ϕ power transformer. The portion with slope s_1 is the linear region and portions with slope s_2 are regions of magnetic saturation. When the core of a power transformer experiences a large flux, it gets pushed into the saturation region. As a result, the 3ϕ magnetizing currents get distorted with harmonic components. In order to model such a non-linear core behavior, the $B-H$ hysteresis curve is linearized as shown by the orange piecewise curves. There are two main types of magnetic saturation experienced by the core of a power transformer. These types are:

i. Symmetrical saturation, where the magnetic flux increases significantly without any dc bias. Internal faults and over-excitation are most causes for this type of magnetic saturation. The symmetrical saturation induces odd harmonics in the magnetizing currents.

ii. Asymmetrical saturation (half-cycle), where the magnetic flux increases significantly with a large dc component. GIC flows are the cause of most of this type of magnetic saturation. The half-cycle saturation induces even harmonics in the magnetizing currents [1], [3].

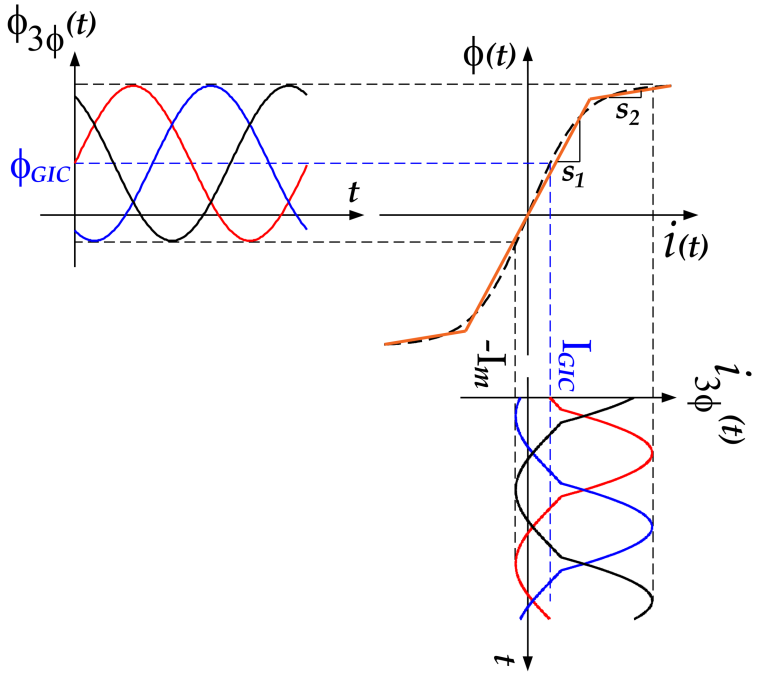


Figure 2.1: A linearized approximation of a transformer saturation curve experiencing a dc flux [3], [47].

2.2.1 Standard Transformer Wiring

Figure 2.2 shows a per-phase conventional circuit-based model of a 3ϕ power transformer. Asymmetrical magnetic saturation affects the magnetizing current i_m of each phase. The 3ϕ magnetizing currents of a 3ϕ power transformer can be stated during steady-state as [1], [3], [4]:

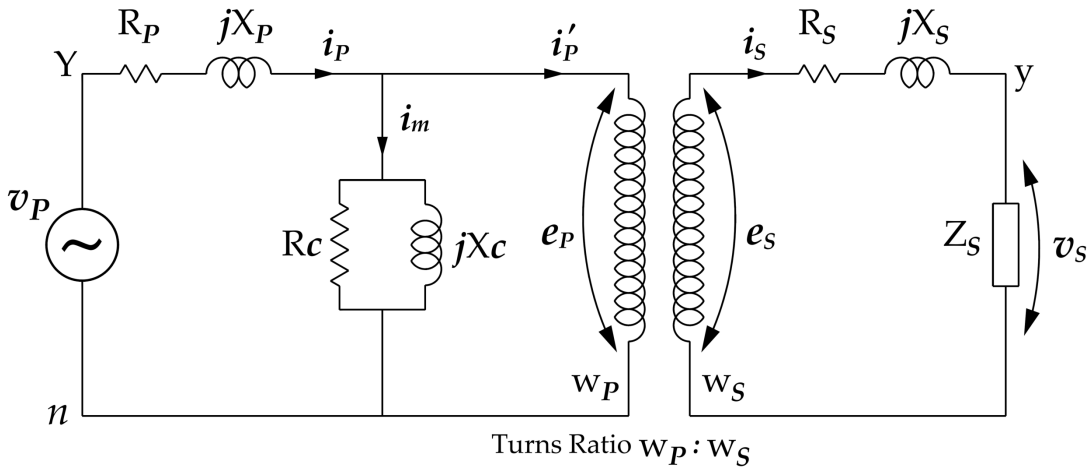


Figure 2.2: A per-phase equivalent circuit of a 3ϕ power transformer

$$i_{ma}(t) = I_m \sin(\omega_s t + \theta) \tag{2.2}$$

$$i_{mb}(t) = I_m \sin\left(\omega_s t + \theta - \frac{2\pi}{3}\right) \tag{2.3}$$

$$i_{mc}(t) = I_m \sin\left(\omega_s t + \theta + \frac{2\pi}{3}\right) \tag{2.4}$$

where I_m is the peak value of the magnetizing current, $\omega_s = 2\pi f_s$ with f_s being the supply frequency, and θ is the phase angle of the magnetizing current in each phase. To account for the effects of GIC, the equations can be altered as [3], [32]:

$$(i_{ma}(t))_G = I_m \sin(\omega_s t + \theta) + I_{GIC} + i_{ad}(t) \tag{2.5}$$

$$(i_{mb}(t))_G = I_m \sin\left(\omega_s t + \theta - \frac{2\pi}{3}\right) + I_{GIC} + i_{bd}(t) \tag{2.6}$$

$$(i_{mc}(t))_G = I_m \sin\left(\omega_s t + \theta + \frac{2\pi}{3}\right) + I_{GIC} + i_{cd}(t) \tag{2.7}$$

where I_{GIC} is the GIC flow and $i_{ad}(t)$, $i_{bd}(t)$, and $i_{cd}(t)$ are distorted components in the magnetizing currents caused by I_{GIC}. These distorted components depend on the core saturation characteristics and level of GIC as:

$$i_{ad}(t) = \begin{cases} k_1 I_m (\sin(\omega_s t + \theta) + k_2) & \beta \leq \omega_s t \leq \pi - \beta \\ 0 & \text{Otherwise} \end{cases} \tag{2.8}$$

$$i_{bd}(t) = \begin{cases} k_1 I_m (\sin(\omega_s t + \theta_b) + k_2) & \beta_b \leq \omega_s t \leq \pi - \beta_b \\ 0 & \text{Otherwise} \end{cases} \tag{2.9}$$

$$i_{bd}(t) = \begin{cases} k_1 I_m (\sin(\omega_s t + \theta_c) + k_2) & \beta_c \leq \omega_s t \leq \pi - \beta_c \\ 0 & \text{Otherwise} \end{cases} \tag{2.10}$$

where β, β_b, β_c, θ_b, and θ_c, are:

$$\beta = \sin^{-1}\left(\frac{I_{GIC}}{I_m}\right) \tag{2.11}$$

$$\beta_b = \beta + \frac{2\pi}{3} \text{ and } \beta_c = \beta + \frac{4\pi}{3} \tag{2.12}$$

$$\theta_b = \theta - \frac{2\pi}{3} \text{ and } \theta_c = \theta + \frac{2\pi}{3} \tag{2.13}$$

and constants k_1 and k_2 are:

$$k_1 = \frac{s_1}{s_2} - 1 \tag{2.14}$$

$$k_2 = \frac{I_{GIC}}{I_m} \tag{2.15}$$

where s_1 and s_2 are the slopes shown in Figure 2.1.

Remarks for (2.5) to (2.7):

- There are negligible hysteresis effects.
- The magnetic coupling between phases is negligible.
- There are no transient conditions (such as magnetizing inrush).
- The magnetizing currents are periodic and stationary.
- The saturation curve can be approximated as piece-wise and linear.

2.2.1.1 Harmonics

The harmonics caused by the distortion in the magnetizing currents can be extracted using Fourier analysis. These harmonic components can be calculated as [3], [32]:

- DC components:

$$i_{adc} = i_{bdc} = i_{cdc} = \frac{k_1 I_m}{2\pi}\left(2\cos(\beta) + k_1(\pi - 2\beta)\right) \tag{2.16}$$

- Fundamental components:

$$i_{ma1} = \frac{k_1 I_m}{\pi}\left(\frac{\pi}{2} - \beta - \frac{1}{2}\sin(2\beta)\right)\sin\left(\omega_s t\right) \tag{2.17}$$

$$i_{mb1} = \frac{k_1 I_m}{\pi}\left(\frac{\pi}{2} - \beta - \frac{1}{2}\sin(2\beta)\right)\sin\left(\omega_s t - \frac{2\pi}{3}\right) \tag{2.18}$$

$$i_{mc1} = \frac{k_1 I_m}{\pi}\left(\frac{\pi}{2} - \beta - \frac{1}{2}\sin(2\beta)\right)\sin\left(\omega_s t + \frac{2\pi}{3}\right) \tag{2.19}$$

- Harmonic components:

$$i_{mah} = \sum_{n=2}^{\infty} \lambda_n \sin\left(n\omega_s t - \gamma_n\right) \tag{2.20}$$

$$i_{mbh} = \sum_{n=2}^{\infty} \lambda_n \sin\left(n\omega_s t - \gamma_n - \frac{2\pi}{3}\right) \tag{2.21}$$

$$i_{mch} = \sum_{n=2}^{\infty} \lambda_n \sin\left(n\omega_s t - \gamma_n + \frac{2\pi}{3}\right) \tag{2.22}$$

where:

$$\lambda_n = \sqrt{a_n^2 + b_n^2} \tag{2.23}$$

$$\gamma_n = \tan^{-1}\left(\frac{b_n}{a_n}\right) \tag{2.24}$$

and where:

$$a_n = \frac{I_m k_1}{4n\pi}\left(n\pi - 2n\beta + \sin(n(2\beta - \pi))\right) \tag{2.25}$$

$$b_n = \frac{I_m k_1 k_2}{n\pi}\sin\left(n\left(\beta - \frac{\pi}{2}\right)\right). \tag{2.26}$$

The results of this analysis can be seen in Figure 2.3, where a series of plots show the impact of varying k_2, which directly relates to varying GIC. As GIC increases, the magnitude of the harmonics increases, while the order of magnitude does not change.

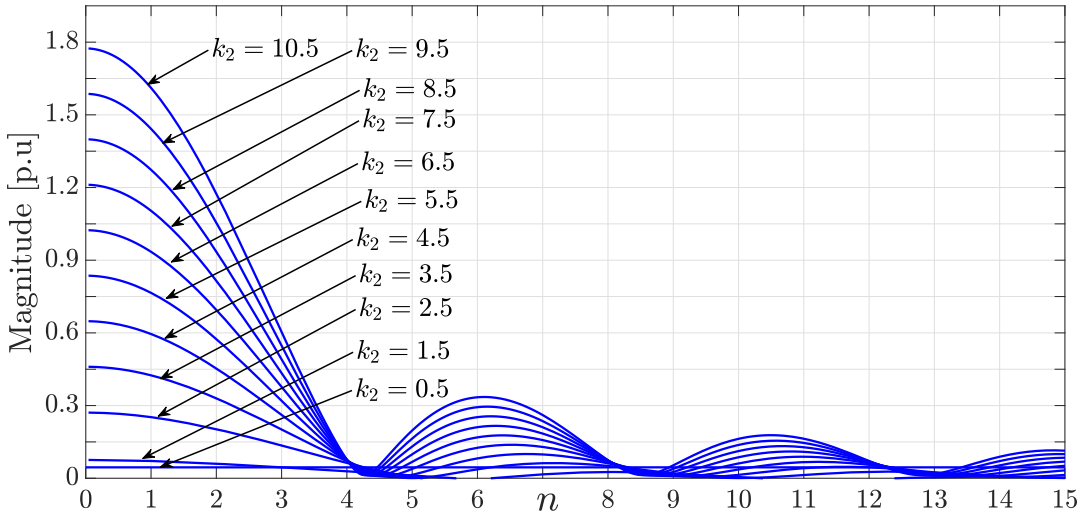


Figure 2.3: Effect of GIC level on harmonics in power transformers.

2.2.2 Autotransformer Wiring

Autotransformers are a popular model of transformer for use in the transmission system, as they can be less expensive to produce due to sharing part of the windings between the primary and secondary sides and requiring smaller cores. This shared winding removes the ability of the transformer to mitigate harmonics and provide electrical isolation, and introduces complexity into the modelling of the half-cycle saturation. Autotransformer saturation can be modelled similarly to a conventional power transformer, but the model first needs to be adjusted to account for the electrical coupling between the primary and secondary side. Figure 2.4 shows a per-phase autotransformer model.

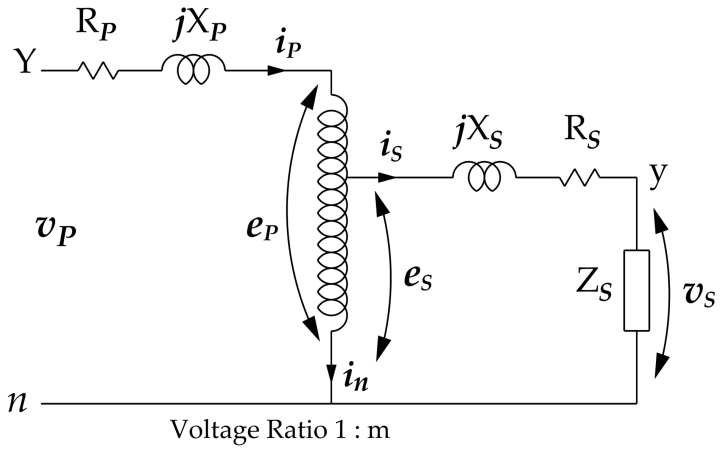


Figure 2.4: A per-phase equivalent circuit of a 3ϕ Y-connected autotransformer.

Figure 2.5 shows the per-phase equivalent circuit of an autotransformer [48], where:

$$w = \frac{w_P}{w_S}, \quad \text{and} \quad m = \frac{|\boldsymbol{v}_P|}{|\boldsymbol{v}_S|}$$

$$R'_S = w^2 R_S, \quad X'_S = w^2 X_S, \quad \text{and} \quad Z'_S = w^2 Z_S$$

$$\widehat{\boldsymbol{i}_S} = \frac{\boldsymbol{i}_S}{w}$$

$$\widehat{\boldsymbol{e}_S} = \boldsymbol{e}_S.w, \quad \widehat{\boldsymbol{v}_S} = \boldsymbol{v}_S.w, \quad \text{and} \quad \widehat{\boldsymbol{v}_P} = \boldsymbol{v}_P.w$$

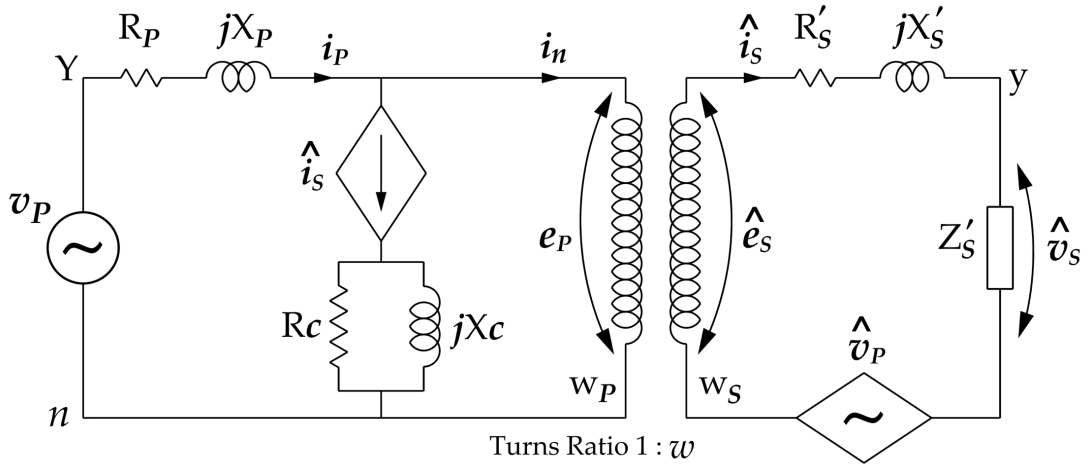


Figure 2.5: A per-phase equivalent circuit of a 3ϕ, Y-connected autotransformer with electrical coupling components [48].

The per-phase model presented in Figure 2.5 can be simplified by referring the secondary side to the primary, as with conventional transformers. With the simplified model, GIC can be accounted for by including it in the magnetizing path. This is shown in Figure 2.6.

The flux generated by the magnetizing current, with a GIC flow, can be shown as:

$$\lambda_m(t) = \lambda_{GIC} + \Lambda_m \sin\left(\omega_s t - \frac{\pi}{2}\right); \Lambda_m = \frac{V_P}{\omega_s . w_P} \tag{2.27}$$

where V_P is the peak value of primary side voltage, ω_s is the angular frequency of the applied ac voltage, w_P is the number of turns of the primary side windings, and

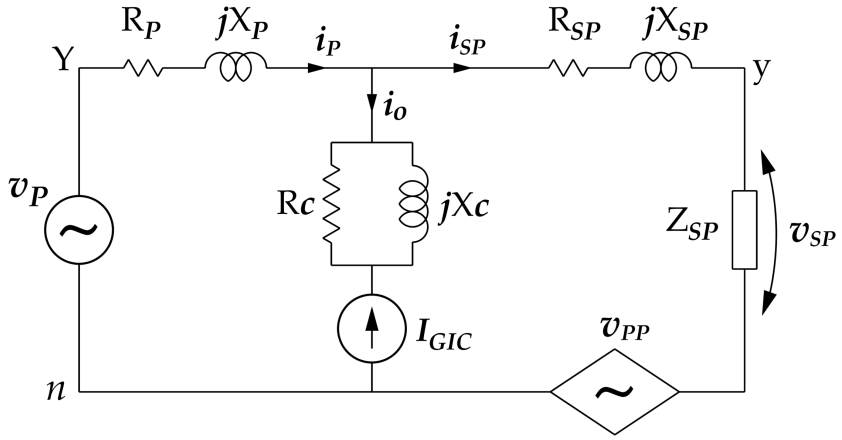


Figure 2.6: A simplified per-phase equivalent circuit of a 3ϕ, Y-connected autotransformer with GIC.

λ_{GIC} is the dc component in λ_m.

The following can be determined by examining Figure 2.6:

$$i_o = \boldsymbol{i}_P - \boldsymbol{i}_{SP} + I_{GIC} \tag{2.28}$$

$$\boldsymbol{v}_P = R_P(\boldsymbol{i}_P) + \frac{d\lambda_1}{dt} \tag{2.29}$$

$$\boldsymbol{v}_{SP} = -R_{SP}(\boldsymbol{i}_{SP}) + \frac{d\lambda_2}{dt} - \boldsymbol{v}_{PP} \tag{2.30}$$

where:

$$\lambda_1 = \lambda_m + L_P(\boldsymbol{i}_P) \approx \Lambda_1 \sin(\omega_s t + g_1) + \lambda_{1d}(t) \tag{2.31}$$

$$\lambda_2 = \lambda_m + L_{SP}(\boldsymbol{i}_{SP}) \approx \Lambda_2 \sin(\omega_s t + g_2) + \lambda_{2d}(t) \tag{2.32}$$

$$L_P = \frac{X_P}{\omega_s} \quad \text{and} \quad L_{SP} = \frac{X_{SP}}{\omega_s} \tag{2.33}$$

with Λ_1 and Λ_2 being the peak value of λ_1 and λ_2, g_1 and g_2 being the phase shift of λ_1 and λ_2, and λ_{1d} and λ_{2d} being non-linear components in λ_1 and λ_2 due to the GIC flow, respectively. Applying Kirchhoff's voltage law around the magnetizing circuit results in:

$$\frac{d\boldsymbol{\lambda}_m}{dt} = \frac{jR_c.X_c}{R_c + jX_c}(\boldsymbol{i}_o - I_{GIC}) \tag{2.34}$$

To simplify (2.34), let:

$$|\boldsymbol{Z}_c|\angle\vartheta = \frac{jR_c.X_c}{R_c + jX_c}$$

Taking the derivative of (2.27) results in:

$$\frac{d\boldsymbol{\lambda}_m}{dt} = \omega_s.\Lambda_m \sin(\omega_s t) \tag{2.35}$$

Substituting (2.35) into (2.34) in turn results in:

$$\boldsymbol{i}_o - I_{GIC} = \frac{\omega_s \Lambda_m}{\sqrt{2}|\boldsymbol{Z}_c|}\angle -\vartheta \tag{2.36}$$

Equation (2.36) can then be brought into the time-domain as:

$$i_o(t) = I_o \sin(\omega_s t - \vartheta) + I_{GIC} + i_d(t);\ I_o = \frac{\omega_s \Lambda_m}{|\boldsymbol{Z}_c|} \tag{2.37}$$

where I_o is the peak value of the magnetizing current, ϑ is the phase angle of the magnetizing current, and $i_d(t)$ is an additional component due to core non-linearity and hysteresis effects [3], [43].

2.2.2.1 Harmonics

Equation (2.37) is structured similarly to (2.5). The analysis that yielded (2.2) through (2.26) remains true, and these equations remain valid for the autotransformer, where:

$$I_m = I_o \tag{2.38}$$

Thus, the same analysis can be conducted to observe the harmonics generated by GIC. Figure 2.7 shows the effect of different levels of GIC on the harmonics induced in an autotransformer. As with the conventional power transformer, the magnitude

of the harmonics increases with I_{GIC}, but the overall order of harmonics remains the same. Additionally, there appears to be a reduction in the magnitude of harmonics relative to those of a conventional power transformer.

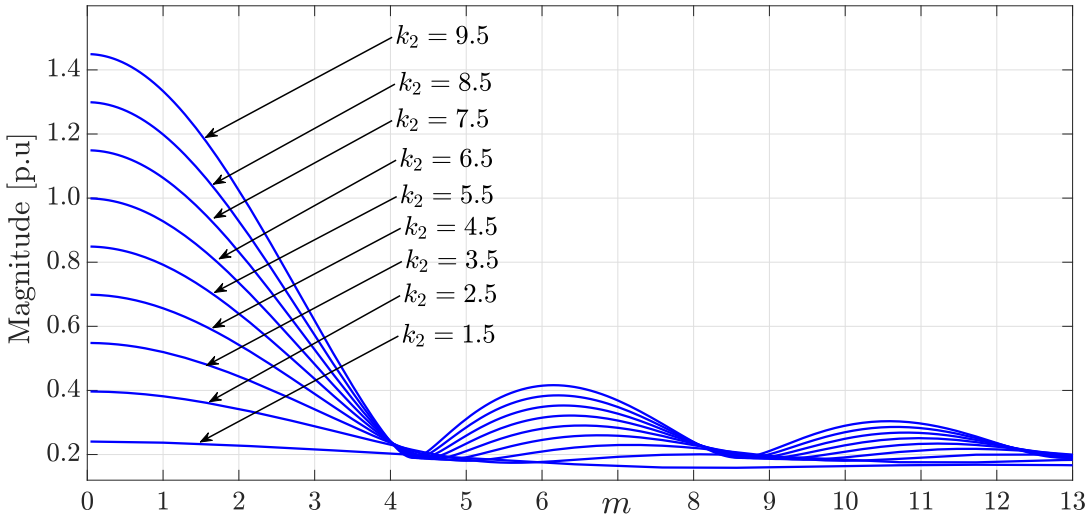


Figure 2.7: Effect of GIC level on harmonics in autotransformers.

2.2.3 Effect of the Loading Level

Prior analysis has not taken into account the transformer loading level, which can have an impact of the flux generated in the core of the transformer. Assuming a constant voltage level, the transformer loading directly relates to the primary current I_{pM}. The flux induced in a transformer can then be related to I_{pM} as:

$$\phi_A(t) = \frac{N_p}{\mathcal{R}_c} I_{pM} \sin\left(\omega_o t - \vartheta\right) \tag{2.39}$$

$$\phi_B(t) = \frac{N_p}{\mathcal{R}_c} I_{pM} \sin\left(\omega_o t - \vartheta - \frac{2\pi}{3}\right) \tag{2.40}$$

$$\phi_C(t) = \frac{N_p}{\mathcal{R}_c} I_{pM} \sin\left(\omega_o t - \vartheta + \frac{2\pi}{3}\right) \tag{2.41}$$

where N_p is the number turns of the primary side windings, $\mathcal{R}_c$ is the reluctance of the magnetic core, and ϑ is the phase angle of the primary side currents.

In turn, assuming no saturation, the fluxes can be related to the magnetizing

currents as [3]:

$$i_{za}(t) = I_Z \sin(\omega_o t - \vartheta) \tag{2.42}$$

$$i_{zb}(t) = I_Z \sin\left(\omega_o t - \vartheta - \frac{2\pi}{3}\right) \tag{2.43}$$

$$i_{zc}(t) = I_Z \sin\left(\omega_o t - \vartheta + \frac{2\pi}{3}\right) \tag{2.44}$$

where:

$$I_Z = \frac{I_{pM}.N_p}{s_1.\mathcal{R}_c} \tag{2.45}$$

where s_1 is the slope of the linearized saturation curve shown in Figure 2.1.

Equations (2.42) through (2.44) are a restatement of (2.2) through (2.4), accounting for the loading of the transformers. As with (2.2) through (2.4), the non-linearity introduced by a GIC flow can be accounted for, restating (2.5) through (2.7) as:

$$(i_{za}(t))_G = I_Z \sin(\omega_o t - \vartheta) + I_{GIC} + i_{ad}(t) \tag{2.46}$$

$$(i_{zb}(t))_G = I_Z \sin\left(\omega_o t - \vartheta - \frac{2\pi}{3}\right) + I_{GIC} + i_{bd}(t) \tag{2.47}$$

$$(i_{zc}(t))_G = I_Z \sin\left(\omega_o t - \vartheta + \frac{2\pi}{3}\right) + I_{GIC} + i_{cd}(t) \tag{2.48}$$

where I_{GIC} is the GIC current, and $i_{ad}(t)$, $i_{bd}(t)$, and $i_{cd}(t)$ are distorted components created by the core magnetic saturation. To account for the loading, (2.14) and (2.15) can be restated as:

$$c_1 = \frac{s_1}{s_2} - 1 \tag{2.49}$$

$$c_2 = \frac{I_G}{I_Z} \tag{2.50}$$

This in turn allows the restating of (2.8) through (2.10) as:

$$i_{ad}(t) = \begin{cases} c_1 I_Z \left(\sin\left(\omega_o t - \vartheta\right) + c_2\right) & \beta_a \leq \omega_o t \leq \pi - \beta_a \\ 0 & \text{Otherwise} \end{cases} \tag{2.51}$$

$$i_{bd}(t) = \begin{cases} c_1 I_Z \left(\sin\left(\omega_o t - \vartheta_b\right) + c_2\right) & \beta_b \leq \omega_o t \leq \pi - \beta_b \\ 0 & \text{Otherwise} \end{cases} \tag{2.52}$$

$$i_{cd}(t) = \begin{cases} c_1 I_Z \left(\sin\left(\omega_o t - \vartheta_c\right) + c_2\right) & \beta_c \leq \omega_o t \leq \pi - \beta_c \\ 0 & \text{Otherwise} \end{cases} \tag{2.53}$$

where the angles ϑ_b, ϑ_c, β, β_b and β_c are:

$$\vartheta_b = \vartheta - \frac{2\pi}{3} \text{ and } \vartheta_c = \vartheta + \frac{2\pi}{3} \tag{2.54}$$

$$\beta = \sin^{-1}\left(\frac{I_G}{I_Z}\right) \tag{2.55}$$

$$\beta_b = \beta + \frac{2\pi}{3} \text{ and } \beta_c = \beta + \frac{4\pi}{3} \tag{2.56}$$

2.2.3.1 Harmonics

As with the previous analyses, the magnetizing currents can be analysed using Fourier analysis to determine the harmonic content of the magnetizing current under load. Expanding on the work of Section 2.2.1.1, the harmonics can be stated as [3]:

- DC components:

$$i_{za0} = i_{zb0} = i_{zc0} = \frac{c_1 I_Z}{2\pi}\left(2\cos(\beta) + c_1(\pi - 2\beta)\right) \tag{2.57}$$

- Fundamental components:

$$i_{za1} = \frac{c_1 I_Z}{\pi}\left(\frac{\pi}{2} - \beta - \frac{1}{2}\sin(2\beta)\right)\sin\left(\omega_o t\right) \tag{2.58}$$

$$i_{zb1} = \frac{c_1 I_Z}{\pi}\left(\frac{\pi}{2} - \beta - \frac{1}{2}\sin(2\beta)\right)\sin\left(\omega_o t - \frac{2\pi}{3}\right) \tag{2.59}$$

$$i_{zc1} = \frac{c_1 I_Z}{\pi}\left(\frac{\pi}{2} - \beta - \frac{1}{2}\sin(2\beta)\right)\sin\left(\omega_o t + \frac{2\pi}{3}\right) \tag{2.60}$$

- Harmonic components:

$$i_{zah} = \sum_{n=2}^{\infty} k_n \sin\left(n\omega_o t - \alpha_n\right) \tag{2.61}$$

$$i_{zbh} = \sum_{n=2}^{\infty} k_n \sin\left(n\omega_o t - \alpha_n - \frac{2\pi}{3}\right) \tag{2.62}$$

$$i_{zch} = \sum_{n=2}^{\infty} k_n \sin\left(n\omega_o t - \alpha_n + \frac{2\pi}{3}\right) \tag{2.63}$$

where:

$$k_n = \sqrt{a_n^2 + b_n^2} \tag{2.64}$$

$$\alpha_n = \tan^{-1}\left(\frac{b_n}{a_n}\right) \tag{2.65}$$

and where:

$$a_n = \frac{I_Z c_1}{4n\pi}\left(n\pi - 2n\beta + \sin(n(2\beta - \pi))\right) \tag{2.66}$$

$$b_n = \frac{I_Z c_1 c_2}{n\pi}\sin\left(n\left(\beta - \frac{\pi}{2}\right)\right) \tag{2.67}$$

Using these equations, plots can be generated to show the effect of loading on the harmonics generated by GIC. As shown in Figure 2.8, increased loading results in slight increases in the harmonics for a given level of GIC.

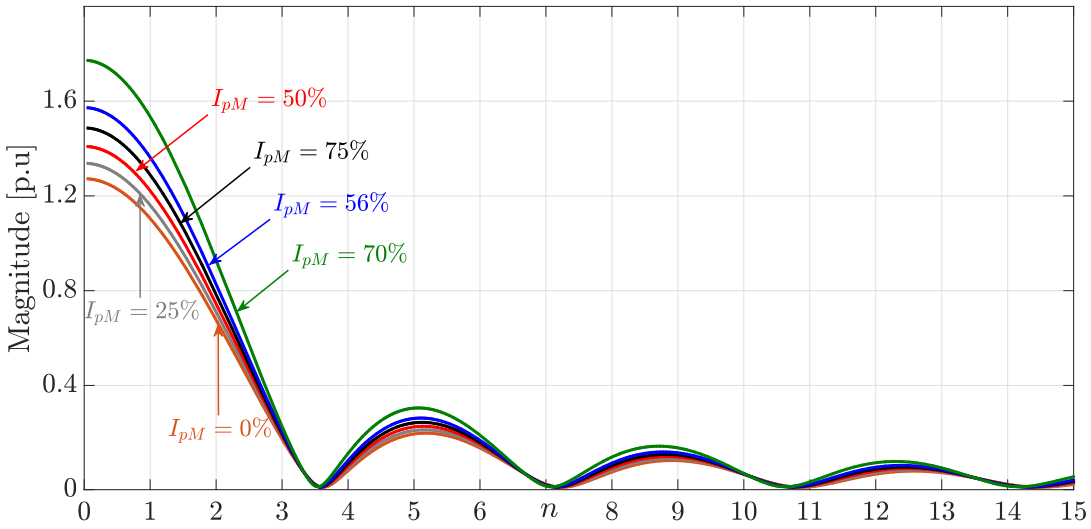


Figure 2.8: Effect of loading level on harmonics due to GIC flows in power transformers [42].

2.2.4 Effect of Grounding System

GIC are known to enter the transmission system through the grounding points of transformers. Many methods of blocking GIC involve some form of grounding equipment [14], [17]–[19], [41]. As such, the grounding system of the transformers can have an impact on the magnitude and severity of the harmonics.

Up to this point, GIC has been modelled as a current source at the neutral point of the affected transformers. To account for the impact of harmonics, the effects of GIC can be modelled as a voltage source at the transformer ground, as [39], [41]:

$$I_{GIC} \approx \frac{E_{GIC}}{3R_G + r_0} \tag{2.68}$$

where E_{GIC} is the ground potential, R_G is the ground resistance of the transformer, and r_0 is the zero-sequence impedance of the transmission system as seen from the transformer ground. The analysis of the resulting currents and saturation effects for a conventional power transformer ((2.2) through (2.15)) remain valid, with the exception that (2.15) can be restated as:

$$k_2 \approx \frac{E_{GIC}}{I_m(3R_G + r_0)} \tag{2.69}$$

2.3 Summary

This section has provided methods for modelling the distortions caused by half-cycle saturation by GIC flows, as well as quantifying the harmonics generated by these distortions. These models have been developed based on a linearized saturation curve for a transformer, and ignore the effects of magnetic coupling between phases (as can be seen on three-limb and five-limb transformers). The resulting distortions are dominated by the 2^{nd} harmonic, and show a positive correlation between GIC level and the induced harmonics.

The effect of transformer type, load level, and grounding system were also analysed. Adjustments to the the modelling equations allow for the model to account for the electrical coupling of autotransformers. The model shows that GIC induced harmonics are moderately reduced in autotransformers, but are still dominated by the 2^{nd} harmonic. In turn, loading level can be shown to affect the magnitude of the harmonics, with a higher loading level resulting in slightly higher harmonic magnitude. Lastly, the models show that introducing a ground resistance can reduce the harmonics caused by a given geomagnetic potential. In both of these cases, the 2^{nd} harmonic remains dominant.

Building off of this modelling, this chapter has shown a potential setup for a detection method based on the 2^{nd} harmonic. Monitoring the differential current between the primary and secondary sides of the transformer for a sustained 2^{nd} harmonic can act as an indicator of the presence of GIC.

The next chapter will build off of this work, showing the results of laboratory testing to confirm the effect of GIC on transformer harmonics. The testing will examine the harmonics generated by 3ϕ power transformers and autotransformers, as well as the effect of loading and grounding systems. It will expand on the work of Chapter 2 by examining both 3ϕ multi-core transformers and 3-limb transformers.

Chapter 3

Analysis of Harmonic Distortion Due to GIC in Power Transformers

3.1 General

Chapter 2 has presented analytical approaches to model the effects of a GIC flow on power transformers. These models have been extended to assess possible impacts of the loading level and grounding system impedance. The presented models have indicated that a GIC flow through the grounded windings of a power transformer can trigger harmonic components in the 3ϕ magnetizing currents. These harmonic components are dominated by even harmonics, mainly the 2^{nd} harmonic.

This chapter presents and discusses the analysis of data collected from two laboratory power transformers, which have different core designs and power ratings. Test power transformers are tested for different levels of GIC flows, loading levels, and grounding impedances. In all tests presented in this chapter, the differential currents of the test power transformers are collected and analyzed for their harmonic components. Finally, tests are conducted for non-GIC flow events to demonstrate the unique signature of a GIC flow in a power transformer. In this chapter, results

obtained from one test power transformer, while the results from the second test transformer are presented in Appendix A.

3.2 Test Power Transformers

The work in this chapter was conducted using two laboratory 3ϕ power transformers to study the effects of GIC flows. One test transformer (Transformer 1) had a multi-core (a bank of three 1ϕ transformers), while the other transformer (Transformer 2) had a 3-limb core. Table 3.1 lists the parameters of the power transformers.

Table 3.1: Specifications of the Laboratory Power Transformers

	Transformer 1	Transformer 2
Rated Power	5.0 kVA	35.0 kVA
Rated Voltage	208/120 V	380/240 V
Rated Frequency	60 Hz	60 Hz
Core Type	Multi-core (3 single cores)	3-Limb Core
Configuration	Y-Δ	Y-Δ
x_1	1.69 Ω	3.8 Ω
r_1	1.87 Ω	0.66 Ω
x_2	3.94 Ω	3.33 Ω
r_2	2.15 Ω	0.90 Ω
x_0	2.18 Ω	2.94 Ω
r_0	1.02 Ω	0.53 Ω

The test power transformers were made part of an experimental setup, where a 3ϕ power supply was used to supply the primary side and a resistive load was connected to the secondary side. A resistive load was used to simplify measuring the changes in reactive demands during any GIC flow. The GIC flows were created by a variable dc source that was connected between the ground and the neutral point of the Y-connected side of the test power transformer. In each test, 3ϕ primary and secondary currents, along with the 3ϕ secondary side voltages, were collected using current and voltages sensors. In addition, active and reactive powers fed to

the primary side were measure using a power meter. A schematic diagram for the experimental setup for both test power transformers is shown in Figure 3.1.

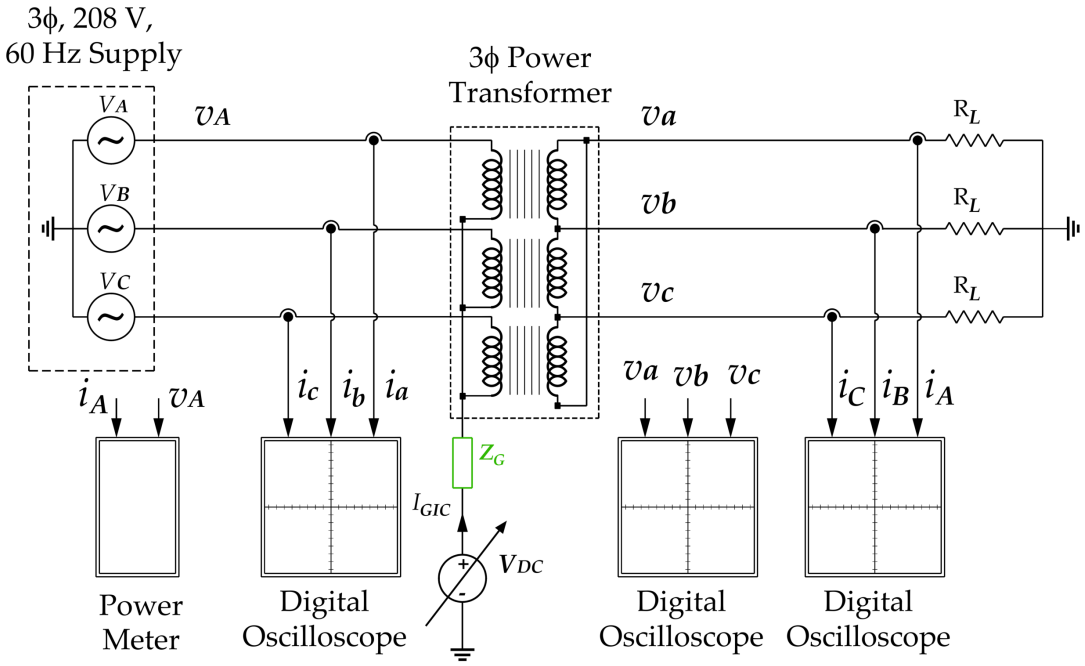


Figure 3.1: A schematic of the test system used for the GIC tests with the power transformers.

3.3 Test Results

In each experimental test, the collected primary and secondary currents were used to determine the 3ϕ differential currents, as given in (1.1). The determined differential currents, together with measured secondary side voltages, were converted to data files in order to extract their harmonic components. The data files were processed a MATLAB/SIMULINK file that had a built-in Fourier analysis function. The obtained harmonic components of the 3ϕ differential currents and 3ϕ secondary side line-to-neutral voltages were averaged as:

$$|I_h| = \frac{|I_h|_A + |I_h|_B + |I_h|_C}{3} \tag{3.1}$$

$$|V_h| = \frac{|V_h|_A + |V_h|_B + |V_h|_C}{3} \tag{3.2}$$

where I_h is the average magnitude of harmonic h of the 3ϕ differential currents, $|I_h|_n$ is the magnitude of harmonic h in the current of phase n, where $n = [A, B, C]$, where V_h is the average magnitude of harmonic h of the 3ϕ secondary side voltages, $|I_h|_n$ is the magnitude of harmonic h in the line-to-neutral voltage of phase n.

3.4 Harmonics Due to a GIC Flow

This experiment aimed to determine the harmonics induced in the power transformers due to the presence of GIC. The transformer was solidly grounded ($Z_G = 0\ \Omega$) on the Y-connected side. The tests on Transformer 1 were conducted with a fixed 3ϕ, Y-connected, resistive load of 0.4 kW/phase. The GIC flow was varied from 0-20 A in steps of 4 A.

3.4.1 5 kVA Transformer

Figure 3.2 shows collected waveforms of the 3ϕ primary currents for each tested GIC flow. In addition, Figure 3.3 shows collected waveforms of the 3ϕ secondary side voltages at each tested GIC flow.

The waveforms in Figure 3.2 show that the 3ϕ primary side currents experienced significant harmonic distortion for each GIC flow. The current waveforms showed that the distortion was asymmetrical in nature, which was due to the half-cycle magnetic saturation created by I_{GIC}. The waveforms in Figure 3.3 demonstrate that secondary side voltages did not experience harmonic distortion at low I_{GIC}. The

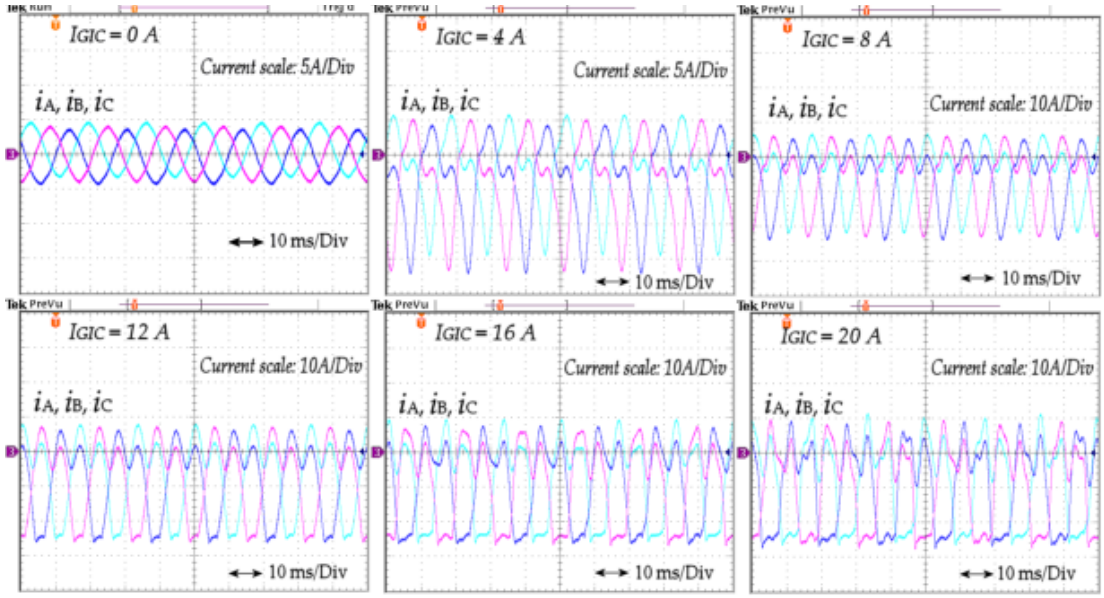


Figure 3.2: Primary side current waveforms showing the distortion caused by GIC in the 5 kVA power transformer.

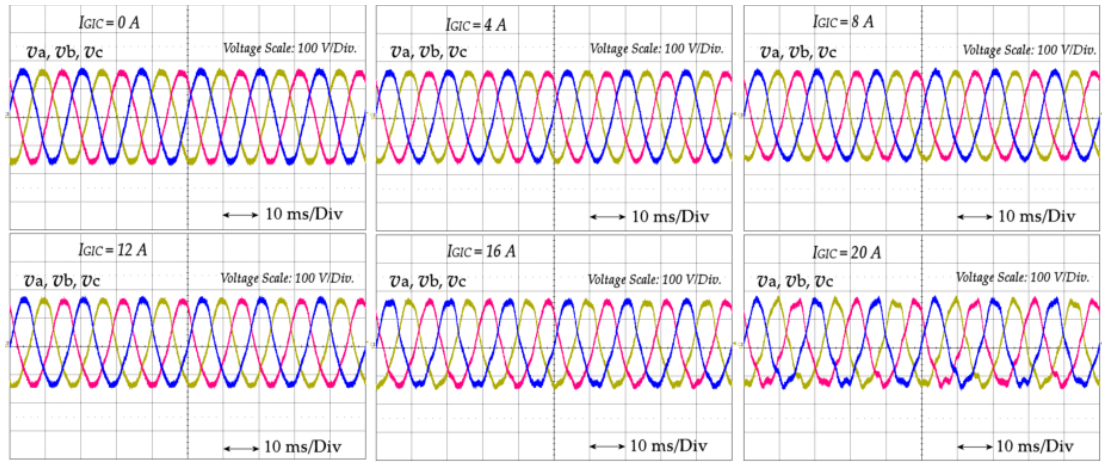


Figure 3.3: Secondary-side voltage waveforms showing the distortion caused by GIC in the 5 kVA power transformer.

distortion in secondary side voltages started to appear for $I_{GIC} \geq 12$ A. This behavior of secondary side voltages was due to the nature of the Δ-connected windings, where the zero-sequence flux could not induce voltage to become part of the voltage distortion on the (Δ-connected) secondary side.

In order to quantify the harmonic distortion due to a GIC flow, a MATLAB/SIMULINK was used to determine current and voltage harmonics. For each set of collected data, the first seven harmonic components of the differential currents

and secondary side voltages were determined. Figure 3.4 shows the waveforms of each voltage and current harmonic at each value of the tested GIC.

The results in Figure 3.4 demonstrate that the dc component increased with I_{GIC}. The fundamental component experienced a linear increase as I_{GIC} increased from 0 to 20 A. Similar to the fundamental component, the 2^{nd} harmonic component increased almost linearly as I_{GIC} was increased. The 3^{rd} harmonic component increased linearly until $I_{GIC} = 10$A, then it slightly decreased before increasing again as I_{GIC} continued to increase. This behavior (increasing, decreasing, and then increasing) was observed in the 4^{th}, 5^{th}, 6^{th}, and 7^{th} harmonic components.

The harmonic components were used to calculate the total harmonic distortion (THD) for both the current and voltage. Additionally, the collected power and reactive power data was plotted. Both can be found in Figure 3.5. The THD for the voltage grows steadily with GIC, but remains quite low, while the THD for the current rises quite high very quickly, and slowly drops as GIC is increased. The reactive power rises rapidly with increasing GIC, but the active power remains nearly constant.

3.5 Effect of the Loading Level

This experiment aimed to determine the effect loading has on the harmonics induced in the power transformers due to the presence of GIC. A variable, 3ϕ, Y-connected, resistive load was connected on the Δ-connected side of the transformer. The load was varied between 0-125% of the rated load. The transformer was solidly grounded ($Z_G = 0\ \Omega$). The dc current used to simulate the GIC was varied from 0-16 A in steps of 4 A.

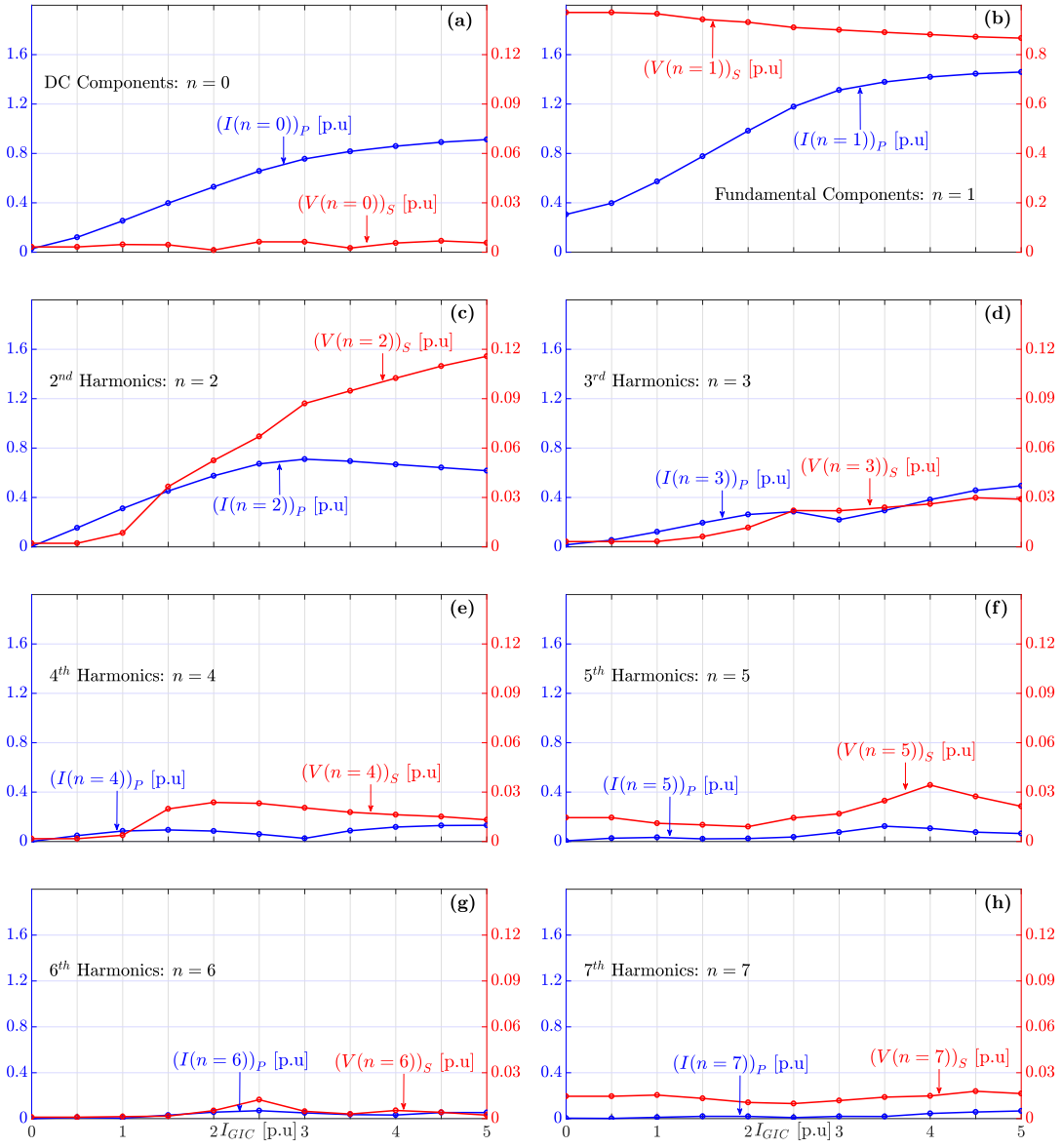


Figure 3.4: Calculated harmonics for the voltages and currents caused by GIC in the 5 kVA power transformer as: a) DC Component; b) Fundamental Component; c) 2nd Harmonic Component; d) 3rd Harmonic Component; e) 4th Harmonic Component; f) 5th Harmonic Component; g) 6th Harmonic Component; and h) 7th Harmonic Component.

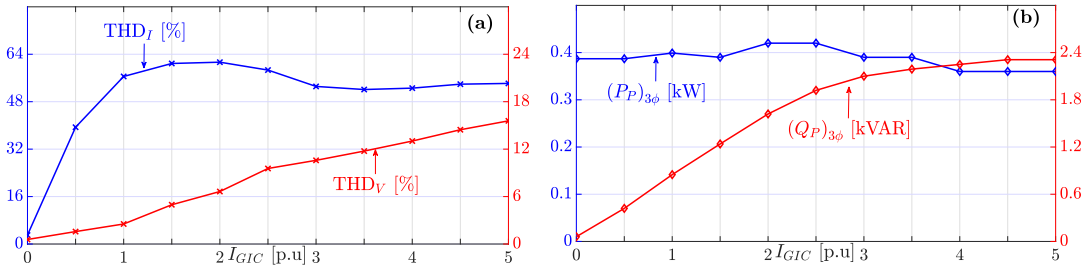


Figure 3.5: Calculated THD for the current and voltage and power/reactive power for the 5 kVA power transformer: a) THD for the current and voltage, and b) Calculated power and reactive power.

3.5.1 5 kVA Transformer

Figure 3.6 shows the collected primary currents for I_{GIC} = 12 A for each load level tested.

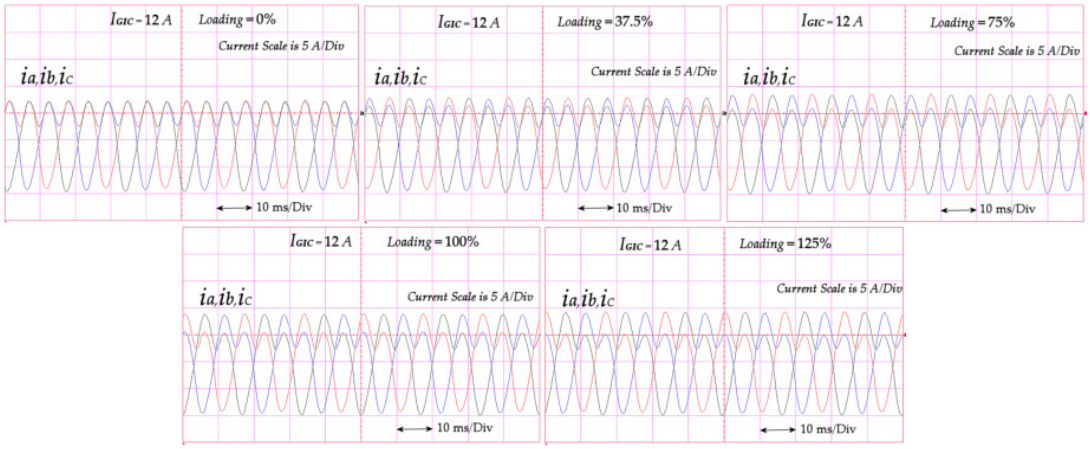


Figure 3.6: Primary side current waveforms showing the distortion caused by I_{GIC} = 12 A in the 5 kVA power transformer for each load level.

The waveforms in Figure 3.6 show that the current experienced significant half-cycle saturation at all loading levels. Observing the positive half of the waveform, the peak current increases with the loading levels. However, the peak current for the bottom half, which is the half-cycle experiencing saturation, does not appear to change significantly with different loading levels.

To quantify the distortion, the harmonics for the current were calculated as discussed in Section 3.3. The results for the first seven harmonics for the differential

currents under all loading levels can be seen in Figure 3.7. All the current harmonics increase at different rates, with the dc, fundamental, and 2nd harmonic components all increasing linearly, while the other harmonics rise and fall at different levels of GIC. As loading increases, it can be seen to slightly increase the levels of harmonic distortion, particularly for the lower order harmonics. After the fundamental, the largest harmonic component remains the 2nd harmonic component for all levels of loading and GIC.

The harmonic components were used to calculate the THD for the current. Additionally, the collected reactive power data was plotted. Both can be found in Figure 3.8. The THD for the current rises with GIC initially, but falls slightly at higher GIC levels. As load is increased, the THD falls. The reactive power rises with increasing GIC, but there is no discernible effect of loading on the reactive power consumption.

3.6 Effect of the Grounding Impedance

This experiment aimed to determine the effect that introducing a ground impedance has on the harmonics induced in the power transformers due to the presence of GIC. The tests of the 5 kVA power transformer were conducted with a fixed 3ϕ, Y-connected, resistive load of 0.75 kW. The dc current used to simulate the GIC was varied from 0-16 A in steps of 4 A.

Transformer grounding impedances can be configured as [41], [49], [50]:

- Solid Grounding, $Z_G = 0\ \Omega$;
- Low Resistance Grounding (LRG), $Z_G = r_{LRG}$;
- High Resistance Grounding (HRG), $Z_G = r_{HRG}$;
- Frequency Selective Grounding (FSG), $Z_G = r_G + jx_G$;

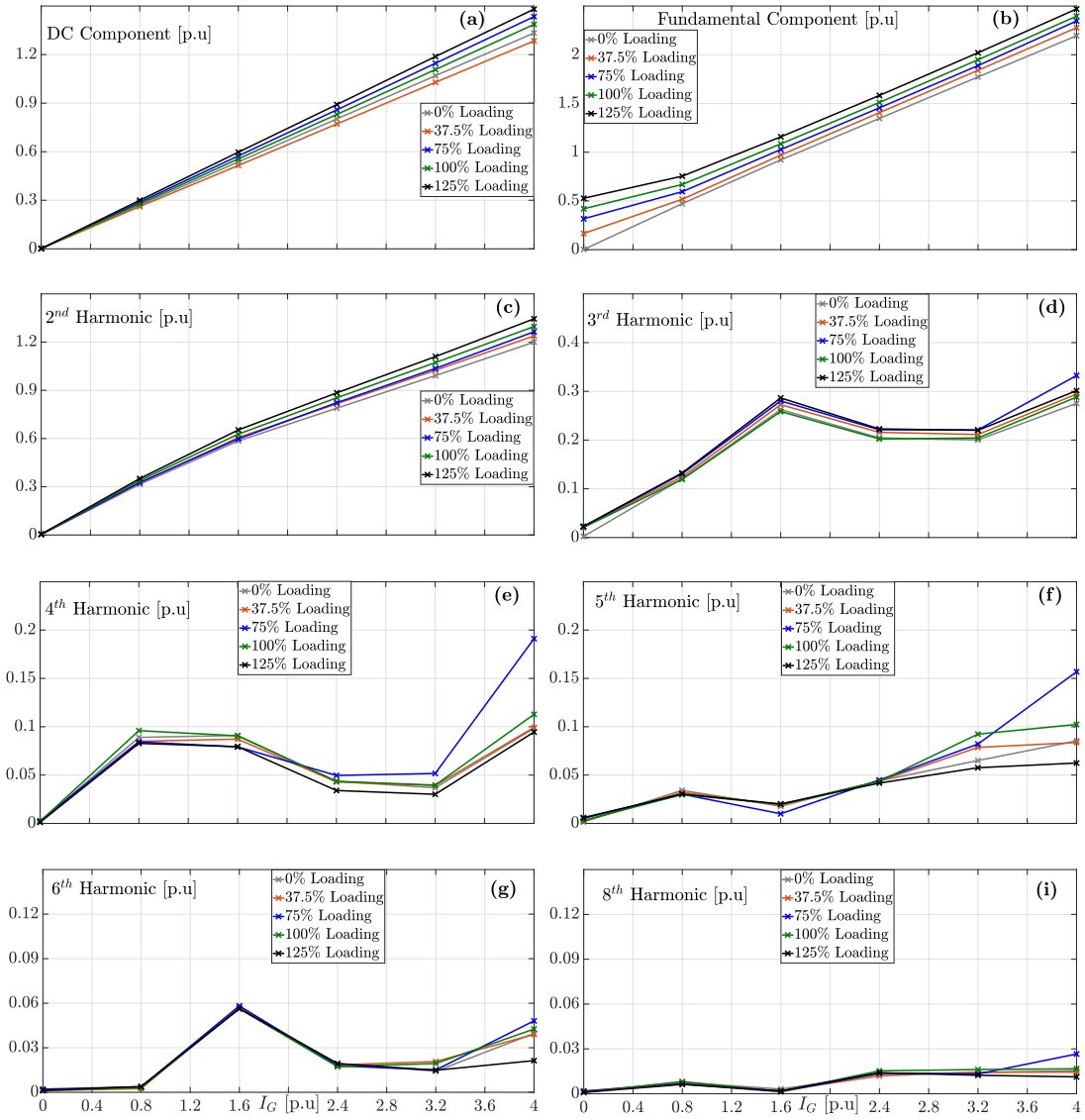


Figure 3.7: Calculated harmonics for the currents caused by GIC in the 5 kVA power transformer for each load level as: a) DC Component; b) Fundamental Component; c) 2nd Harmonic Component; d) 3rd Harmonic Component; e) 4th Harmonic Component; f) 5th Harmonic Component; g) 6th Harmonic Component; and h) 7th Harmonic Component.

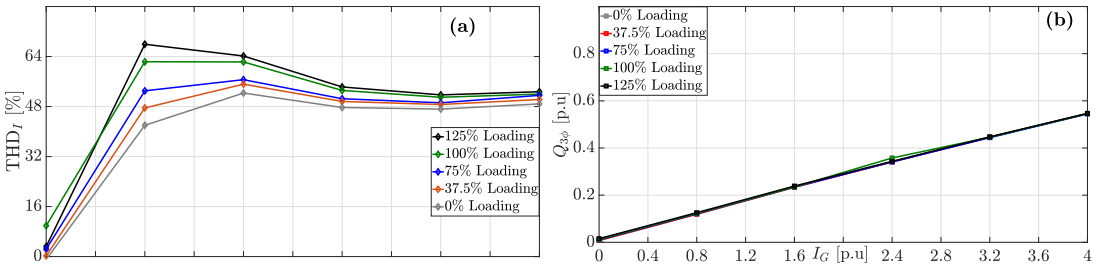


Figure 3.8: Calculated THD for the current and reactive power for the 5 kVA power transformer at each loading level: a) THD for the current, and b) Calculated reactive power.

- Isolated Grounding (IG),$Z_G = \infty$; and
- Inductive Grounding (XG) $Z_G = jx_G$;

As GIC is modelled in these tests as a dc current, XG is not used as it has no steady state effect on dc currents. As IG would result in no ability for GIC to flow, it has not been used in these tests. The rest of the grounding types have been used with the parameters established as [41]:

- Solid Grounding, $Z_G = 0\ \Omega$;
- Low Resistance Grounding, $Z_G = 5\ \Omega$;
- High Resistance Grounding, $Z_G = 10\ \Omega$; and
- Frequency Selective Grounding, $Z_G = 5 - j53\ \Omega$.

3.6.1 5 kVA Transformer

Figure 3.9 shows the collected primary currents for $I_{GIC} = 12$ A for each grounding system tested.

The waveforms in Figure 3.9 show that the current experienced significant half-cycle saturation regardless of the grounding system used. The greatest saturation can be seen with solid grounding, while the least saturation can be seen for the

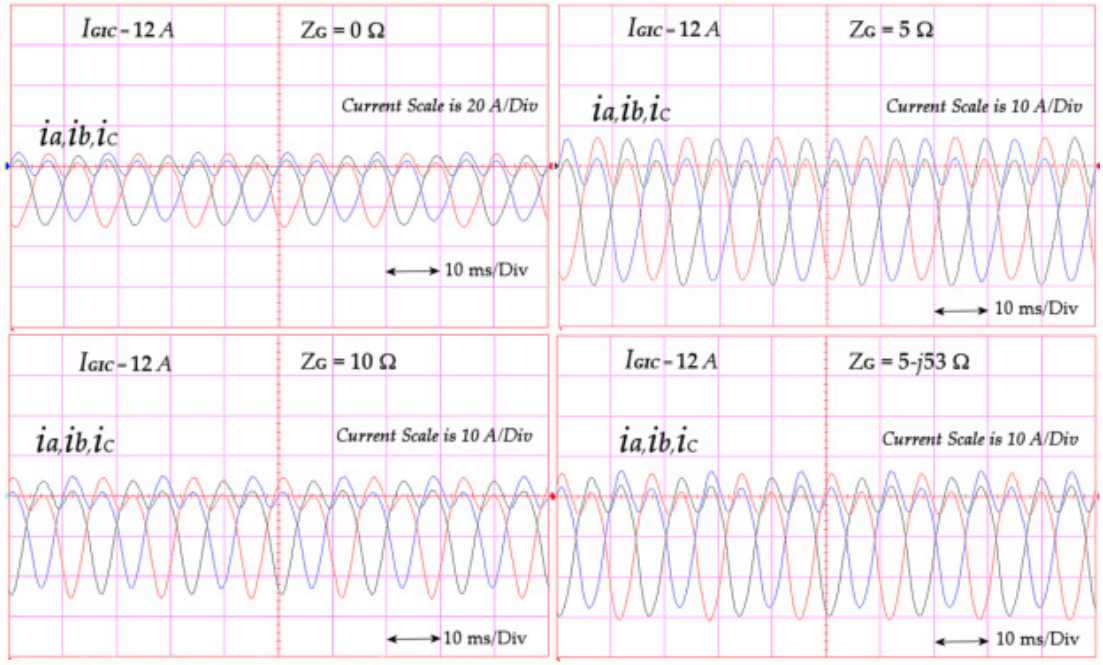


Figure 3.9: Primary side current waveforms showing the distortion caused by I_{GIC} = 12 A in the 5 kVA power transformer for each grounding system tested.

HRG. Most notably, the LRG and FSG do not have significant differences in the distortion and both have a moderate level of saturation.

To quantify the distortion, the harmonics of the differential current were calculated as discussed in Section 3.3. The results for the first seven harmonics for the currents for each grounding impedance can be seen in Figure 3.10. The direct effect of the grounding systems can be best seen in the dc components, where the dc current is reduced, particularly by the HRG. This in turn reduces the magnitude of the harmonic components. The HRG reduces the harmonics the most, with there being little difference between the FSG and LRG, as the capacitive component of the FSG acts as an open circuit for dc currents (like the simulated GIC). Observing the magnitudes of the harmonic components, regardless of grounding type or GIC level, the 2nd harmonic component remains strongly dominant, at about four times the magnitude of the next largest harmonic.

The harmonic components were used to calculate the THD for the differential current. Additionally, the collected reactive power data was plotted. Both can be

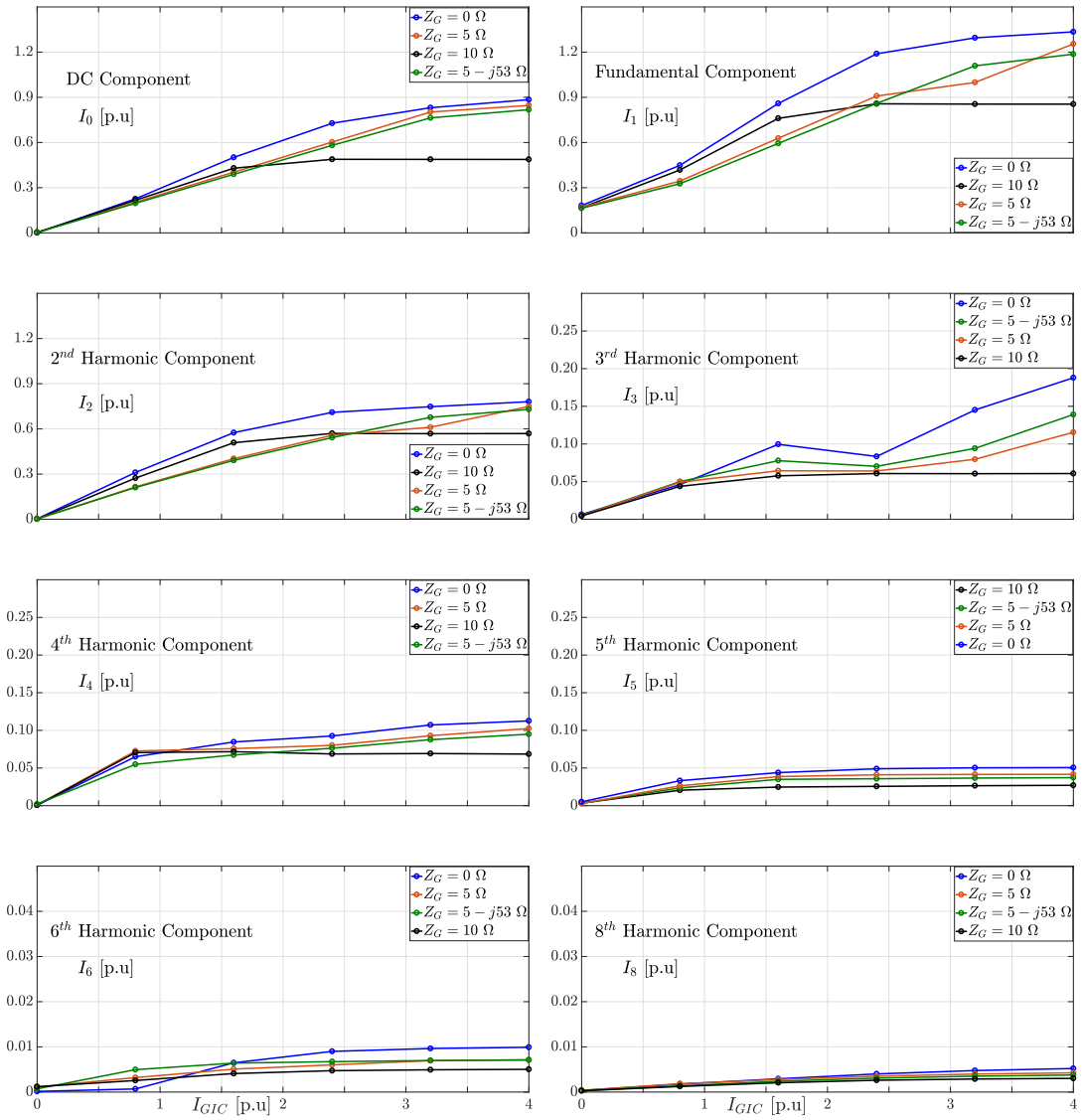


Figure 3.10: Calculated harmonics for the currents caused by GIC in the 5 kVA power transformer for each grounding type used as: a) DC Component; b) Fundamental Component; c) 2nd Harmonic Component; d) 3rd Harmonic Component; e) 4th Harmonic Component; f) 5th Harmonic Component; g) 6th Harmonic Component; and h) 7th Harmonic Component.

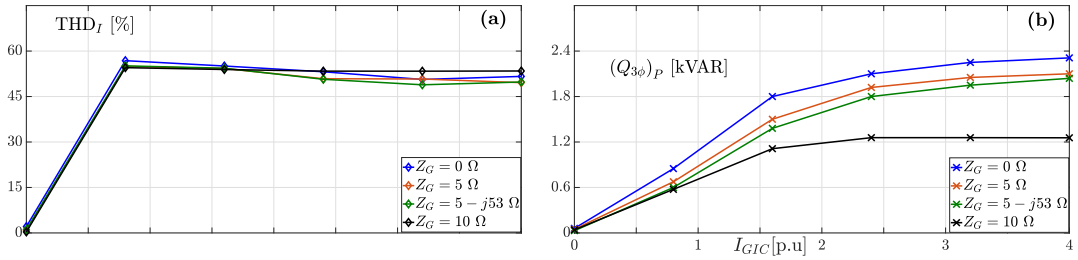


Figure 3.11: Calculated THD for the current and reactive power for the 5 kVA power transformer for each grounding type: a) THD for the current, and b) Calculated reactive power.

found in Figure 3.11. The THD for the current rises with GIC initially, but plateaus around 50% for all grounding systems. The reactive power rises with increasing GIC for all grounding systems, but the greatest rise is seen with the solid grounding, while the lowest rise is seen with the HRG.

3.7 Non-GIC Events

This chapter has thus far verified the presence of the 2$^{\text{nd}}$ harmonic component in the differential current of transformers affected by GIC. It has shown that the 2$^{\text{nd}}$ harmonic increases with rising levels of GIC, and that it in all cases it is the largest harmonic component. It is always the largest harmonic component, regardless of the grounding system used or the level of loading on the transformer. This verifies that the 2$^{\text{nd}}$ harmonic can be used as a method to identify the presence of GIC. However, other power system events can result in large harmonic distortion as well.

This section looks to compare the 2$^{\text{nd}}$ harmonic component of distortion caused by line-to-neutral faults, line-to-line faults, and transformer energization to that caused by GIC flows. The ratio of the 2$^{\text{nd}}$ harmonic component of each event to the fundamental component, as calculated in (1.4), will be used to compare these events to determine how well this metric can be used to discriminate between events.

The test setup used is very similar to the one used in Section 3.5. A vari-

able, 3ϕ, Y-connected, resistive load was connected on the secondary side of the transformer, ranging from 0-125% of the rated load. A series of cases were then tested.

The five cases that were tested for the transformer were:

- Normal Operation: In this case, the transformer was monitored without any harmonic inducing events to establish a base case.
- GIC: In this case, a dc source was connected between the ground and the transformer neutral. A GIC flow of 16 A was used.
- Line-Neutral Fault: In this case, a fault was created between one phase and ground. To avoid the tripping of the source, a fault resistance of 10 Ω was used. For the 5 kVA transformer, the fault was introduced on Phase B.
- Line-Line Fault: In this case, a fault was created between two phases. To avoid the tripping of the source, a fault resistance of 20 Ω was used. For the 5 kVA transformer the fault was introduced between Phase A and Phase C.
- Transformer Energization: In this case, the transformer was energized by suddenly connecting the transformer to the 3ϕ 120/208 V source. The transient response was captured and analysed.

The results of these test cases were then analysed and compared to each other to identify differences in the 2^{nd} harmonic component ratios.

3.7.1 5 kVA Transformer

Figure 3.12 shows the collected primary currents for each test case at 100% of rated load. These figures show significant distortion for a number of the test cases. The GIC case shows the half-cycle saturation typical of GIC events. The fault cases show an imbalance between the phases, with the faulted phases drawing large fault

currents. The transformer energization case shows unbalanced and distorted currents with a transient response that quickly disappears.

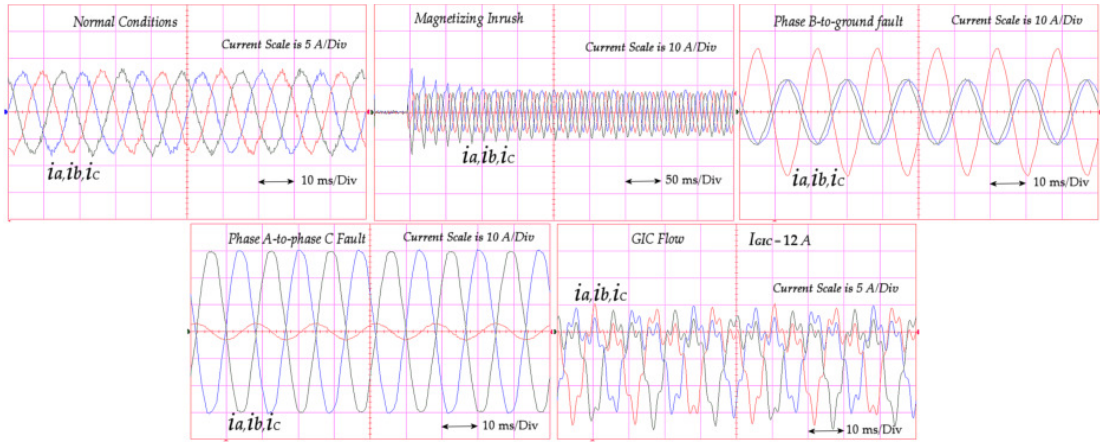


Figure 3.12: Primary side current waveforms showing the distortion caused for each test case for a 5 kVA power transformer at a load level of 100%.

The harmonics for each test case were then calculated as discussed in Section 3.3. The 2nd harmonic ratios were then calculated from those results, and are compared in Figure 3.13. This figure shows that only two of the events had an increase in the 2nd harmonic ratio: GIC and transformer energization. Despite the large imbalance caused by the fault currents, most of their energy was not in the 2nd harmonic, but in the fundamental. This resulted in a reduction in the 2nd harmonic ratio for those cases. The GIC showed a slight increase in the ratio with an increasing load, while the transformer energization's ratio was greatly reduced as the load was increased. However, due to the high 2nd harmonic ratio in the case of transformer energization, an additional criterion will be necessary to distinguish between these events.

As discussed in Section 1.4, one discriminator that can be used is duration. Figure 3.12 shows the sustained nature of the GIC, with the transformer inrush disappearing after a few cycles. This offers support to the use of a sustained 2nd harmonic ratio as the signature of a GIC event.

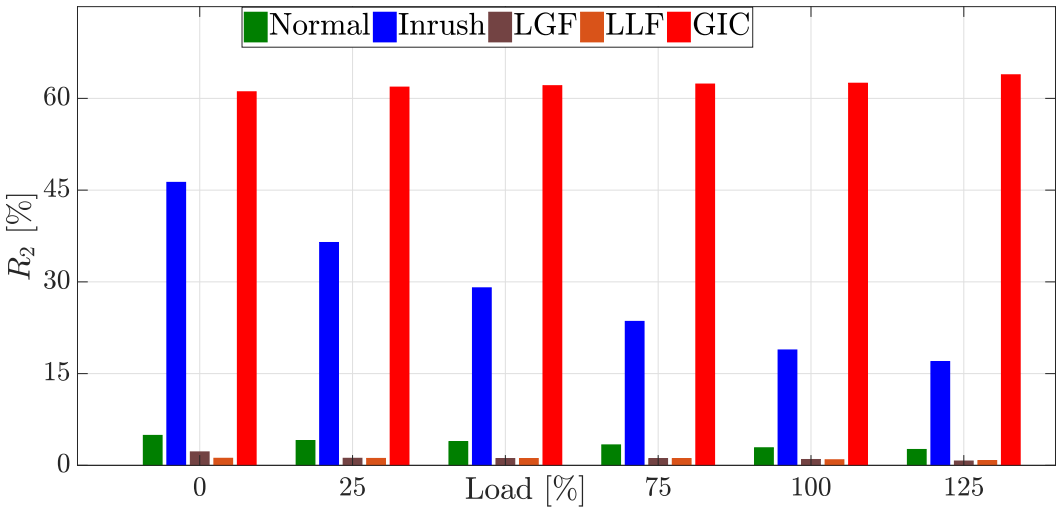


Figure 3.13: A comparison of the 2nd harmonic ratio for each event for the 5 kVA power transformer.

3.8 Summary

This chapter has presented a series of experimental test cases to verify the dominance of the 2nd harmonic in the half-cycle saturation caused by GIC. It has looked at the harmonic components that result from saturation, showing that in all cases the 2nd harmonic component is a large part of the distortion caused by GIC. In most cases it is the largest harmonic component, regardless of the the loading level or the grounding system type. The 2nd harmonic component will be present whenever a transformer is experiencing sufficient GIC to cause saturation.

This chapter has also compared the harmonic content of other power system events, showing that the ratio of the 2nd harmonic in the differential current allows GIC to stand out against both line-to-line and line-to-neutral faults. This comparison confirmed, however, that transformer energization also has a significant 2nd harmonic ratio. It also showed that the harmonics caused by transformer energization are transient. This demonstrates the effectiveness of using a sustained 2nd harmonic ratio as an indicator of saturation due to the presence of GIC.

The next chapter will present the results of testing done on autotransformers to verify that this detection method remains usable for autotransformers.

Chapter 4

Analysis of Harmonic Distortion Due to GIC in Autotransformers

4.1 General

Test results for power transformers experiencing GIC flows have confirmed the strong presence of harmonic components due to GIC flow. These harmonic components have been observed in the 3ϕ differential currents, as well as the 3ϕ currents flowing the grounded windings of test power transformers. The salient feature of the determined harmonic components has been the 2^{nd} harmonic, which has dominated harmonic components at different loading levels and grounding impedance values.

This chapter extends the testing of the impacts of GIC flows on power transformers to autotransformers. Similar to tests presented in Chapter 3, this chapter presents and discusses tests of 3ϕ autotransformers during different GIC flows. Furthermore, testing is extended to include GIC flows at different loading levels. In addition, this chapter provides a generic comparison between harmonic components due to GIC flows in 3ϕ power transformers and autotransformers.

4.2 Test Autotransformers

The work in this chapter was conducted using two laboratory 3ϕ autotransformers to study the effects of GIC flows. One test autotransformer (Transformer 1) had a multi-core, while the other autotransformer (Transformer 2) had a 3-limb core. Table 4.1 lists the parameters of the autotransformers.

Table 4.1: Specifications of the Laboratory Autotransformers

	Transformer 1	Transformer 2
Rated Power	5.0 kVA	35.0 kVA
Rated Voltage	208/120 V	380/240 V
Rated Frequency	60 Hz	60 Hz
Core Type	Multi-core (3 single cores)	3-Limb Core
Configuration	Y-Y	Y-Y
x_1	1.69 Ω	3.8 Ω
r_1	1.87 Ω	0.66 Ω
x_2	3.94 Ω	3.33 Ω
r_2	2.15 Ω	0.90 Ω
x_0	2.18 Ω	2.94 Ω
r_0	1.02 Ω	0.53 Ω

The test autotransformers were made part of an experimental setup similar to that described in Section 3.2, where a 3ϕ power supply was used to supply the primary side and a resistive load was connected to the secondary side. The GIC flows were created by a variable dc source that was connected between the ground and the neutral point of the test autotransformer. In each test, 3ϕ primary and secondary currents, along with the 3ϕ secondary side voltages, were collected using current and voltages sensors. In addition, active and reactive powers fed to the primary side were measured using a power meter. A schematic diagram for the experimental setup for both test autotransformers is shown in Figure 4.1.

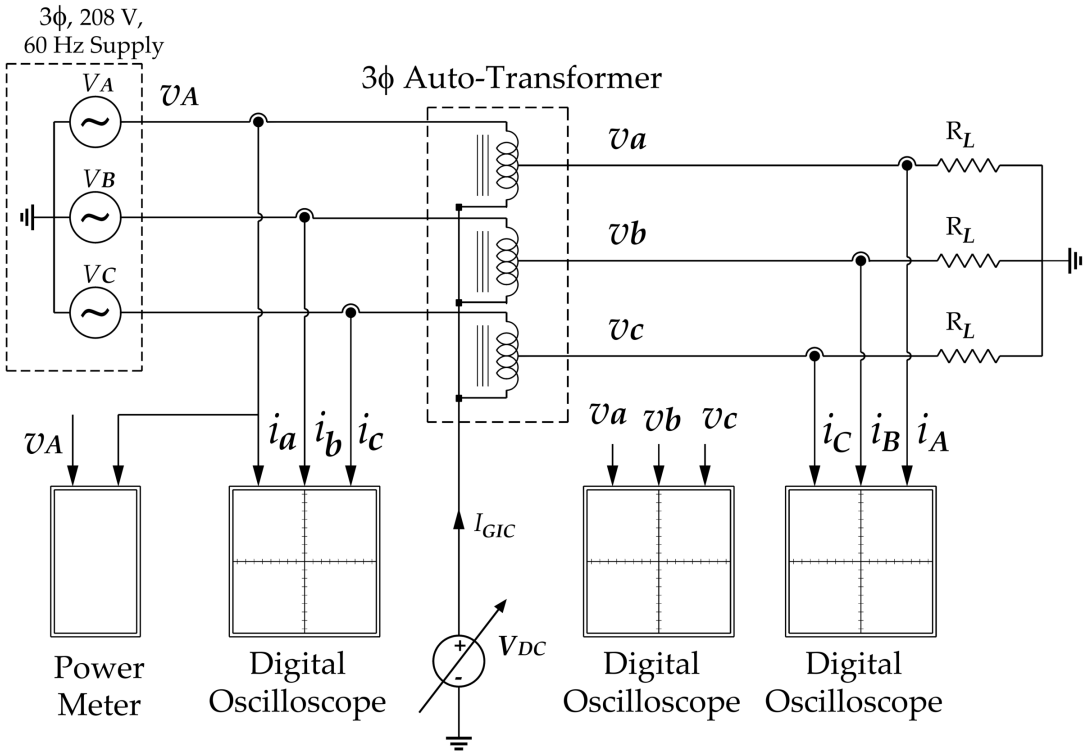


Figure 4.1: A schematic of the test diagram used for the GIC tests with the Y-Y autotransformers [43].

4.3 Harmonics due to a GIC Flow in Autotransformers

This experiment aimed to determine the harmonics induced in the Y-Y autotransformers due to the presence of GIC. A fixed, 3ϕ Y-connected resistive load was used. The transformer was solidly grounded ($Z_G = 0\ \Omega$) at the neutral point.

4.3.1 5 kVA Autotransformer

For the 5 kVA autotransformer, a load of 0.6 kW/phase was used. The dc current used to simulate the GIC was varied from 0-16 A in steps of 2 A. Figure 4.2 shows the collected primary currents for each level of GIC tested. Figure 4.3 shows collected waveforms for the secondary voltages.

The waveforms in Figure 4.2 show that the current experienced significant

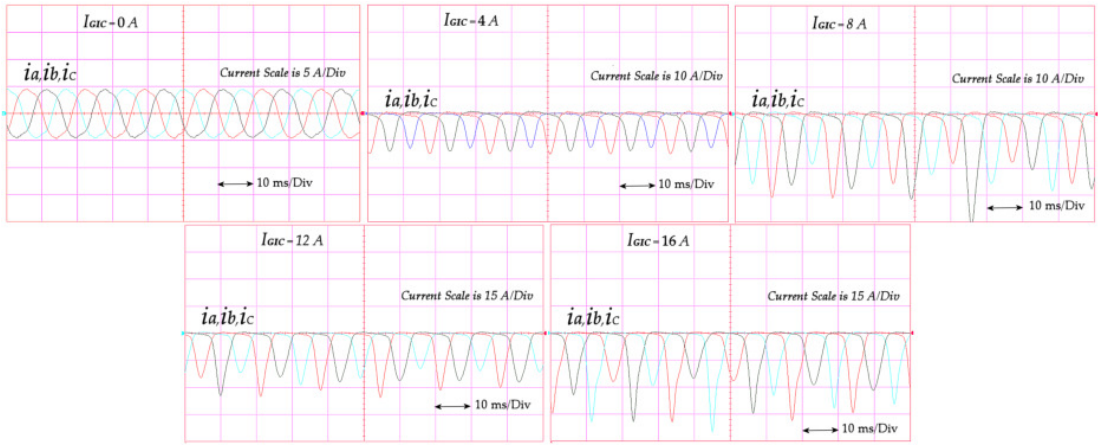


Figure 4.2: Primary side current waveforms showing the distortion caused by GIC in the 5 kVA autotransformer.

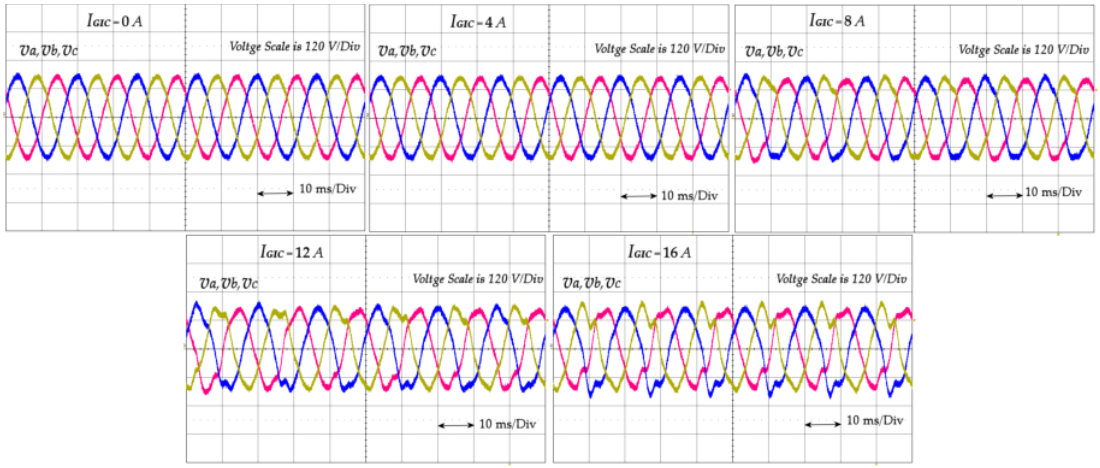


Figure 4.3: Secondary-side voltage waveforms showing the distortion caused by GIC in the 5 kVA autotransformer.

harmonic distortion at even the lower levels of I_{GIC}. Compared to the conventional power transformers, the autotransformer appears to experience more half-cycle saturation, with very little of the signal in the positive half-cycle. The waveforms in Figure 4.3 show far less distortion, though are slightly more distorted than for the corresponding power transformer.

To quantify the distortion, the harmonics for the voltage and current were calculated as discussed in Section 3.3. The results for the first seven harmonics for both currents and voltages can be seen in Figure 4.4. All the current harmonics increase with GIC, with the lower order harmonics generally increasing linearly.

The fundamental component increases with GIC as well. At all levels of GIC, the 2nd harmonic remains dominant, with the magnitude of the harmonics dropping off rapidly after the 3rd harmonic component. The voltage harmonics produced by GIC are far smaller, with a dominant 3rd harmonic. The fundamental component does not increase, though most of the harmonics increase slowly with GIC.

The harmonic components were used to calculate the THD for both the current and voltage. Additionally, the collected power and reactive power data was plotted. Both can be found in Figure 4.5. The THD for the voltage grows steadily with GIC, but remains quite low, while the THD for the current rises quite high very quickly, then slowly drops as GIC is increased. Both the power and reactive power rise with increasing GIC, but the reactive power rises far more rapidly than the active power.

4.3.2 35 kVA Autotransformer

For the 35 kVA autotransformer, a load of 2.5 kW was used. The dc current used to simulate the GIC was varied from 0-40 A in steps of 4 A. Figure 4.6 shows the collected primary currents for each level of GIC tested. Figure 4.7 shows the secondary voltages.

The waveforms in Figure 4.6 show that the current experienced distortion even at low levels of GIC. The current can be seen shifting due to the presence of a dc current, with distortion appearing at $I_{GIC} = 4$ A and growing with GIC. The waveforms in Figure 4.7 show far less distortion. No distortion is visible at any level of GIC.

To quantify the distortion, the harmonics for the voltage and current were calculated as discussed in Section 3.3. The results for the first seven harmonics for both currents and voltages can be seen in Figure 4.8. The current harmonics grow with GIC, indicating the transformer is more susceptible to GIC than a typical 3-

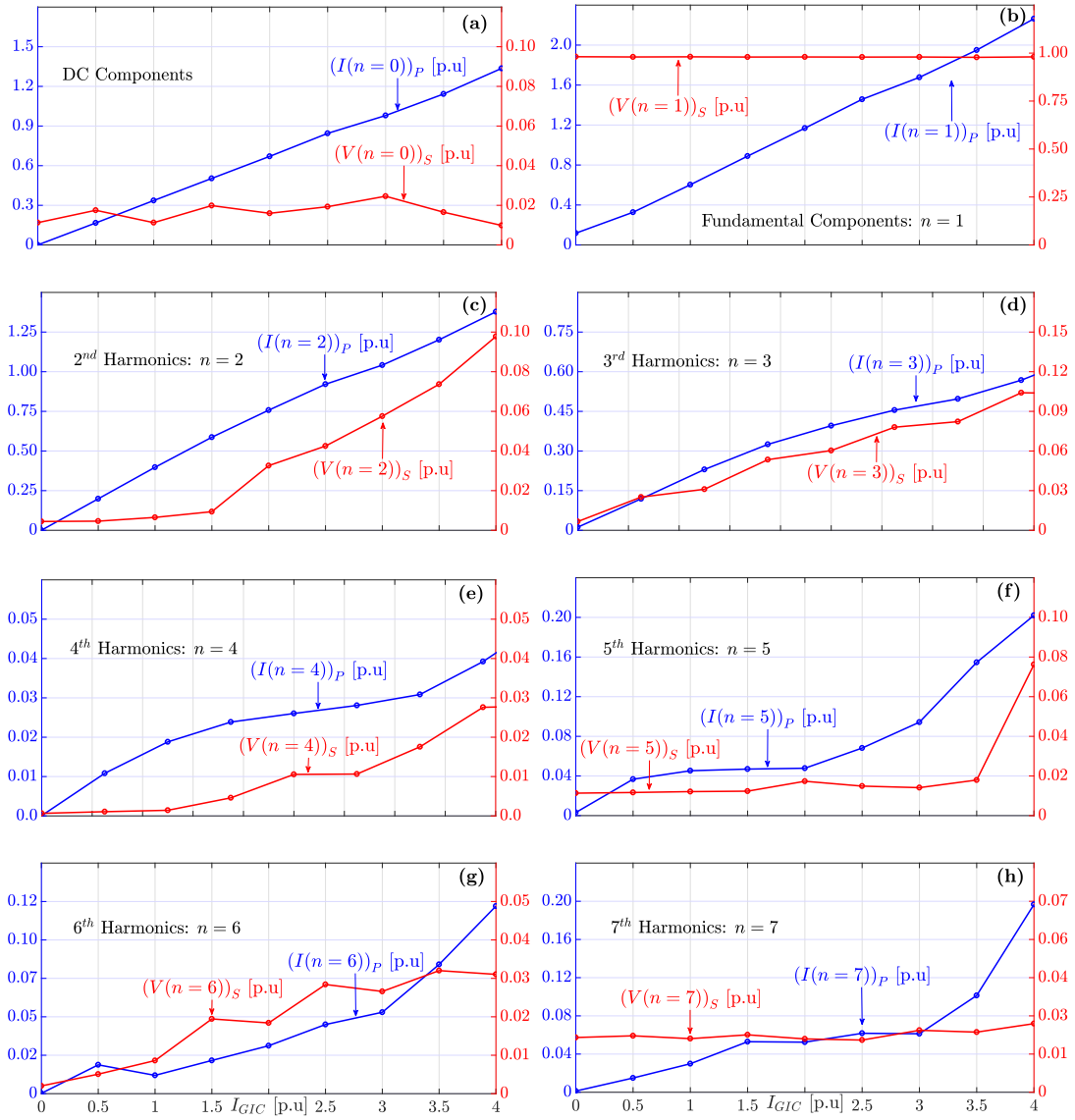


Figure 4.4: Calculated harmonics for the voltages and currents caused by GIC in the 5 kVA autotransformer as: a) DC Component; b) Fundamental Component; c) 2nd Harmonic Component; d) 3rd Harmonic Component; e) 4th Harmonic Component; f) 5th Harmonic Component; g) 6th Harmonic Component; and h) 7th Harmonic Component.

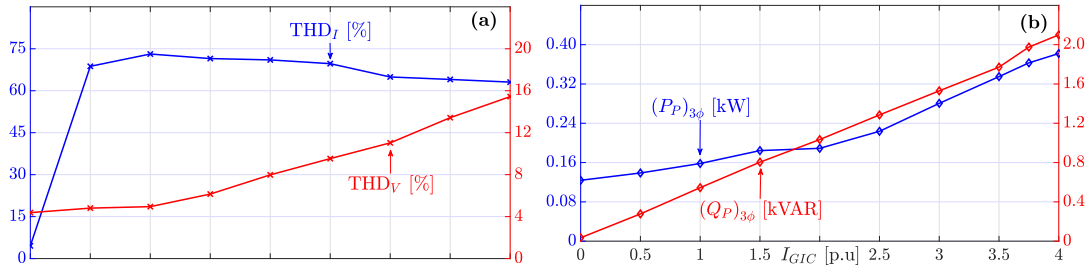


Figure 4.5: Calculated THD for the current and voltage and power/reactive power for the 5 kVA autotransformer: a) THD for the current and voltage, and b) Calculated power and reactive power.

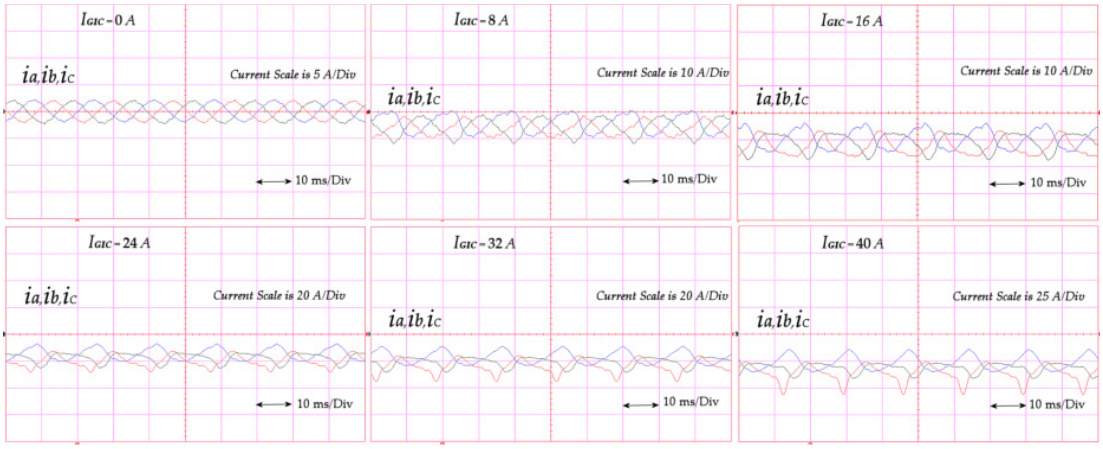


Figure 4.6: Primary side current waveforms showing the distortion caused by GIC in the 35 kVA autotransformer.

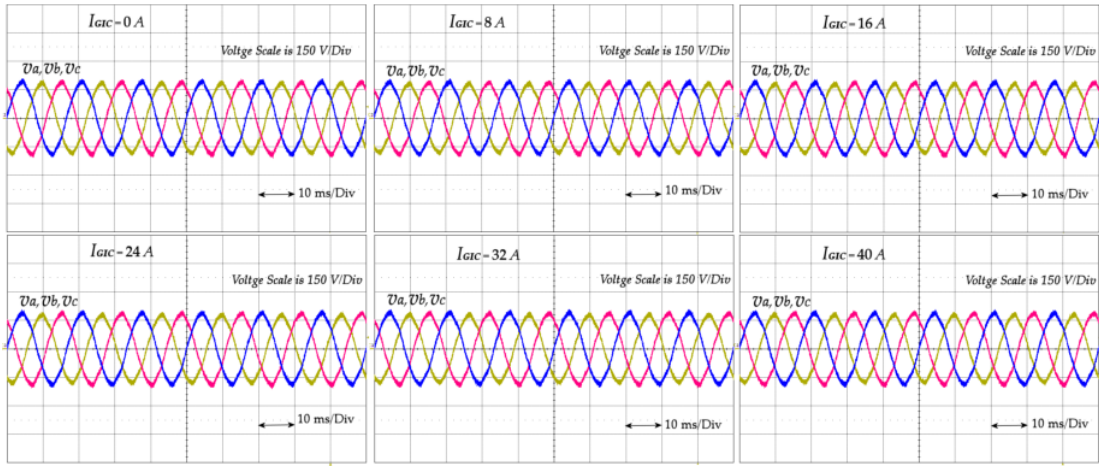


Figure 4.7: Secondary-side voltage waveforms showing the distortion caused by GIC in the 35 kVA autotransformer.

limb transformer. As can be seen, the harmonic content of the voltages remains very low throughout, and does not change significantly as I_{GIC} increases.

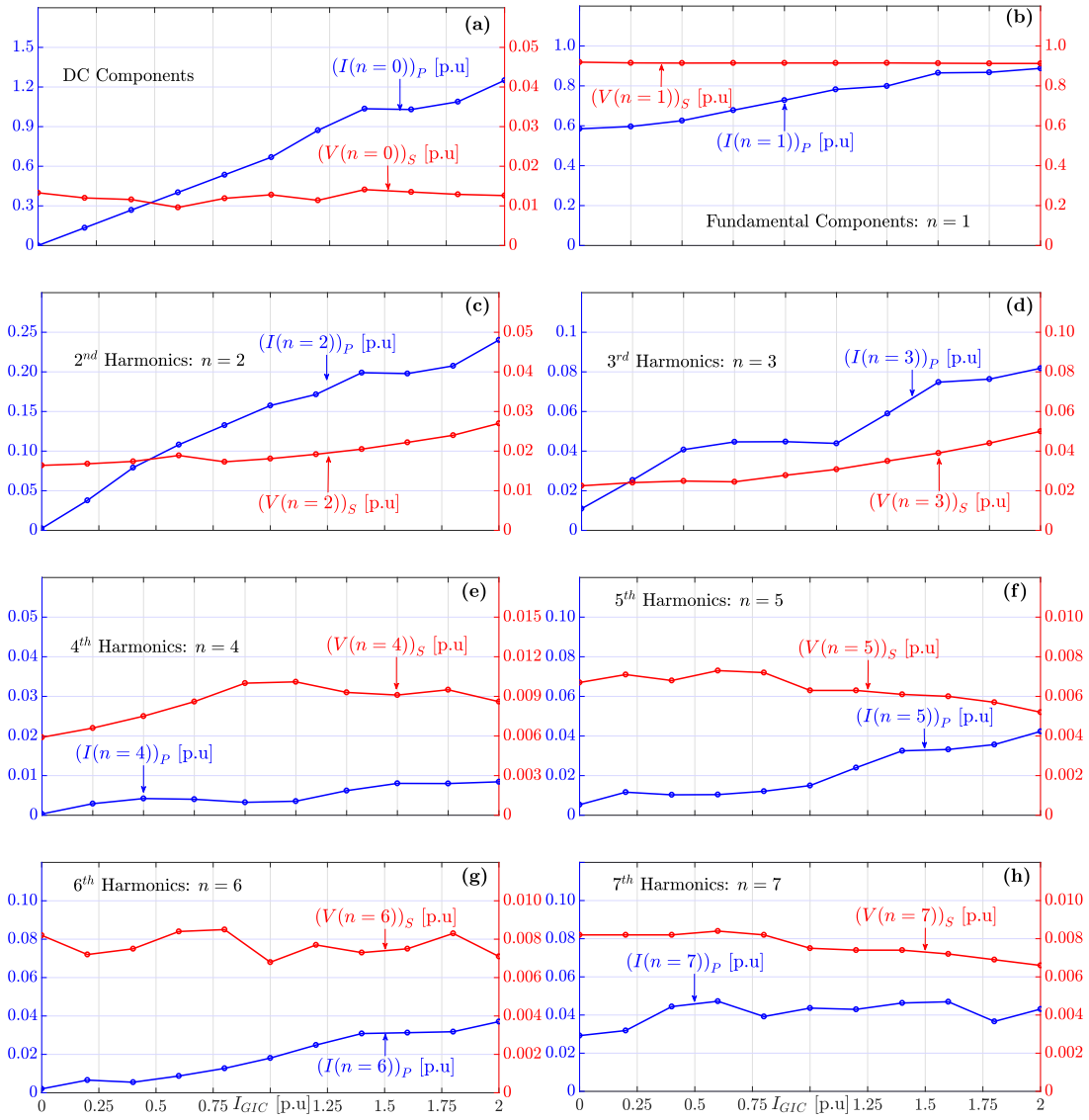


Figure 4.8: Calculated harmonics for the voltages and currents caused by GIC in the 35 kVA autotransformer as: a) DC Component; b) Fundamental Component; c) 2^{nd} Harmonic Component; d) 3^{rd} Harmonic Component; e) 4^{th} Harmonic Component; f) 5^{th} Harmonic Component; g) 6^{th} Harmonic Component; and h) 7^{th} Harmonic Component.

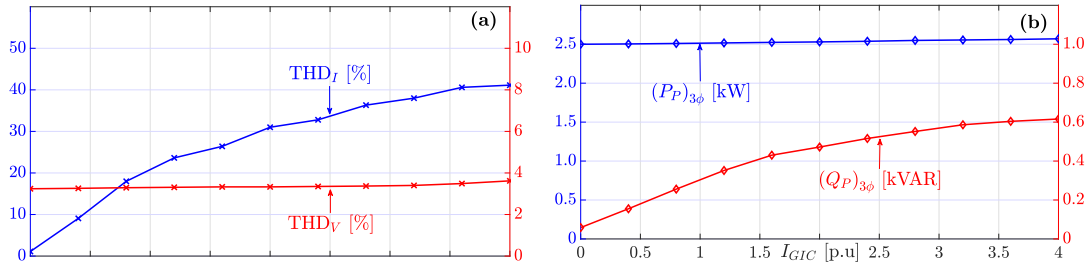


Figure 4.9: Calculated THD for the current and voltage and power/reactive power for the 35 kVA autotransformer: a) THD for the current and voltage, and b) Calculated power and reactive power.

The harmonic components were used to calculate the THD for both the current and voltage. Additionally, the collected power and reactive power data was plotted. Both can be found in Figure 4.9. The THD for the voltage remains very stable, while the THD for the current rises as GIC is increased. The active power also remains stable, while the reactive power rises with increasing GIC.

4.4 Effect of the Loading Level

This experiment aimed to determine the effect loading has on the harmonics induced in the autotransformers due to the presence of GIC. A variable load was connected on the low-voltage side of the transformer. The transformer was solidly grounded ($Z_G = 0\ \Omega$).

4.4.1 5 kVA Autotransformer

For the 5 kVA autotransformer, the load was varied between 0-125% of the rated load. The dc current used to simulate the GIC was varied from 0-20 A in steps of 4 A. Figure 4.10 shows the collected primary currents for $I_{GIC} = 16$ A for each load level tested.

The waveforms in Figure 4.2 show that the current experienced significant half-cycle saturation at all loading levels. Observing the positive half of the wave-

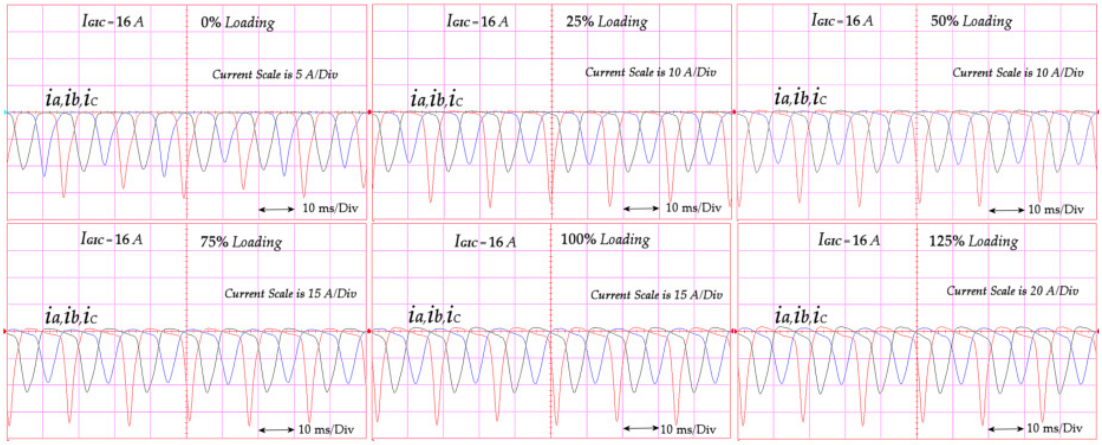


Figure 4.10: Primary side current waveforms showing the distortion caused by I_{GIC} = 16 A in the 5 kVA autotransformer for each load level.

form, the peak current increases slightly with the loading levels. However, the peak current for the bottom half, which is experiencing the saturation, does not appear to change with different loading levels, except appearing smaller for the no load case.

To quantify the distortion, the harmonics for the current were calculated as discussed in Section 3.3. The results for the first seven harmonics for the currents under all loading levels can be seen in Figure 4.11. All the current harmonics increase with GIC. The impact of loading on the harmonics generated are less clear than with the conventional power transformer, with there being no consistent effect of a higher loading level. The largest harmonic component remains the 2nd harmonic component for all levels of loading and GIC.

The harmonic components were used to calculate the THD for the current. Additionally, the collected reactive power data was plotted. Both can be found in Figure 4.12. The THD for the current rises with GIC initially, but falls very slightly as GIC increases. Broadly, as load is increased, the THD falls. The reactive power rises with increasing GIC, but there is no discernible effect of loading on the reactive power consumption.

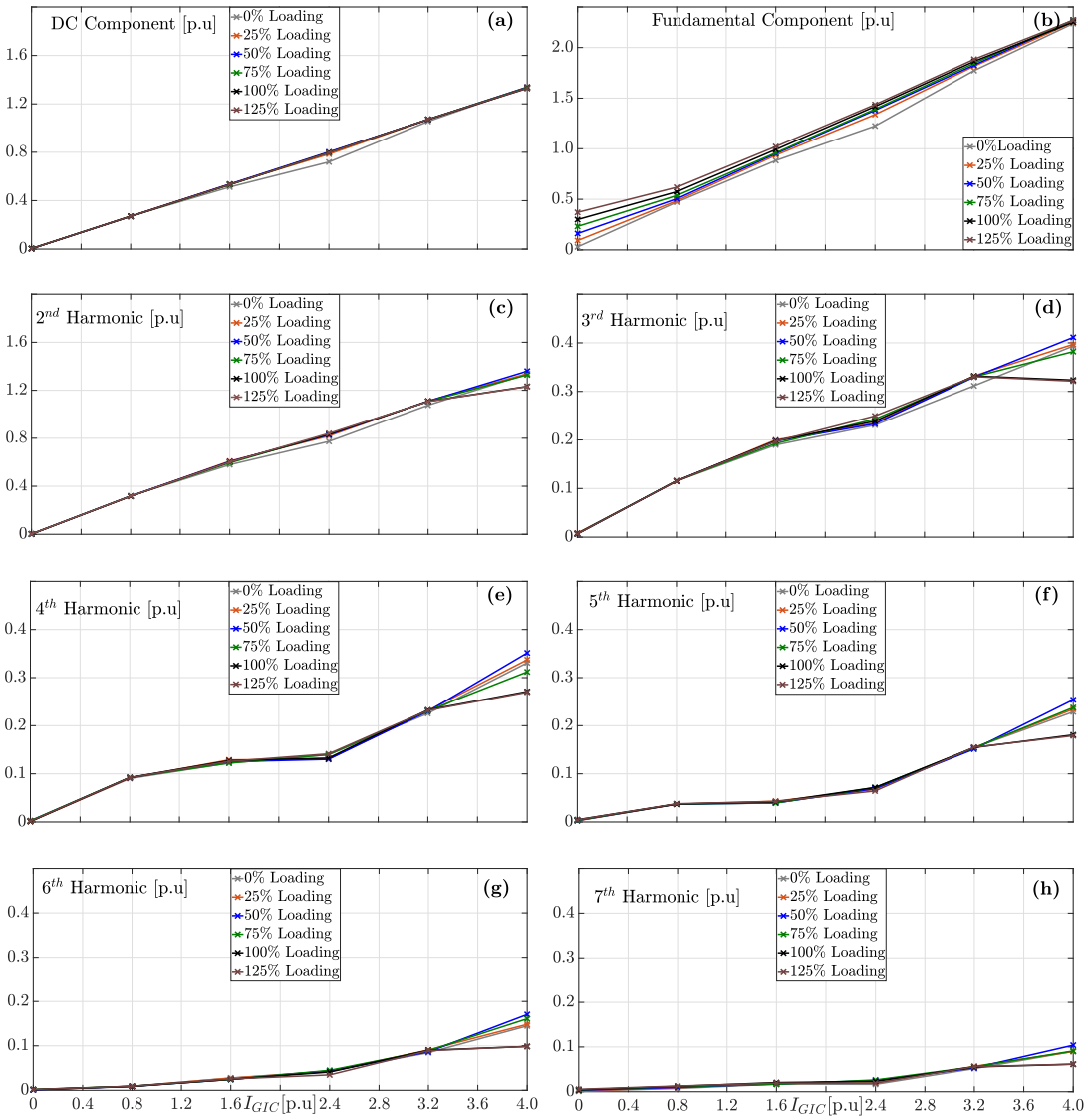


Figure 4.11: Calculated harmonics for the currents caused by GIC in the 5 kVA autotransformer for each load level as: a) DC Component; b) Fundamental Component; c) 2^{nd} Harmonic Component; d) 3^{rd} Harmonic Component; e) 4^{th} Harmonic Component; f) 5^{th} Harmonic Component; g) 6^{th} Harmonic Component; and h) 7^{th} Harmonic Component

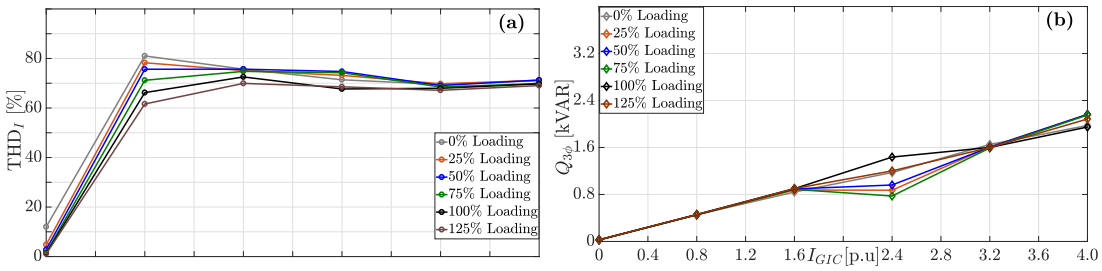


Figure 4.12: Calculated THD for the current and reactive power for the 5 kVA autotransformer at each loading level: a) THD for the current, and b) Calculated reactive power.

4.4.2 35 kVA Autotransformer

For the 35 kVA autotransformer, the load was varied between 0-28%. The dc current used to simulate the GIC was varied from 0-36 A in steps of 6 A. Figure 4.13 shows the collected primary currents for $I_{GIC} = 30$ A for each load level tested.

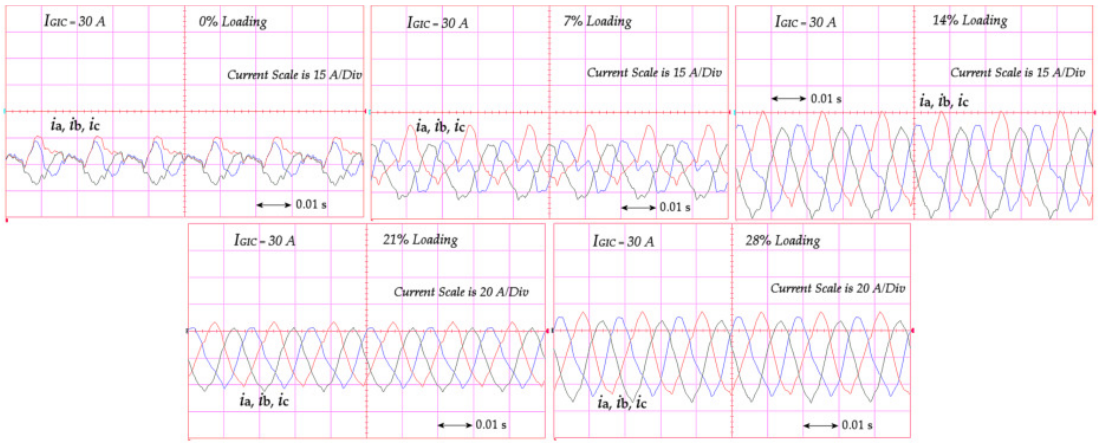


Figure 4.13: Primary side current waveforms showing the distortion for $I_{GIC} = 30$ A in the 35 kVA autotransformer for each load level.

The waveforms in Figure 4.13 show that the transformer experienced a moderate amount of distortion due to the presence of GIC. The effects of saturation are visible at low loading levels, but begin to be overwhelmed by the loading at higher levels.

To quantify the distortion, the harmonics for the current were calculated as discussed in Section 3.3. The results for the first seven harmonics of the differential

current can be seen in Figure 4.14. The 2nd, 3rd, 4th, and 6th harmonic components all trend upwards with GIC, with other harmonics remaining constant. The effects of loading are not consistent, only having a discernible effect on the fundamental, 5th, and 7th harmonic components. Regardless, the 2nd harmonic component is dominant for all levels of loading and GIC.

The harmonic components were used to calculate the THD for the current. Additionally, the collected reactive power data was plotted. Both can be found in Figure 4.15. The THD for the current rises steadily with GIC. An increase in loading results in a very small drop in THD. The reactive power rises with increasing GIC, but there is no discernible effect of loading on the reactive power consumption, except for a small rise at high GIC with no loading.

4.5 Non-GIC Events

This chapter has confirmed that the 2nd harmonic component is dominant in autotransformers experiencing GIC. The last part of this chapter will examine the harmonics introduced by other power system events for autotransformers to determine if the 2nd harmonic can reliably distinguish between events, as it can for power transformers.

The same test cases were used as in Section 3.7. The harmonic ratio is calculated as per that section, as well.

4.5.1 5 kVA Autotransformer

For the 5 kVA autotransformer, the load was varied between 0-125% of the rated load. Figure 4.16 shows the collected primary currents for each test case at 100% of rated load. These figures show significant distortion for a number of the test cases. The GIC case shows the half-cycle saturation, while the fault cases show an

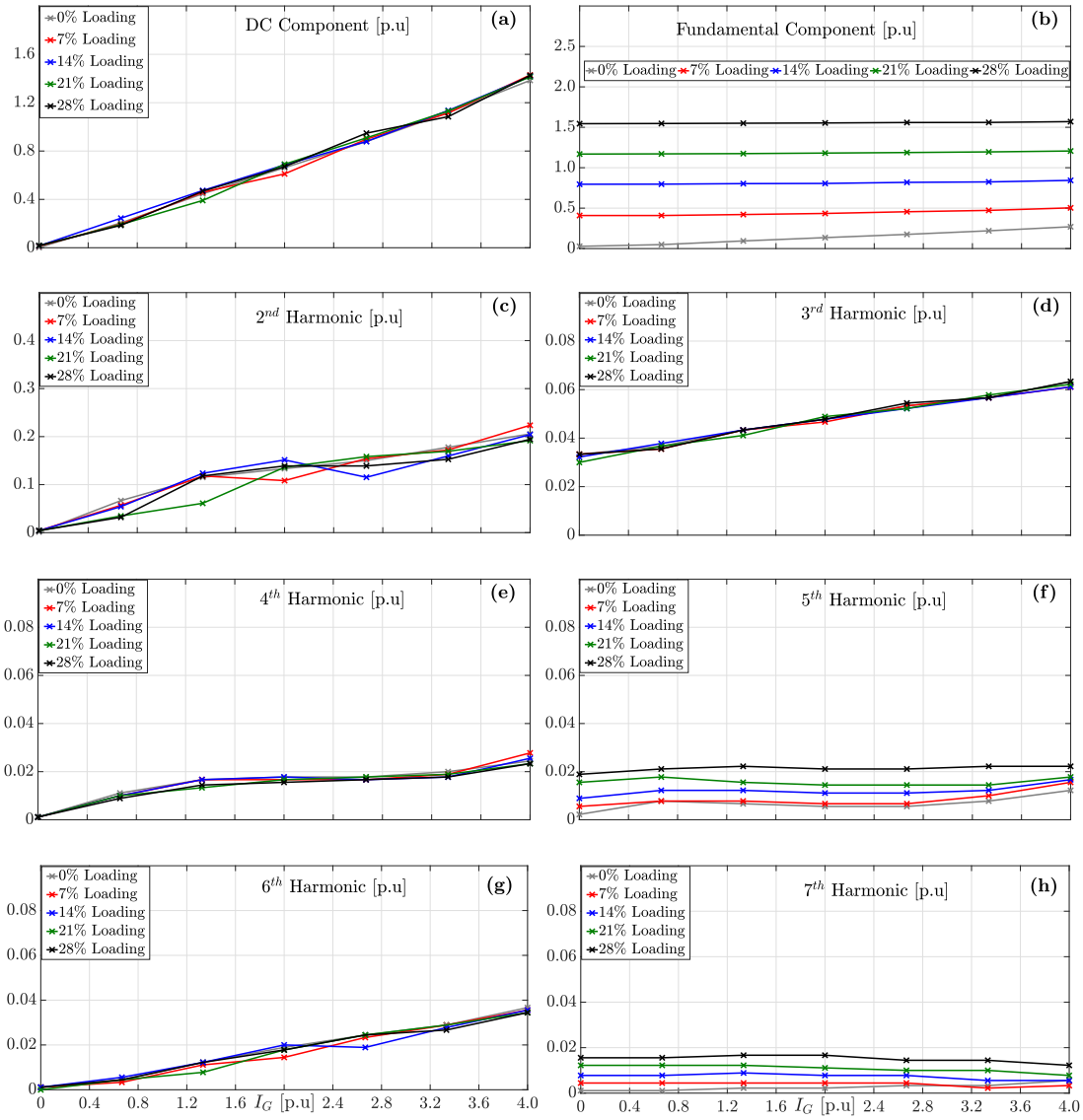


Figure 4.14: Calculated harmonics for the currents caused by GIC in the 35 kVA autotransformer for each load level as: a) DC Component; b) Fundamental Component; c) 2nd Harmonic Component; d) 3rd Harmonic Component; e) 4th Harmonic Component; f) 5th Harmonic Component; g) 6th Harmonic Component; and h) 7th Harmonic Component.

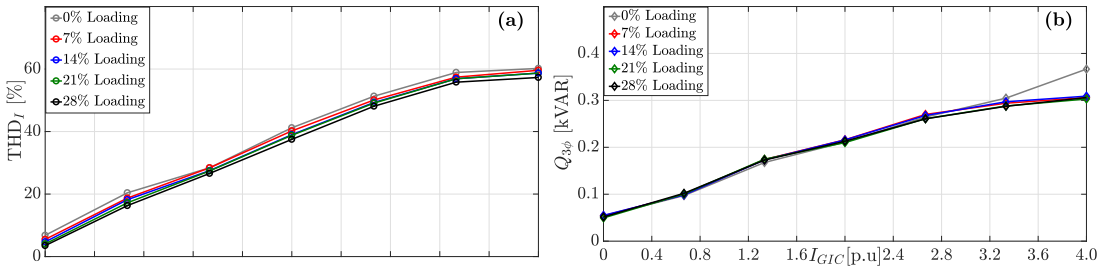


Figure 4.15: Calculated THD for the current and reactive power for the 35 kVA autotransformer at each loading level: a) THD for the current, and b) Calculated reactive power.

imbalance between the phases. The faulted phases draw large fault currents, resulting in distortion in the case of the line-to-neutral fault. The transformer energization case shows unbalanced and distorted currents with a transient response that quickly disappears.

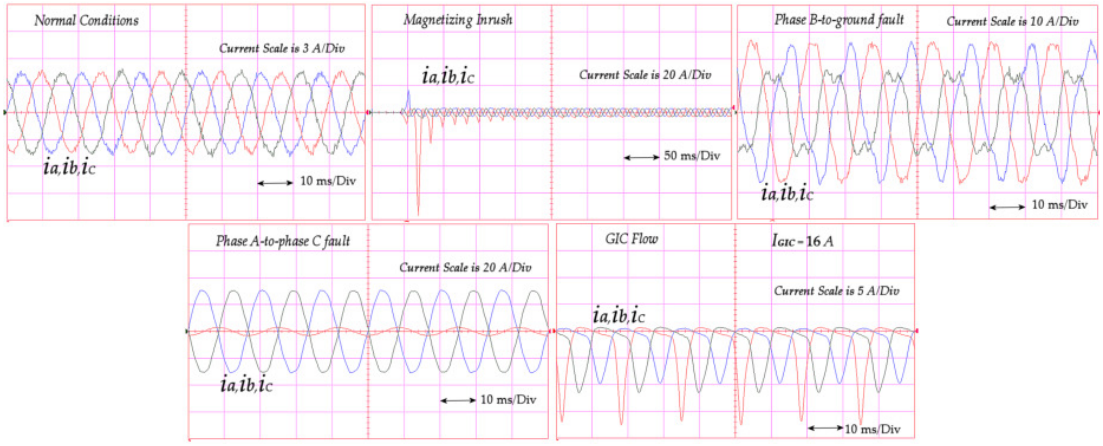


Figure 4.16: Primary side current waveforms showing the distortion caused by each test case for a 5 kVA autotransformer at a load level of 100%.

The harmonics for each test case were then calculated as discussed in Section 3.3. The 2nd harmonic ratios were then calculated from those results, and are compared in Figure 4.17. This figure shows that only GIC and transformer energization had an increase in the 2nd harmonic ratio, relative to the base case. Despite the large imbalance caused by the fault currents, most of their energy was not in the 2nd harmonic, but in the fundamental. This resulted in a reduction in the 2nd harmonic ratio for those cases, particularly the line-to-line fault. The GIC ratio showed very

little increase with an increasing load, while the transformer energization's ratio was greatly reduced as the load was increased. These results are very similar to the results with a conventional power transformer.

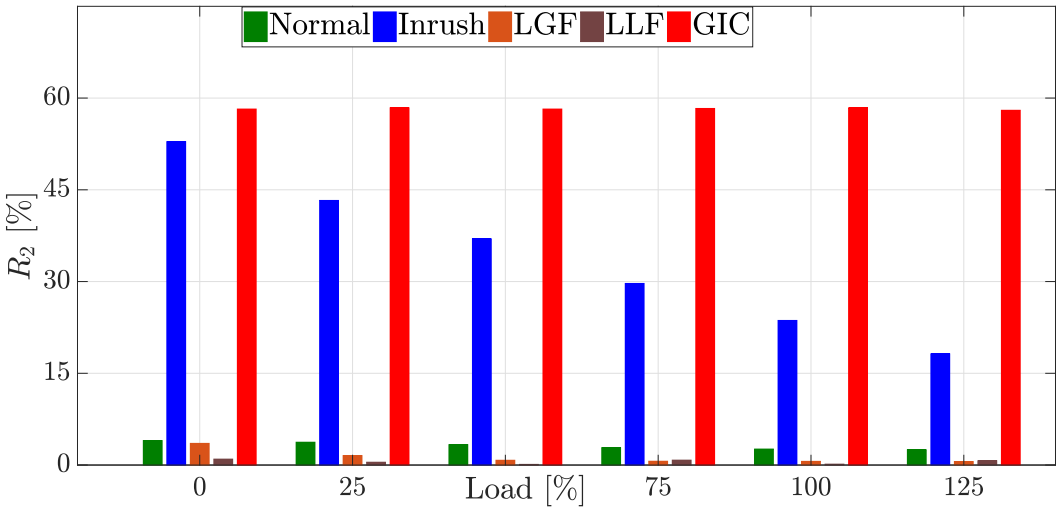


Figure 4.17: A comparison of the 2nd harmonic ratio for each event for a 5 kVA autotransformer.

The use of the duration of the 2nd harmonic ratio as a distinguishing feature of GIC can work with the autotransformer. Figure 4.16 shows the sustained nature of the GIC, with the transformer inrush disappearing after a few cycles. This indicates that a sustained 2nd harmonic ratio will work as a signature of GIC events in autotransformers as well.

4.5.2 35 kVA Autotransformer

For the 35 kVA autotransformer, the load was varied between 0-18% of the rated load and the GIC test was conducted with $I_{GIC} = 30$ A. Figure 4.18 shows the collected primary currents for each test case at 12% of rated load. These figures show some distortion for a number of the test cases. The GIC case shows half-cycle saturation, with less distortion than the 5 kVA autotransformer. The fault cases show an imbalance between the phases for the duration of the fault, with the faulted phases drawing large fault currents. The energizing case shows very small transient

currents that disappear quickly.

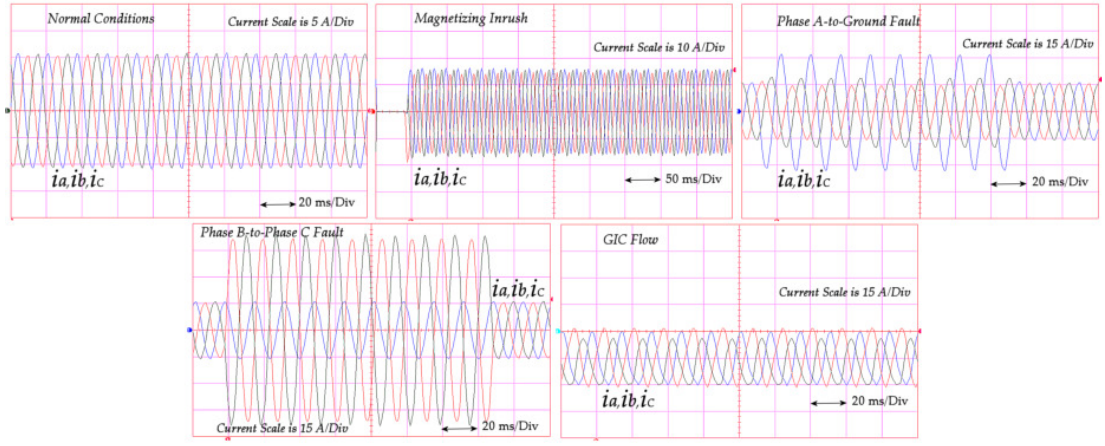


Figure 4.18: Primary side current waveforms showing the distortion caused by each test case for a 35 kVA autotransformer at a load level of 12%.

The harmonics for each test case were then calculated as discussed in Section 3.3. The 2nd harmonic ratios were then calculated from those results, and are compared in Figure 4.19. This figure agrees with the results for the 5 kVA autotransformer. The test cases with the largest 2nd harmonic ratios were the transformer energization and the GIC cases. The fault cases had smaller 2nd harmonic ratios, though the line-to-neutral fault had growth in the 2nd harmonic ratio, relative to the base case. The transformer energization's ratio was greatly reduced as the load was increased, dropping below the ratio of the line-to-neutral fault with the highest loading level.

These results again support the use of a sustained 2nd harmonic ratio as a useful discriminator between transformer energization and GIC for autotransformers. Figure 4.18 shows the sustained nature of the GIC, while the small transformer inrush disappears quickly.

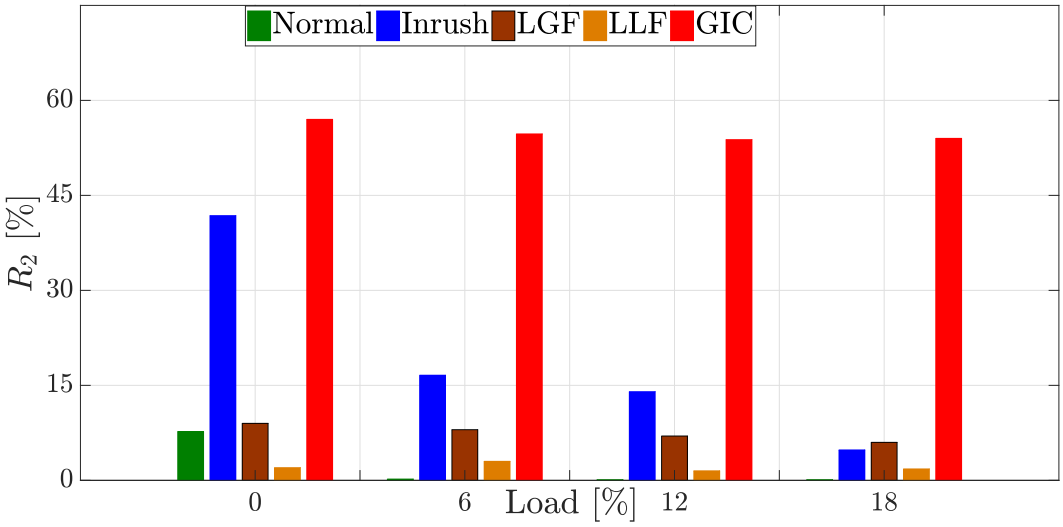


Figure 4.19: A comparison of the 2nd harmonic ratio for each event for a 35 kVA 3-limb autotransformer.

4.6 Summary

This chapter has presented and discussed impacts of GIC flows on 3ϕ power autotransformers. 3ϕ differential currents collected from two 3ϕ power autotransformers have been analyzed to extract their harmonic components. Experimental tests have been conducted for different GIC flows at different loading levels. Analysis of the collected data has shown that the 2nd harmonic dominates all harmonic components triggered by a GIC flow. This signature of GIC flows has been shown to be accurate for different loading levels. Test results of 3ϕ power autotransformers have been found in agreement with those obtained from testing 3ϕ transformers. In both test results, the 2nd harmonic component has been found with significant magnitude (high $R2$ ratio). In addition, the ratio $R2$ has been found to be higher than the non-GIC events. Finally, test results for 3ϕ power transformers and autotransformers support the proposed method to use the sustained 2nd harmonic component, extracted from the 3ϕ differential current, as an accurate signature to detect a GIC flow.

Chapter 5

Conclusion

5.1 Summary

This thesis has presented and discussed adverse effects of GIC flows on 3ϕ power transformers and autotransformers, which have grounded windings. Such effects include the severe harmonic distortion, magnetic saturation of the core(s), overheating of windings, and degraded overall performance. The main cause of these undesired effects is the half-cycle (asymmetrical) magnetic saturation of the core that occurs when GIC flows through grounded windings. Such a flow induces a dc flux in the core and leads to half-cycle magnetic saturation of the core. This phenomena has been modeled using linearized $B - H$ hysteresis curves of magnetic cores that are used in 3ϕ power transformers and autotransformers. In this thesis, derived models have been extended to include effects of the loading level on harmonic components triggered by a GIC flow. In addition, derived models of 3ϕ power transformers and autotransformers have been further extended to include the effects of the grounding impedance on harmonic components triggered by a GIC flow. The analysis, along with experimental test results, have shown that harmonic components triggered by a GIC mainly depend on the magnitude of the GIC, transformer core design, and the

value of the grounding impedance. Moreover, analysis and test results have demonstrated that loading levels have minor effects on the harmonic components triggered by a GIC flow.

Extensive experimental tests have been conducted to identify the order, type, and dominating harmonic components due to different GIC flows when a 3ϕ power transformer or autotransformer has different loading levels or grounding impedances. Test results have shown that the harmonic distortion (quantified using the THD factors) and reactive power demands of a 3ϕ power transformer or autotransformer increase with the increase in the GIC, regardless of the loading level. Moreover, the values of THD and reactive power demands have been found to decrease as the grounding impedance is increased. In all test results, any GIC flow (in a 3ϕ power transformer or autotransformer) triggers a severe harmonic distortion with the 2^{nd} harmonic component being the dominant one.

In order to verify the that a GIC uniquely induces a large 2^{nd} harmonic component, other events have been tested and analyzed. The ratio $R2$ has been introduced to compare GIC events with other non-GIC events. Tested non-GIC events have been normal load changes, line-to-ground faults, line-to-line faults, and transformer energization. Test results have revealed that $R2$ for a GIC flow tend to be higher than for non-GIC events and lasts for as long as the GIC is present. As a result, the proposed use of a sustained high $R2$ ratio as a signature of a GIC flow can provide a simple approach to detect and identify GIC flows in 3ϕ power transformers and autotransformers

5.2 Conclusions

The objectives of this thesis have been stated to model and quantify the effects of a GIC flow on 3ϕ power transformers and autotransformers. Furthermore, this thesis

has focused on developing and testing a new approach to detect and identify a GIC flow in a 3ϕ power transformer or autotransformer. Models have been developed for the impacts of a GIC flow on 3ϕ power transformers and autotransformers. These models have been extended to include the effects of loading level and grounding impedance. Extensive experimental tests have been conducted to verify and analyze effects of a GIC flow on 3ϕ power transformers and autotransformers. The work presented in this thesis supports the following conclusions:

- A GIC flow creates half-cycle saturation in the magnetic core of a 3ϕ power transformer or autotransformer. Such a saturation type triggers harmonic components in magnetizing currents and 3ϕ currents flowing in the grounded windings of a 3ϕ power transformer or autotransformer.

- Harmonic components due to a GIC flow are dominated by the 2^{nd} harmonic component. The magnitudes of such harmonic components directly depend on the level of GIC flow and core design of the 3ϕ power transformer or autotransformer at hand. In addition, the magnitudes of harmonic components due to a GIC flow decrease as the grounding impedance increases.

- The loading level of a 3ϕ power transformer or autotransformer has negligible effects on the magnitudes of harmonic components triggered by a GIC flow.

- The ratio $R2$ (the ratio of the 2^{nd} harmonic component to the fundamental component) has a very large, sustained value in a 3ϕ power transformer or autotransformer when experiencing a GIC flow.

5.3 Contributions

The work presented in this thesis has contributed to the detection of GIC flows in power transformers. This thesis contributes the following:

- A series of models for power transformers that allow modelling the GIC flows to determine the harmonic contents for a given transformer.
- A harmonic analysis of the differential current of conventional power transformers and autotransformers with both multi-cores and 3-limb cores under GIC flows.
- An assessment of the effect of loading levels on the harmonic components generated by GIC flows in power transformers.
- An assessment of the effect of power transformer grounding on the harmonic components generated by GIC flows in power transformers.
- A comparison of the harmonic contents of non-GIC power system events to the harmonic contents of GIC flows.

5.4 Future Works

The work completed in this thesis can provide the background for future research activities. The following are possible avenues for future research works:

- Analysis and modeling of GIC effects (at different loading levels and grounding impedance) on solid-state power transformers.
- The use of developed models and analyses to study effects on common-mode currents and voltages in variable frequency motor drives.
- The utilization of the developed models and analyses to investigate effects of dc ground current circulation in HVDC systems.

References

[1] "IEEE guide for establishing power transformer capability while under geomagnetic disturbances," *IEEE Std C57.163-2023 (Revision of IEEE Std C57.163-2015)*, pp. 1–56, 2024.

[2] D. Boteler, "Geomagnetically induced currents: Present knowledge and future research," *IEEE Transactions on Power Delivery*, vol. 9, no. 1, pp. 50–58, 1994.

[3] S. A. Saleh, E. W. Zundel, G. Young-Morris, *et al.*, "Investigating harmonic distortion in power transformers due to geomagnetically induced current flows," *IEEE Transactions on Industry Applications*, pp. 1–11, 2023.

[4] J. Taylor, "Analysis of geomagnetic disturbance (GMD) related harmonics," Electric Power Research Institute, Tech. Rep., 2014.

[5] J. G. Kappenman, V. D. Albertson, and N. Mohan, "Current transformer and relay performance in the presence of geomagnetically-induced currents," *IEEE Transactions on Power Apparatus and Systems*, vol. PAS-100, no. 3, pp. 1078–1088, 1981.

[6] B. Bozoki, S. Chano, L. Dvorak, *et al.*, "The effects of GIC on protective relaying," *IEEE Transactions on Power Delivery*, vol. 11, no. 2, pp. 725–739, 1996.

[7] K. Burhanudin, M. H. Jusoh, Z. I. A. Latiff, M. H. Hashim, and N. D. K. Ashar, "The estimation of the geomagnetically induced current based on simulation

and measurement at the power network: A bibliometric analysis of 42 years (1979–2021)," *IEEE Access*, vol. 10, pp. 56 525–56 549, 2022.

[8] R. Girgis and K. Vedante, "Effects of GIC on power transformers and power systems," in *PES T&D 2012*, 2012, pp. 1–8.

[9] H. C. Tay and G. W. Swift, "On the problem of transformer overheating due to geomagnetically induced currents," *IEEE Transactions on Power Apparatus and Systems*, vol. PAS-104, no. 1, pp. 212–219, 1985.

[10] N. Takasu, T. Oshi, F. Miyawaki, S. Saito, and Y. Fujiwara, "An experimental analysis of DC excitation of transformers by geomagnetically induced currents," *IEEE Transactions on Power Delivery*, vol. 9, no. 2, pp. 1173–1182, 1994.

[11] I. Boguslawsky, N. Korovkin, V. Popov, and O. Sokolova, "Synchronous machine performance under geomagnetic disturbances," *High Voltage*, vol. 6, no. 5, pp. 894–903, 2021.

[12] A. Rezaei-Zare, "Behavior of single-phase transformers under geomagnetically induced current conditions," *IEEE Transactions on Power Delivery*, vol. 29, no. 2, pp. 916–925, 2014.

[13] M. Lahtinen and J. Elovaara, "GIC occurrences and GIC test for 400 kV system transformer," *IEEE Transactions on Power Delivery*, vol. 17, no. 2, pp. 555–561, 2002.

[14] L. Bolduc, M. Granger, G. Pare, J. Saintonge, and L. Brophy, "Development of a DC current-blocking device for transformer neutrals," *IEEE Transactions on Power Delivery*, vol. 20, no. 1, pp. 163–168, 2005.

[15] M. Eitzmann, R. Walling, M. Sublich, *et al.*, "Alternatives for blocking direct current in AC system neutrals at the Radisson/LG2 complex," *IEEE Transactions on Power Delivery*, vol. 7, no. 3, pp. 1328–1337, 1992.

[16] R. J. Pirjola, A. T. Viljanen, and A. A. Pulkkineni, "Research of geomagnetically induced currents (GIC) in Finland," in *2007 7th International Symposium on Electromagnetic Compatibility and Electromagnetic Ecology*, 2007, pp. 269–272.

[17] E. Arajärvi, R. Pirjola, and A. Viljanen, "Effects of neutral point reactors and series capacitors on geomagnetically induced currents in a high-voltage electric power transmission system," *Space Weather*, vol. 9, no. 11, 2011.

[18] F. R. Faxvog, W. Jensen, G. Fuchs, *et al.*, "Power grid protection against geomagnetic disturbances (GMD)," in *2013 IEEE Electrical Power & Energy Conference*, 2013, pp. 1–13.

[19] A. A. Hussein and M. H. Ali, "Fuzzy logic controlled variable resistor for suppressing GIC in transformers," *IET Generation, Transmission & Distribution*, vol. 11, no. 6, pp. 1494–1501, 2017.

[20] B. Kovan and F. de León, "Mitigation of geomagnetically induced currents by neutral switching," *IEEE Transactions on Power Delivery*, vol. 30, no. 4, pp. 1999–2006, 2015.

[21] A. Hesami Naghshbandy, A. Ghaderi Baayeh, and A. Faraji, "Mitigating the effects of geomagnetically induced currents in the power network," *IET Generation, Transmission & Distribution*, vol. 14, no. 23, pp. 5514–5525, 2020.

[22] W. Viana, R. Micaleff, S. Young, F. Dawson, and E. Dick, "Transformer design considerations for mitigating geomagnetic induced saturation," *IEEE Transactions on Magnetics*, vol. 35, no. 5, pp. 3532–3534, 1999.

[23] M. Kazerooni and T. J. Overbye, "Transformer protection in large-scale power systems during geomagnetic disturbances using line switching," *IEEE Transactions on Power Systems*, vol. 33, no. 6, pp. 5990–5999, 2018.

[24] M. A. F. K. Alakula and S. Lindha, "Method and equipment for the protection of power systems against geomagnetically induced currents," *US Patent 7489485 B2*, 2009.

[25] "IEEE guide for protecting power transformers," *IEEE Std C37.91-2021 (Revision of IEEE Std C37.91-2008)*, pp. 1–160, 2021.

[26] W. G. Enright, O. Nayak, and N. R. Watson, "Three-phase five-limb unified magnetic equivalent circuit transformer models for PSCAD V3," in *IPST '99 Proceedings*, 1999, pp. 462–467.

[27] R. Hamilton, "Analysis of transformer inrush current and comparison of harmonic restraint methods in transformer protection," *IEEE Transactions on Industry Applications*, vol. 49, no. 4, pp. 1890–1899, 2013.

[28] M. H. Rashid, *Power Electronics Handbook.* Butterworth-Heinemann, 2017, vol. 4th ed, ISBN: 9780128114070.

[29] G. Buticchi and E. Lorenzani, "Detection method of the DC bias in distribution power transformers," *IEEE Transactions on Industrial Electronics*, vol. 60, no. 8, pp. 3539–3549, 2013.

[30] C.-H. Gao, H. Gao, W.-L. Liu, H.-P. Shi, S.-T. Yan, and Q.-R. Zhang, "Geomagnetically induced current-monitoring method based on high voltage wires for transformers," *IEEE Access*, vol. 10, pp. 54 208–54 213, 2022.

[31] L. Marti, J. Berge, and R. K. Varma, "Determination of geomagnetically induced current flow in a transformer from reactive power absorption," *IEEE Transactions on Power Delivery*, vol. 28, no. 3, pp. 1280–1288, 2013.

[32] J. Chen, C. Liu, M. Wang, and T. Wang, "Power system responses to geomagnetic disturbances recognized using phasor measurement recordings," *International Journal of Electrical Power & Energy Systems*, vol. 113, pp. 932–940, 2019, ISSN: 0142-0615.

[33] H. C. Tay and G. W. Swift, "A novel method of detecting asymmetrical transformer core saturation due to GIC," *IEEE Power Engineering Review*, vol. PER-4, no. 1, pp. 42–43, 1984.

[34] D. Tousignant, L. Bolduc, and A. Dutil, "A method for the indication of power transformer saturation," *Electric Power Systems Research*, vol. 37, no. 2, pp. 115–120, 1996, ISSN: 0378-7796.

[35] S. A. Saleh, E. W. Zundel, G. Young-Morris, *et al.*, "Second harmonic-based approach to identify a GIC flow in power transformers," *2024 IEEE/IAS 60th Industrial and Commercial Power Systems Technical Conference (I&CPS)*, 2024.

[36] B. Ahmadzadeh-Shooshtari and A. Rezaei-Zare, "Advanced transformer differential protection under GIC conditions," *IEEE Transactions on Power Delivery*, vol. 37, no. 3, pp. 1433–1444, 2022.

[37] B. Ahmadzadeh-Shooshtari and A. Rezaei-Zare, "A waveform-based approach for transformer differential protection under GIC conditions," *IEEE Transactions on Power Delivery*, vol. 37, no. 6, pp. 5366–5375, 2022.

[38] B. Ahmadzadeh-Shooshtari and A. Rezaei-Zare, "Transformer differential protection during geomagnetic disturbances: A hybrid protection scheme and real-time validation tests," *IEEE Transactions on Power Delivery*, vol. 39, no. 1, pp. 13–28, 2024.

[39] S. Wang, P. Dehghanian, L. Li, and B. Wang, "A machine learning approach to detection of geomagnetically induced currents in power grids," *IEEE Transactions on Industry Applications*, vol. 56, no. 2, pp. 1098–1106, 2020.

[40] A. A. Ademola, X. Li, A. Pinceti, *et al.*, "Effects-based monitoring of geomagnetically induced current using a convolutional neural network," *IEEE Transactions on Power Delivery*, vol. 38, no. 1, pp. 85–94, 2023.

[41] S. A. Saleh, E. W. Zundel, G. Young-Morris, *et al.*, "Effect of grounding impedance on the second harmonic component produced by GIC flows," *2024 IEEE/IAS 60th Industrial and Commercial Power Systems Technical Conference (I&CPS)*, 2024.

[42] S. A. Saleh, E. W. Zundel, G. Young-Morris, *et al.*, "Impacts of transformer loading on the harmonic distortion created by GIC flows," *IEEE Transactions on Industry Applications*, pp. 1–11, 2024.

[43] S. A. Saleh, E. W. Zundel, G. Young-Morris, *et al.*, "Harmonic distortions in 3ϕ auto-transformers due to geomagnetically induced current flows," *2024 IEEE/IAS 60th Industrial and Commercial Power Systems Technical Conference (I&CPS)*, 2024.

[44] S. A. Saleh, E. W. Zundel, G. Young-Morris, *et al.*, "Impacts of loading level on harmonic distortions in 3ϕ auto-transformers during GIC flows," *2024 IEEE/IAS 60th Industrial and Commercial Power Systems Technical Conference (I&CPS)*, 2024.

[45] "IEEE recommended practice and requirements for harmonic control in electric power systems," *IEEE Std 519-2014 (Revision of IEEE Std 519-1992)*, pp. 1–29, 2014.

[46] E. Ragonese, A. Scuderi, T. Biondi, and G. Palmisano, *Integrated Inductors and Transformers: Characterization, Design and Modeling for RF and MM-Wave Applications*. Auerbach Publishers, 2010.

[47] S. Zhang, L.-G. Liu, and H. Li, "GIC influence on UHV power grids based on Kalman filter and WAMS data," *IEEE Access*, vol. 8, pp. 202 379–202 386, 2020.

[48] M. A. Sharkirov, "The equivalent circuit of a two-winding autotransformer with mapping of magnetic fluxes," *Russia Electrical Engineering*, vol. 88, no. 1, pp. 289–295, 2017.

[49] S. A. Saleh, E. Ozkop, M. E. Valdes, *et al.*, "Experimental assessment of ground fault protection in frequency-selective grounded systems fed by a single transformer," *IEEE Transactions on Industry Applications*, vol. 59, no. 2, pp. 2386–2399, 2023.

[50] S. A. Saleh, D. Jewett, and S. A. R. Panetta, "The analysis, modeling, and capabilities of grounding system designs," *IEEE Transactions on Industry Applications*, vol. 58, no. 5, pp. 5908–5920, 2022.

Appendix A

35 kVA Power Transformer Results

A.1 Harmonics Due to a GIC Flow

This experiment aimed to determine the harmonics induced in the power transformer due to the presence of GIC. The transformer was solidly grounded ($Z_G = 0\ \Omega$). For the 35 kVA power transformer, defined in Table 3.1, a fixed 3ϕ, Y-connected, resistive load of 0.85 kW was used. The dc current used to simulate the GIC was varied from 0-36 A in steps of 4 A.

Figure A.1 shows the collected primary currents for each level of GIC tested. Figure A.2 shows the secondary voltages.

The waveforms in Figure A.1 show that the current experienced very little distortion at low levels of GIC. The current can be seen shifting due to the presence of a dc current, but distortion does not start occurring until $I_{GIC} = 24$ A. This is consistent with the fact that 3-limb transformers are far less susceptible to saturation due to GIC. The waveforms in Figure A.2, as with the 5 kVA transformer, show far less distortion. No distortion is visible at any level of GIC.

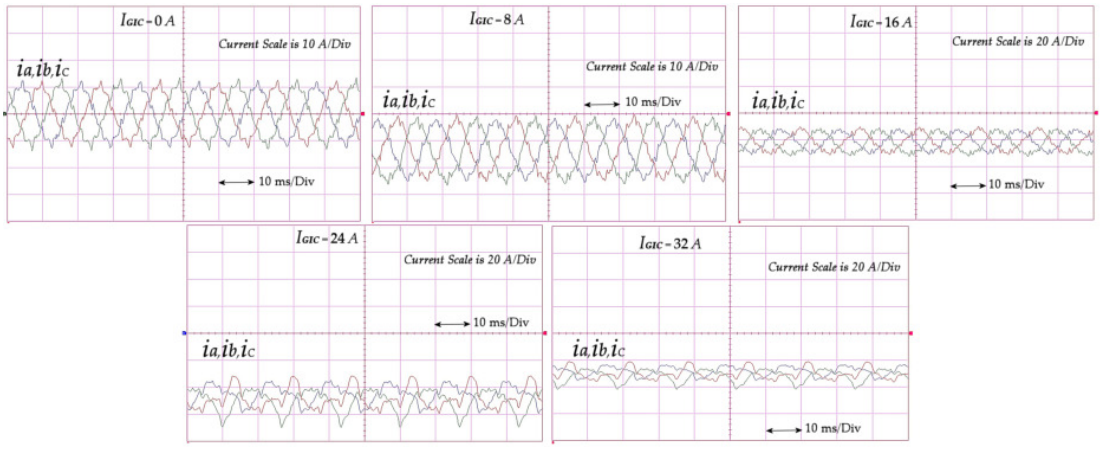


Figure A.1: Primary side current waveforms showing the distortion caused by GIC in the 35 kVA power transformer.

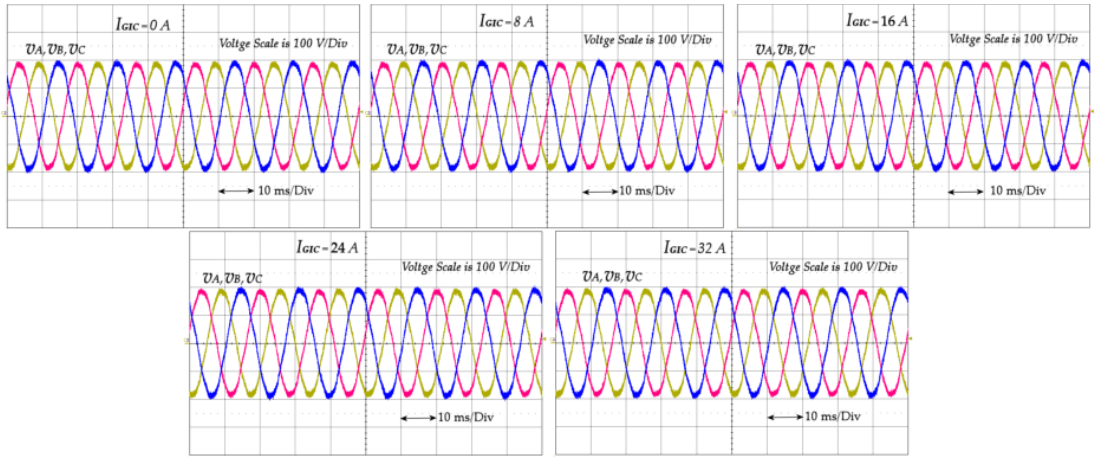


Figure A.2: Secondary-side voltage waveforms showing the distortion caused by GIC in the 35 kVA power transformer.

To quantify the distortion, the harmonics for the voltage and current were calculated as discussed in Section 3.3. The results for the first seven harmonics for both currents and voltages can be seen in Figure A.3. The current harmonics increase very slowly until experiencing a sudden jump around $I_{GIC} = 24$ A. From that point on, the current harmonics grow quite large and are dominated by the 4^{th} harmonic component, with the 2^{nd} harmonic component also quite large. As can be seen, the harmonic content of the voltages remains very low throughout, and does not change significantly as I_{GIC} increases.

The harmonic components were used to calculate the THD for both the cur-

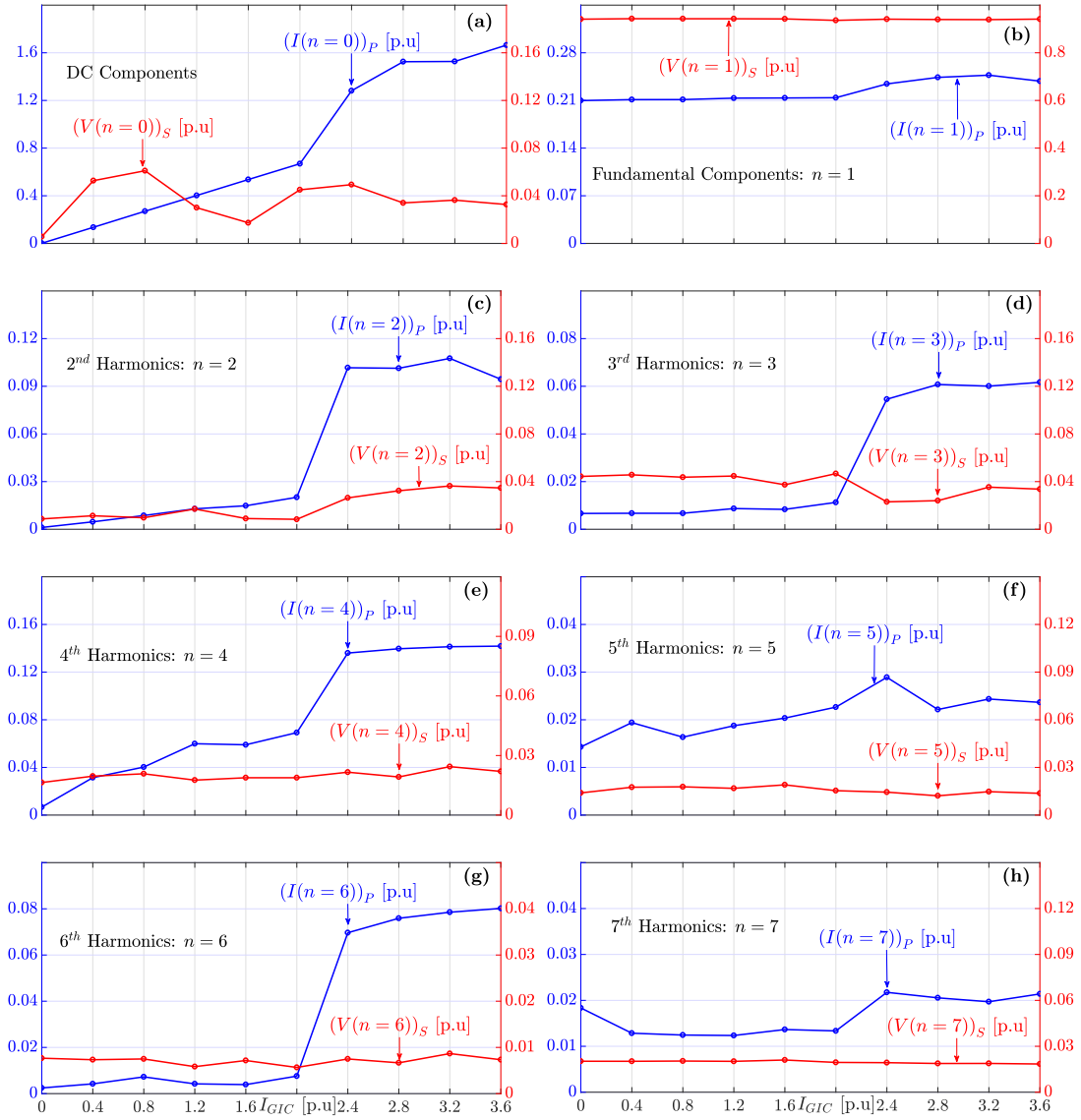


Figure A.3: Calculated harmonics for the voltages and currents caused by GIC in the 35 kVA power transformer as: a) DC Component; b) Fundamental Component; c) 2^{nd} Harmonic Component; d) 3^{rd} Harmonic Component; e) 4^{th} Harmonic Component; f) 5^{th} Harmonic Component; g) 6^{th} Harmonic Component; and h) 7^{th} Harmonic Component.

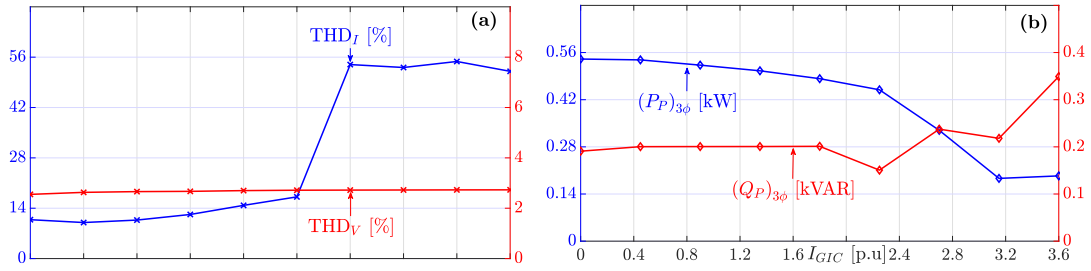


Figure A.4: Calculated THD for the current and voltage and power/reactive power for the 35 kVA power transformer: a) THD for the current and voltage, and b) Calculated power and reactive power.

rent and voltage. Additionally, the collected power and reactive power data was plotted. Both can be found in Figure A.4. The THD for the voltage remains very stable, while the THD for the current rises slowly, before spiking quickly to a new plateau as GIC reaches higher levels. The active power falls as GIC rises, while the reactive power remains quite low, before increasing at higher levels of GIC.

A.2 Effect of the Loading Level

This experiment aimed to determine the effect loading has on the harmonics induced in the autotransformers due to the presence of GIC. A variable, 3ϕ, Y-connected, resistive load was connected on the secondary side of the transformer. The load was varied between 0-54.8% of the rated load. The transformer was solidly grounded ($Z_G = 0\ \Omega$). The dc current used to simulate the GIC was varied from 0-36 A in steps of 6 A.

Figure A.5 shows the collected primary currents for $I_{GIC} = 30$ A for each load level tested.

The waveforms in Figure A.5 show that the transformer experienced a moderate amount of distortion due to the presence of GIC. Compared to the 5 kVA transformer, there is less saturation, and the loading starts to make the effects of distortion harder to discern as it is increased.

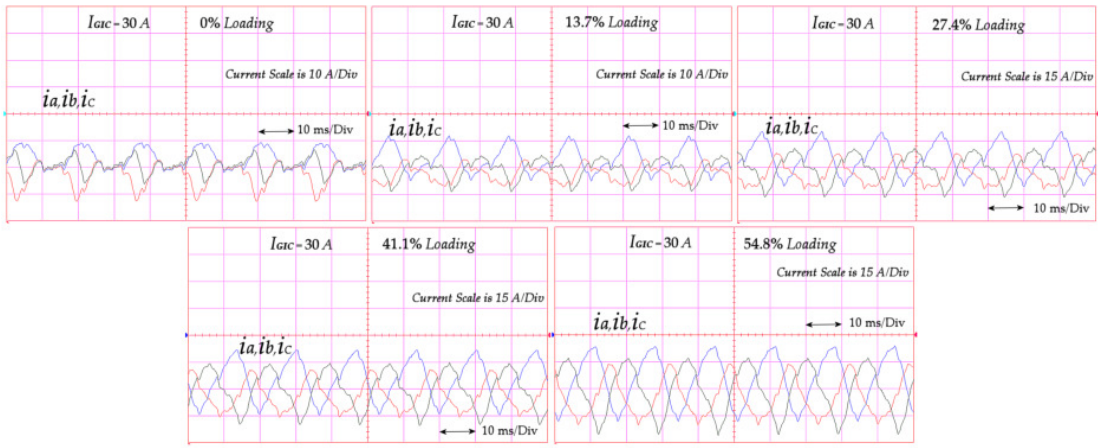


Figure A.5: Primary side current waveforms showing the distortion for $I_{GIC} = 30$ A in the 35 kVA power transformer for each load level.

To quantify the distortion, the harmonics for the current were calculated as discussed in Section 3.3. The results for the first seven harmonics for both currents and voltages can be seen in Figure A.6. The harmonics all trend upwards, with the 2$^{\text{nd}}$ harmonic component the largest of the higher order harmonics. Due to the lower level of susceptibility to saturation of a 3-limb transformer, the effects of GIC are reduced on the transformer. Unlike the 5 kVA transformer, the effects of loading on the harmonic distortion are less clear, seeming to have little consistent effect on the magnitude of the harmonics. Regardless, the 2$^{\text{nd}}$ harmonic component is dominant for all levels of loading and GIC.

The harmonic components were used to calculate the THD of the differential current. Additionally, the collected reactive power data was plotted. Both can be found in Figure A.7. The THD for the current rises with GIC initially, but falls slightly at higher GIC levels. There is no consistent effect of loading on the THD. The reactive power rises with increasing GIC, but there is no discernible effect of loading on the reactive power consumption.

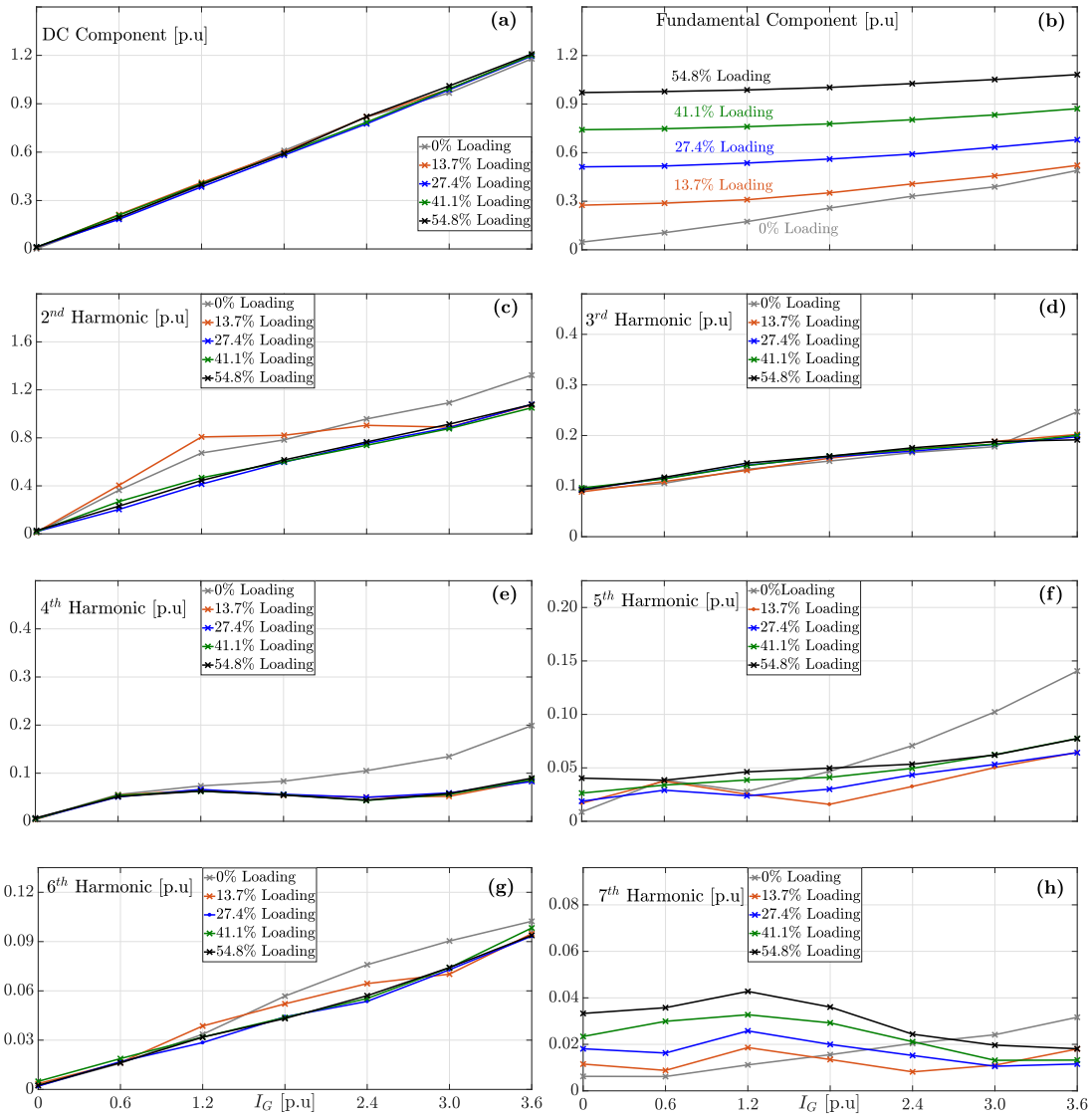


Figure A.6: Calculated harmonics for the currents caused by GIC in the 35 kVA power transformer for each load level as: a) DC Component; b) Fundamental Component; c) 2nd Harmonic Component; d) 3rd Harmonic Component; e) 4th Harmonic Component; f) 5th Harmonic Component; g) 6th Harmonic Component; and h) 7th Harmonic Component.

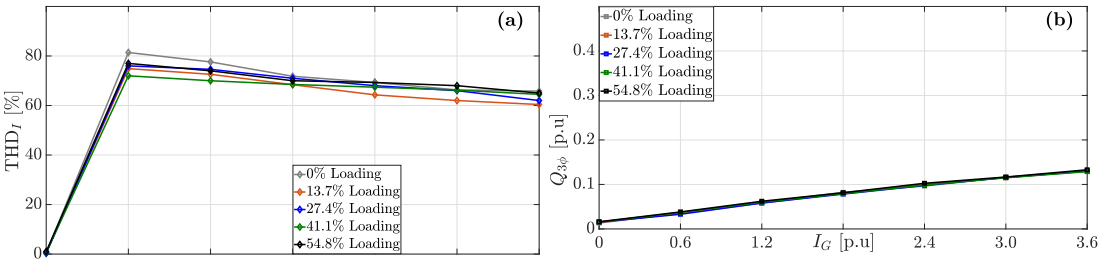


Figure A.7: Calculated THD for the current and reactive power for the 35 kVA power transformer at each loading level: a) THD for the current, and b) Calculated reactive power.

A.3 Effect of the Grounding Impedance

This experiment aimed to determine the effect that introducing a ground impedance has on the harmonics induced in the power transformer due to the presence of GIC. The tests of the 35 kVA power transformer were conducted with a fixed, 3ϕ, Y-connected, resistive load of 1 kW. The dc current used to simulate the GIC was varied from 0-40 A in steps of 8 A.

Figure A.8 shows the collected primary currents for $I_{GIC} = 12$ A for each grounding system tested.

The waveforms in Figure A.8 show that using any form of grounding system radically reduced the harmonics seen by the system. The greatest saturation can be seen with solid grounding, while the least saturation can be seen for the HRG. As with the 5 kVA transformer, the LRG and FSG do not have significant differences in the distortion. This reduced distortion may be a result of the low excitation of the transformer, as well as the low susceptibility of the transformer to saturation due to the 3-limb core. Any reduction in GIC flow could thus have an outsized effect on the resulting harmonics.

To quantify the distortion, the harmonics for the differential current were calculated as discussed in Section 3.3. The results for the first seven harmonics for the currents under all loading levels can be seen in Figure A.9. The sharp drop in

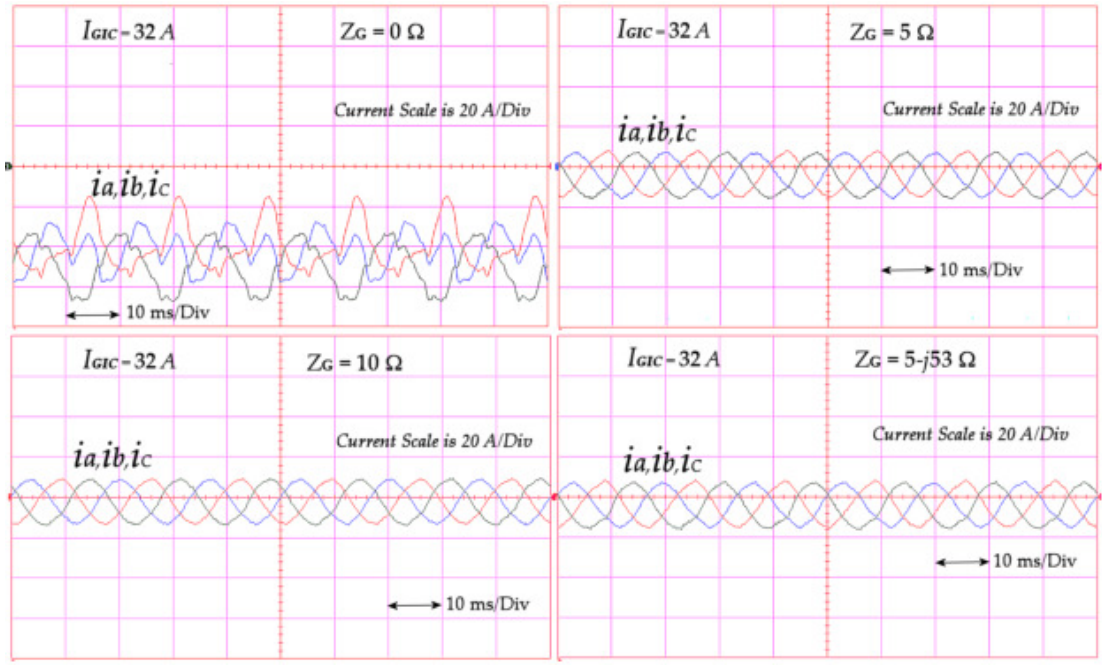


Figure A.8: Primary side current waveforms showing the distortion caused by I_{GIC} = 12 A in the 35 kVA power transformer for each grounding system tested.

distortion with the addition of a grounding system is reflected in the magnitude of the harmonic components. As before, there is little difference between the FSG and LRG. The HRG reduces the harmonics the most, but any level of grounding greatly reduces the levels of harmonics. Observing the magnitudes of the harmonic components, including a grounding source results in the 2nd and 3rd harmonic components being of similar magnitudes. This represents a risk for using the 2nd harmonic component as an indicator of saturation with with LRG and HRG grounding systems. However, the use of these systems already greatly reduce the saturation of the transformer, and close examination of the 2nd harmonic component shows that it both still increases with GIC and is consistently slightly larger than any other harmonic component.

The harmonic components were used to calculate the THD for the current. Additionally, the collected reactive power data was plotted. Both can be found in Figure A.10. For all grounding systems except solid grounding the THD remains quite low; for solid grounding, the THD rises before plateauing around 45%. The reactive power rises with increasing GIC for solid grounding, but there is no discernible

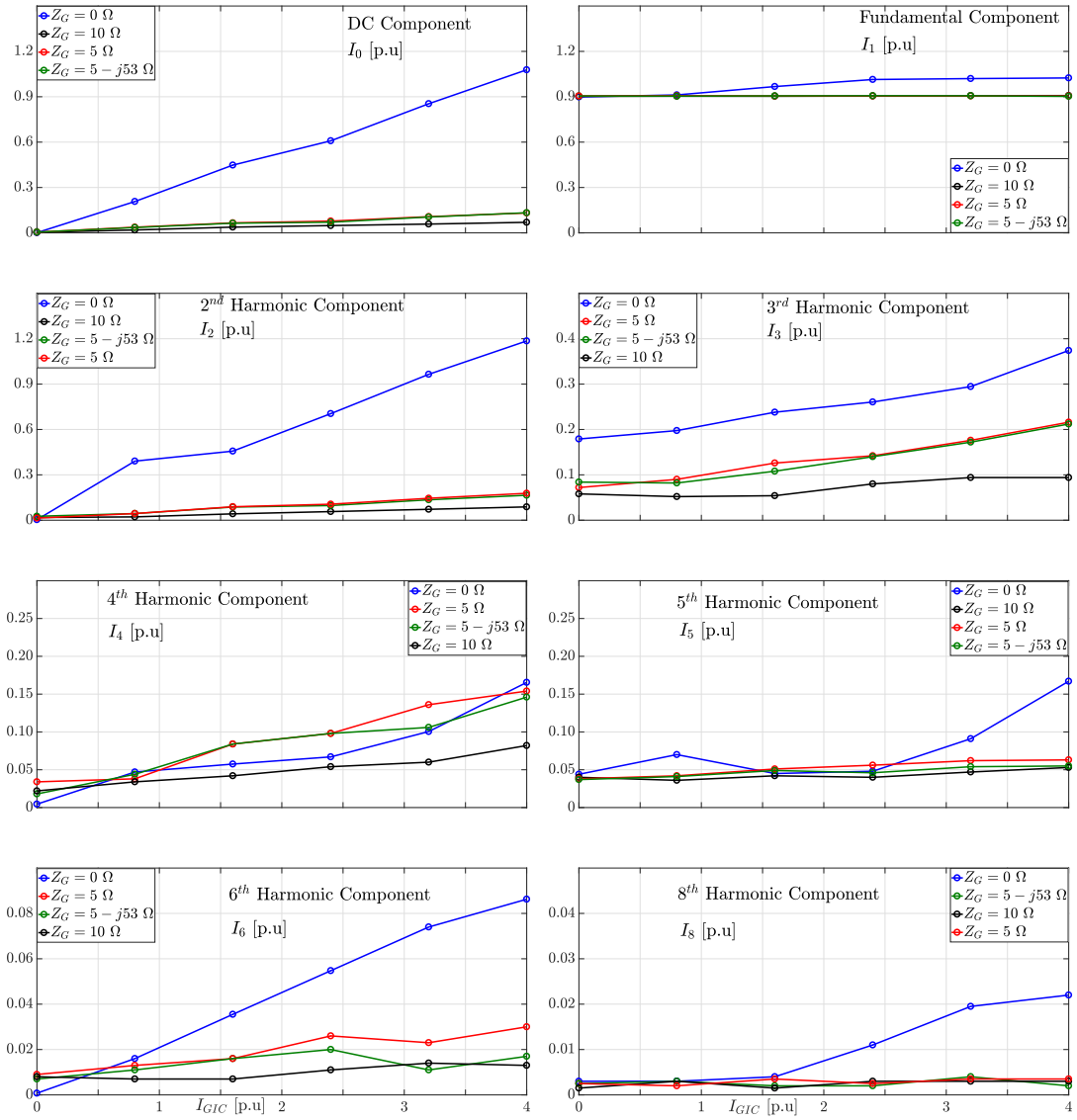


Figure A.9: Calculated harmonics for the currents caused by GIC in the 35 kVA power transformer for each grounding type used as: a) DC Component; b) Fundamental Component; c) 2nd Harmonic Component; d) 3rd Harmonic Component; e) 4th Harmonic Component; f) 5th Harmonic Component; g) 6th Harmonic Component; and h) 7th Harmonic Component.

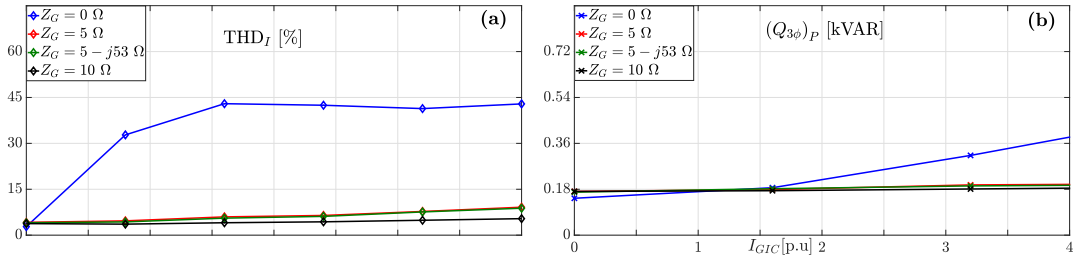


Figure A.10: Calculated THD for the curren and reactive power for the 35 kVA power transformer for each grounding type: a) THD for the current, and b) Calculated reactive power.

rise in reactive power consumption for the other grounding systems.

A.4 Non-GIC Events

The test set-up used is very similar to the one used in Section 3.5. A variable, 3ϕ, Y-connected, resistive load, ranging from 0-18% of the rated load, was connected on the secondary side of the transformer. The same series of tests performed on the 5 kVA multi-core transformer were performed, with the GIC test conducted with I_{GIC} = 30 A.

Figure A.11 shows the collected primary currents for each test case for 12% of rated load. These figures show some distortion for a number of the test cases. The GIC case shows some half-cycle saturation, but is less distorted than the 5 kVA transformer. The fault cases again show an imbalance between the phases, with the faulted phases drawing a large fault current. The energizing case shows transient unbalanced and distorted currents that slowly disappear, taking far longer than for the 5 kVA transformer.

The harmonics for each test case were then calculated as discussed in Section 3.3. The 2^{nd} harmonic ratios were then calculated from those results, and are compared in Figure A.12. This figure agrees with the results for the 5 kVA transformer, and shows that only two of the events had an increase in the 2^{nd} harmonic ratio:

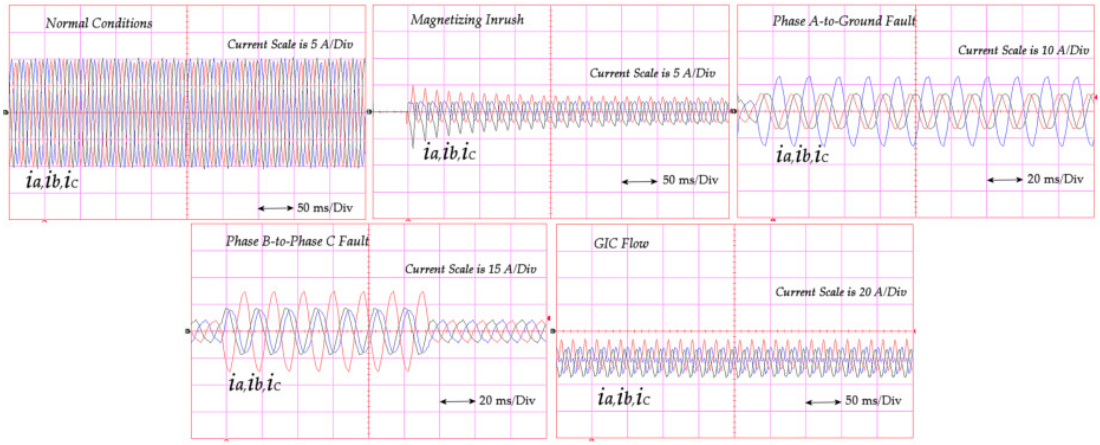


Figure A.11: Primary side current waveforms showing the distortion caused by each test case for a 35 kVA power transformer at a load level of 12%.

GIC and transformer energization. Despite the large imbalance caused by the fault currents, most of their energy was not in the 2nd harmonic, but in the fundamental. This resulted in a reduction in the 2nd harmonic ratio for those cases relative to the base case. The transformer energization's ratio was greatly reduced as the load was increased, with the GIC ratio only dropping slightly.

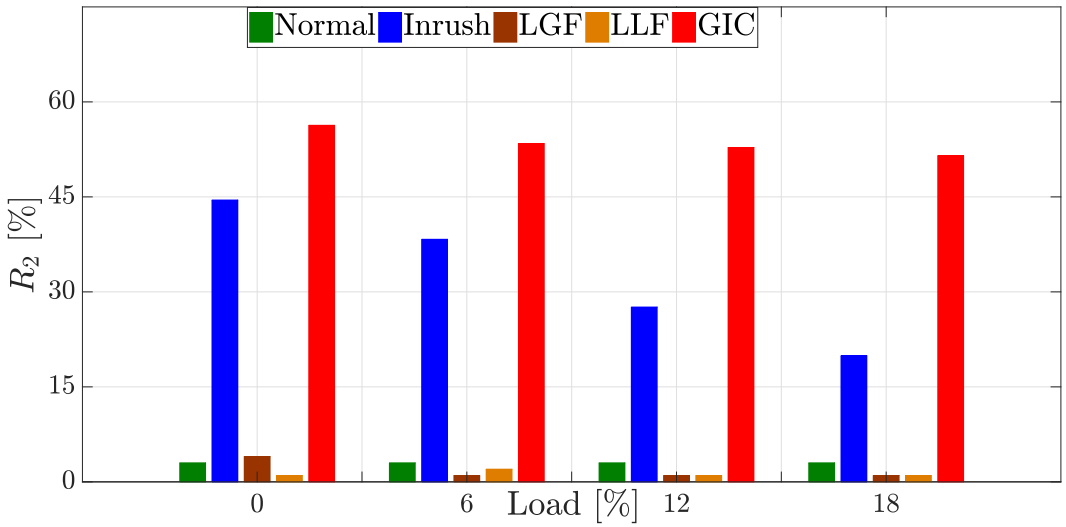


Figure A.12: A comparison of the 2nd harmonic ratio for each event for the 35 kVA power transformer.

These results again support the use of a sustained 2nd harmonic ratio as a useful discriminator between inrush and GIC. Figure A.11 shows the sustained nature of the GIC, while the transformer inrush disappears gradually. This offers support

to the use of a sustained 2^{nd} harmonic ratio as the signature of a GIC event, with a sufficiently long delay time to allow for the transformer inrush to fully disappear.

Vita

Candidate's full name: Eric Walter Zundel
University attended:

- Bachelor of Science in Engineering, Major in Electrical Engineering
  University of New Brunswick, Sept. 2016 - May 2022.

Publications:

- S. A. Saleh, E. W. Zundel, G. Young-Morris, *et al.*, "Investigating harmonic distortion in power transformers due to geomagnetically induced current flows," *IEEE Transactions on Industry Applications*, pp. 1–11, 2023
- S. A. Saleh, E. W. Zundel, G. Young-Morris, *et al.*, "Impacts of transformer loading on the harmonic distortion created by GIC flows," *IEEE Transactions on Industry Applications*, pp. 1–11, 2024
- S. A. Saleh, M. Valdes, P.E. Sutherland, and M. Haj-Ahmed, and E. W. Zundel, "Phaselet-Based Arc Flash Relay Against Low Voltage Side Arcing Current Faults in MV-LV Power Transformers", *IEEE Trans. on Industry Applications*, Vol. 59, No. 6, pp. 7462–7474, 2023.
- S. A. Saleh, O. Betancourt, E. Ozkop, R. Ahshan, E. Zundel, Z. Sanchez, and J. Meng, "The Analysis and Modeling of Voltage Survivability in Power Systems", *Accepted for publication in the IEEE Trans. on Industry Applications*, December, 2023.

Conference Presentations:

- S. A. Saleh, E. W. Zundel, G. Young-Morris, *et al.*, "Harmonic distortions in 3ϕ auto-transformers due to geomagnetically induced current flows," *2024 IEEE/IAS 60th Industrial and Commercial Power Systems Technical Conference (I&CPS)*, 2024
- S. A. Saleh, E. W. Zundel, G. Young-Morris, *et al.*, "Impacts of loading level on harmonic distortions in 3ϕ auto-transformers during GIC flows," *2024 IEEE/IAS 60th Industrial and Commercial Power Systems Technical Conference (I&CPS)*, 2024

- S. A. Saleh, E. W. Zundel, G. Young-Morris, *et al.*, "Effect of grounding impedance on the second harmonic component produced by GIC flows," *2024 IEEE/IAS 60th Industrial and Commercial Power Systems Technical Conference (I&CPS)*, 2024

- S. A. Saleh, E. W. Zundel, G. Young-Morris, *et al.*, "Second harmonic-based approach to identify a GIC flow in power transformers," *2024 IEEE/IAS 60th Industrial and Commercial Power Systems Technical Conference (I&CPS)*, 2024

- S. A. Saleh, E. W. Zundel, D. Jewett, E. F. S. Hill, J. Meng, G. Y. Morris and S. Brown "Case Studies of Harmonic Distortion in Power Transformers Due to Geomagnetically Induced Current Flow", *In Proc. of the 59-th IEEE IAS Industrial and Commercial Power Systems Technical Conference (ICPS 2023)*, Las Vegas, NV, May 2023.

- S. A. Saleh, E. W. Zundel, E. F. S. Hill, G. Y. Morris, S. Brown, J. Meng, and J. Cardenas "Effects of Loading Levels on Harmonic Distortion in Power Transformers Due to GIC Flows", *In Proc. of the 58-th IEEE IAS'23 Annual Meeting Conference*, Nashville, TN, October 2023.

- S. A. Saleh, E. Ozkop, O. Betancourt, R. Ahshan, E. Zundel, Z. Sanchez, and J.Meng "Voltage Survivability Analysis of Power Systems", *In Proc. of the 58-th IEEE IAS'23 Annual Meeting Conference*, Nashville, TN, October 2023.